1-1-2019

Field testing and simulation of vadose-zone recharge wells in the Mississippi river valley alluvial aquifer as an artificial recharge method

Kyungwon Kwak

FIELD TESTING AND SIMULATION OF VADOSE-ZONE RECHARGE WELLS IN THE MISSISSIPPI RIVERVALLEY ALLUVIAL AQUIFER AS AN ARTIFICIAL RECHARGE METHOD

A Thesis
presented in partial fulfillment of requirements
for a Master's degree in Engineering Science
in the Department of geology and geological engineering
The University of Mississippi

by

KYUNGWON KWAK

August 2019

Abstract

Increasing concerns regarding depletion of groundwater in the Delta region of Mississippi have led to a need to augment natural recharge. Infiltration basins are often one of the simplest means of artificially recharging aquifers. However, the Delta has a layer of clay and silt at the surface, so it is a better idea to use vadose-zone recharge wells that are not limited by the surficial layer of fine soils. The purpose of this study is to use full-scale field testing to assess the feasibility of using vadose-zone wells for artificial recharge of the Mississippi River Valley alluvial aquifer by using a combination of field, laboratory, and computer simulation techniques. From field tests data, the calculated transmissivity ranged from 5800 to 7800 m^2/day. The calculated hydraulic conductivity ranged from 150 to 220 m/day. The calculated storativity of the aquifer ranged from 0.19 to 0.22. Field tests indicated that there is inverse correlation between barometric pressure and water level in the monitoring wells, indicating a barometric efficiency of approximately 60%. Despite 50 hours of injection test, there were small water table rises from well recharge. Water table rises decreased with increasing distance from the vadose-zone wells, ranging from 1 to 4 cm. Small water-table rises likely are due to the high hydraulic conductivity of the aquifer, vertical heterogeneity, screen location of the monitor wells, or some combination of these factors. Eight soil samples were collected from the site, and for some samples their saturated hydraulic conductivities (K_{sat}) and wetting/draining curves were determined using falling head permeability test, METER Hyprop, and hanging water-column method. An axisymmetric model was developed using VS2DTI software. The simulations were run with a

range of K_{sat} and porosity (n) values. The results of the simulations show that head changes at the nearest monitor well will occur faster and be smaller with a greater ratio of K_{sat}/n and vice versa. In addition, 3D numerical variably-saturated model was developed using HYDRUS-3D software. This model simulated the injection of water from four vadose-zone wells in an alluvial aquifer. Simulated pressure head differences in five observation nodes that are located 0.17 m below the water table showed that the observation node that is below the vadose-zone well had the largest water level increase and the observation node that is furthest from the vadose-zone well had the smallest water level increase, ranging from 0.6 to 2 cm. Different water-table responses between the final field test and model simulations are likely due to the differences in the amount of water injected into the system and the positions of the monitor wells. A total of 272 m^3/day of water was injected during the field test whereas only 88 m^3/day of water was injected during the HYDRUS simulation, and the field monitor wells were screened deeper than the depths of the observation nodes in HYDRUS. This research provides understanding of the hydraulic properties controlling vadose-zone wells and operation of the artificial recharge system. As most alluvial aquifers have similar geological settings as the Delta, results are expected to be relevant to other areas.

DEDICATION

Dedicated to my mother and father for their countless support and unconditional love

ACKNOWLEDGEMENTS

I would like to thank Dr. J.R. Rigby and Wesley Bolton from USDA-ARS National Sedimentation Laboratory for their technical support, hard work, and collaboration. I would like to thank Mississippi Department of Environmental Quality for funding, drilling wells, and installation of pump and instrumentation. I would like to thank Dr. Robert Holt for his service on my thesis committee and his helps on developing 2D/3D numerical models.

Lastly, I would like to thank my advisor, Dr. Andrew O'Reilly. He served as an outstanding mentor, advisor, and teacher and I cannot thank him enough for his patience, kindness, hard work, and guidance to the field of hydrology. This research would not have been possible without his numerous support. It was an absolute pleasure working with him.

TABLE OF CONTENTS

LIST OF TABLES

LIST OF FIGURES

INTRODUCTION

Significant demands for irrigation water in the Delta region of Mississippi have resulted in heavy depletion of groundwater in the aquifer to the extent of unsustainability of groundwater resources (Brandon, 2015). To augment natural recharge, infiltration basins are commonly used for artificially recharging aquifers (Bouwer, 2002). However, most alluvial aquifers, including the Mississippi River Valley alluvial aquifer (MRVAA), have capping layers of fine soils that significantly reduce the infiltration of water to the subsurface (Pyne, 1995).

Therefore, it is a better idea to use vadose-zone recharge wells, instead of infiltration basins, since they are not limited by the surficial layer of fine soils that impedes infiltration. Instead, the wells are drilled through the capping layer and screened in the unsaturated (vadose) zone of the aquifer (Bouwer, 2002). Recent research based on a series of numerical simulations reported that the simulation results reveal the significant advantages of using small-diameter, shallow vadose-zone wells compared to surface infiltration basins, demonstrating possible flow rates of 76 gallons per minute (gpm) ($414 m^3$/day) (Handel et al., 2014).

The purposes of this study are to perform full-scale field tests of vadose-zone wells in order to i)determine properties controlling well hydraulics such as saturated hydraulic conductivities, flow rate, groundwater storage, and unsaturated hydraulic properties of the aquifer and ii) assess feasibility of the use of vadose-zone wells for artificial recharge of the MRVAA.

To address these project objectives, a combination of field, laboratory, and numerical

modeling methods were applied. Two initial field tests were conducted for planning the final aquifer recharge test. Final field test was conducted consisting of eight hours of pumping the nearby production well (only to an adjacent pond) and followed by 50 hours of injection into four vadose-zone wells. Eight soil samples were collected from the site and their saturated hydraulic conductivities (K_{sat}), wetting/draining curves, and unsaturated hydraulic properties of the soil samples were determined using falling head permeability test, METER Hyprop, and hanging water-column method. An axisymmetric model was developed using VS2DTi software from the U.S. Geological Survey (USGS). Simulations were run with a range of K_{sat} and porosity (n) values in order to estimate potential water-table response to these parameters. Finally, a three-dimensional (3D) numerical variably-saturated flow model was developed using HYDRUS-3D software to simulate the injection of water into four vadose-zone wells.

This research provides better understanding of the hydraulic properties controlling vadose-zone wells. In addition, the research assesses feasibility of operation of the artificial recharge system using small-diameter vadose-zone wells in the shallow alluvial aquifer in order to address drawdown problems in the Delta. As most alluvial aquifers have similar geological settings as the Delta, results are expected to be relevant to other areas.

I. BACKGROUND

Mississippi River Valley Alluvial Aquifer

The Mississippi River alluvial plain in Mississippi is locally called the “Delta”. The Delta is a lens-shaped area about 320 kilometers long. The MRVAA underlies about 650 square kilometers (km^2) of the region of Delta in most parts of the 19 counties in northwestern Mississippi. The MRVAA broadly underlies approximately 85,000 square kilometers located within Mississippi, Arkansas, and Louisiana, extending to small portions of Tennessee, Illinois, and Kentucky (Miller, 1994; Maupin and Barber, 2005) (Fig. 1).

The alluvial aquifer consists of unconsolidated alluvium and terrace deposits of Quaternary age (Ackerman, 1996). The MRVAA predominately consists of two hydrogeologic units: an upper surficial confining layer of clay, silt, and fine sand and a lower coarse sand and gravel aquifer (Ackerman, 1996; Arthur, 1994) (Fig. 2). The aquifer grades from coarse sand or gravel at the bottom of the aquifer to fine-grained sand at the top. Lenses of clay, slit, or sandy silt occur at many places in the alluvial aquifer besides the confining layer at the surface (Ackerman, 1996). The upper confining layer has average thickness of between 6.1 – 9.1 meters in most areas, however, in some parts of Mississippi and Arkansas, the thickness of the upper confining layer unit can range from 18.3 to 30.5 meters locally (Ackerman, 1996).

Sources of recharge to the aquifer are: infiltration from land surface, leakage from adjacent rivers, streams, and lakes; and lateral interflow from sediments and aquifers of the Bluff Hills that lie along the eastern boundary of Delta (Barlow and Clark, 2011). Natural groundwater

recharge from infiltration is typically limited due to presence of the overlying clay and fine-grained soil in the upper part of the aquifer. A previous study has shown that only 5 percent (6.6 cm) of the average annual rainfall typically recharges the aquifer (Arthur, 2001). Main sources of recharge are leakage from the Mississippi River and lateral recharge from the Bluff Hills.

The Delta is a prime area for agriculture due to its fertile soils, a long growing season, heavy annual rainfall rate, and a productive alluvial aquifer. The MRVAA produces roughly 35 million cubic meters per day (m^3/day) of groundwater and the aquifer is the third most used aquifer in the U.S. (Maupin and Barber, 2005). Among the total withdrawals from the MRVAA, 98 percent of groundwater was used for irrigation purposes (Maupin and Barber, 2005) (Fig. 3).

However, many studies have reported that the groundwater resources of the aquifer are not sustainable, and better solutions are required to halt the declines of groundwater all across the Delta (Ackerman, 1996; Barlow and Clark, 2011; Konikow, 2013). Using annual water-level data, Yazoo Mississippi Delta Joint Water Management District (YMD) reported that the average drawdown in groundwater storage since 1987 resulted in a cumulative loss of groundwater of approximately 4.09 cubic kilometers (km^3) from 1987 to 2009 (Yazoo Mississippi Delta Joint Water Management District, 2010).

Artificial Recharge Methods

In order to mitigate groundwater drawdown problems, one approach is to store extra water during periods of low demand. Surface reservoirs have been widely used to store water, however, this approach is limited due to high evaporation rate of stored water, economic efficiency, potential of structural failure, and adverse environmental, ecological, and socio-cultural issues (Bouwer, 2002). Therefore, artificial recharge methods (managed aquifer

recharge) has been increasingly recognized as an alternative approach to address water problems (Lowry and Anderson, 2006). Artificial recharge methods are the systems of spreading or injecting water on/into the ground to increase recharge to the aquifer in order to augment groundwater resources (Bouwer, 2002). Artificial recharge systems are typically achieved using infiltration basins and trenches, abandoned quarries, large-diameter, high-capacity injection wells, and vadose-zone wells (dry wells).

An infiltration basin is one of the means of artificially recharging aquifers. The source water is spread on the ground and infiltrates into the ground and moves down to the groundwater (Bouwer, 2002). Surface infiltration methods are cost effective and most commonly used, however, they have a number of disadvantages compared to well-based methods (Minsley at al., 2011). The disadvantages include the following: greater land area requirement, loss of stored water due to evaporation, and vulnerability to contamination (Minsley at al., 2011). Moreover, a permeable surficial soil layer is required to obtain a high flux of recharged water for infiltration basin systems (Bouwer, 2002). This is the main disadvantage especially for alluvial aquifers such as MRVAA. Also, subsurface soil layers should not be contaminated by past or current activities since the water will infiltrate though the soil, potentially dissolve some contaminants, and directly recharge the groundwater with poor quality water.

Artificial recharge wells are another methods of artificially recharging aquifers. Artificial recharge wells can be classified into shallow vadose-zone wells and deep wells that are screened into the targeted aquifer under the groundwater table (Fig. 4). Recently, deep artificial recharge wells have broadly been used as an alternative to surface reservoirs and infiltration basins (Handel at al., 2014). However, they are often not cost-efficient since they require a lot of logistical and infrastructure support for operation and maintenance of the wells.

A recent paper presented the development of a new artificial recharge method for shallow, unconsolidated aquifers using small-diameter, low-cost vadose-zone wells installed with direct-push (DP) technology (Handel at al., 2014). DP technology uses hydraulic rams supplemented with vehicle weight and high-frequency percussion hammers to rapidly advance small-diameter tools. DP technology has been used for installing small-diameter vadose-zone wells in shallow, unconsolidated aquifers, and there were no significant performance differences between DP wells and wells installed with other drilling techniques in sandy aquifers (Kram et al., 2001; Parker et al., 2011). The main advantages of using the DP technique are its cost efficiency and lesser subsurface disturbance compared to conventional drilling techniques.

Smaller diameter vadose-zone wells typically are constructed similar to a conventional water well, while larger diameter wells may be filled with coarse sand or fine gravel. The well is screened over only part of the vadose-zone. Water is injected directly into the vadose zone of the aquifer and the water naturally moves down to the water table predominantly by gravity. The main advantage of a vadose-zone well is that it is not limited by any surficial fine-grained layers (Bouwer, 2002).

Handel et al. (2014) performed a series of numerical simulations using HYDRUS-2D and reported that the simulation results reveal the significant advantages of using small-diameter, shallow wells installed by using DP technology over surface infiltration basins. They show that one shallow vadose-zone well was able to recharge a good amount of water into the vadose zone, noting that the asymptotic recharge rate of an infiltration basin 10m by 6m in surface area is equivalent to that of 5 cm small-diameter vadose-zone wells. The general applicability of the small-diameter DP wells has been also shown by numerical modeling and field experiments in Austria, Germany, and USA (Handel et al., 2016; Liu et al., 2012). These experimental and

numerical assessment results clearly indicate that the small-diameter DP wells have great potential for use in shallow unconsolidated aquifers. Therefore, it might be feasible to use small-diameter wells to address groundwater drawdown problems in the Delta.

II. METHODS

Field Site

The field site of this study is located in LeFlore County, Mississippi, between Minter City and Ruleville approximately 1 km north of Highway 8 (Figs. 5 and 6). The property lies along Dugand Bayou and a small pond. The geologic setting of the field site is similar to that of typical MRVAA setting. The field site generally consists of 3 layers: upper clayey layer with depth of approximately 10 m from surface, mid sand layer with depth from 10 to 27.4 m, and lower gravel layer with depth from 27.4 to 42.7 m. Due to the thick clay layer near the surface, it is almost impossible to enter this area during wet seasons or after heavy rainfall. The area become flooded at times, so that it was impossible to conduct the final field test until May 2019.

According to a driller's log from a well at the site, the aquifer is more heterogeneous, consisting of the following lithology: clay from ground level to 9.8m, coarse sand from 9.8 m to 11.9 m, sand and pea gravel from 11.9 m to 17.7 m, large gravel from 17.7 m to 18.3 m, coarse sand from 18.3 m to 20.7 m, sand and gravel from 20.7 m to 29.0 m, and large gravel from 29.0 m to 39.6 m (Appendix A). The YMD survey well A053 is the closest known well with historical water-level measurements. The water table at the well has been recorded since 1976 and the depth to water table in 2016 was approximately 15 m with a strong downward trend. The water table varies by about 60 cm between spring and fall measurements (Rigby, 2015).

Wells

Ten 10-cmdiameter wells, consisting of four vadose-zone recharge wells and six monitoring wells, and one supply well were installed in the field site using the mud rotary technique by the Mississippi Department of Environmental Quality (MDEQ) (Fig. 7). The vadose-zone wells are screened over depths of approximately 8.6 to 13.15 m (top part of sand layer) (Rigby, 2015) (Fig. 8). The monitoring wells are screened over depths ranging from 22.25 to28.34 m and from 24.38 to 30.48 m (Table 1). Pressure transducer and specific conductance sensors are installed in each monitoring well and in two of the four vadose-zone wells (V-1 and V-2), and water level, temperature, and specific conductance were recorded at 15-minute intervals initially and at 1-minute intervals for the final test. However, during the final field test, transducers in M1, M3, and M6 were not functioning, so the water levels were measured manually using an electric groundwater-level measurement tape every hour for M1, M3, and M6 and every two hours for the other wells.

The production well (supply well) was planned to be installed far from the vadose-zone and monitoring wells so that the water table at these wells would not be affected by a cone of depression. However, the well was installed nearby the vadose-zone and monitoring wells close enough to affect the groundwater table during pumping. The pumping well is screened deeper than the vadose-zone wells, at the depth of 19.81 to 28.96 m. A portable generator was used to run the pump to withdraw water from the production well (Fig. 9).

Groundwater from the supply well is directly injected into the recharge wells through PVC pipes at the surface, and four flow meters are installed on the pipes to measure flow rates into the vadose-zone wells (pitot-tube pressure flowmeter, model F-300 from Blue-White Industries). Vadose-zone wells are intended to inject surface water, thereby augmenting recharge

to the aquifer, which requires treatment of water before injection in order to mitigate potential water-quality impacts. Therefore, groundwater is being used to conduct the vadose-zone well tests in order to avoid an unregulated injection of surface water. The water is injected through a smaller diameter PVC pipe that extends to the bottom of the vadose well.

Field Pumping Test

Three preliminary field tests were conducted on August 10, 2018, August 27, 2018, and October 22, 2018. These tests were for planning the larger final pumping test. Initially, the pump was run and the water discharged to the adjacent pond for two hours in order to obtain sustainable pumping flow rate. Then, one of the vadose-zone wells was run for another 5 hours. In addition, the water level in the vadose-zone and observation wells were measured hourly using an electric water-level meter and at 15-minute intervals by the transducers. Transmissivity and storativity were determined by using the drawdown data and the Cooper and Jacob method (Cooper and Jacob, 1946).

On March 28, 2019, an 8-hour test was conducted in order to estimate the effect of pumping on the water table at each monitoring well. Groundwater was pumped from the production well and discharged only to the pond for 8 hours. The water table was monitored by transducers in the observation wells every one minute and by using the electric water-level meter every hour manually. Also, the flow rate of pump discharge to the pond was measured using a 5-gallon bucket and a stopwatch. After the pumping test, transmissivity and storativity were determined by using the drawdown data and the Cooper and Jacob method.

The final field test was conducted from May 28 to 31, 2019. Initially, to obtain a sustainable pumping flow rate, the pump was turned on and water discharged only to the nearby

pond at 8:00 PM, May 28th and kept running over night (approximately 8.5 hours of pumping only to the pond). On May 29th, pumping stopped at about 5:30 AM due to lack of gasoline in the portable generator. Pumping only to the pond was restarted at 7:40 AM and the valves to all four vadose-zone wells were opened at 9:46 AM on May 29th (the valve to the pond was closed after 10 minutes). Due to multiple overflows in the vadose-zone wells, the valve to the pond was slightly opened to inject less water into the vadose-zone wells. The injection test was conducted for approximately 50 hours and the test was finished at 12:15 PM, May 31st. The water table was monitored by transducers in the observation wells every one minute. Also, the water table was measured using the water-level meter every hour manually for the wells that did not have transducer data and every two hours manually for the wells that did have operating transducers. Flow rate of pump discharge to the pond was measured periodically using a 5-gallon bucket and a stopwatch.

Sample Collection

Eight soil samples were collected from the field site on May 24, 2018. The first soil sample was collected using a Hyprop sample ring (8 cm diameter and 5 cm high) (Fig. 10) and the other seven soil samples were collected using SoilMoisture Equipment Corporation sample rings (5.38 cm inner diameter and 6 cm high) (Fig. 11). A 10-cm diameter auger from SoilMoisture Equipment Corporation (Fig. 12) was used to hand auger the borehole. At a location approximately 2 m south of V1, cores were taken at depths of 0.27, 0.48, 0.94, 1.43, 1.67, 2.13, 2.59, and 3.01 m.

Laboratory Measurements

Falling Head Permeability Test

Saturated hydraulic conductivities were determined by using falling head permeability tests. The tests were conducted using a 2816G1 Chameleon Station from SoilMoisture Equipment Corporation. The reservoir cylinder is filled with water and attached by a flexible plastic tube to the Tempe cell that holds the soil core. The soil core is capped by the Tempe cell and a filter that retains the soil sediments and allows for water to flow upward from the base to exit the top of the core and overflow through an open tube. Also, a pressure transducer is attached to the port of the reservoir cylinder (Fig. 13). This transducer monitors pressure head and sends the data to the computer automatically. The software provided with the instrumentation calculates the saturated hydraulic conductivity of the soil sample automatically.

Sample A-8(3.01 m depth) and sample A-3 (0.94 m depth) were tested in order to measure representative saturated hydraulic conductivity values of the clay layer at the field site. Due to the thickness of the clay layer at the field site, a sample of sand from the vadose-zone could not be collected by hand auger. Therefore, for a representative saturated hydraulic conductivity of the sand layer, sample SL-1-11 collected near Sky Lake, northwest of Belzoni, Mississippi was tested. In 2016, Jenkins (2017) and Moore (2017) collected sample SL-1-11 consisting of a bagged sample and a core sample, and performed a grain-size analysis, which indicated 98.3% passed #18 sieve, 50.4% passed #60 sieve, and 7.1% passed #200 sieve. With less than 10% silt- and clay-sized particles, this sample is a sand according to the U.S. Department of Agriculture (USDA) textural classification.

METER Hyprop Device

Hyprop is an automated measuring and evaluation system to determine unsaturated hydraulic properties of a soil sample (draining curve) (Fig. 14). The two tensiometer shafts at different levels in the device measure the water tensions at two levels. The soil sample is installed on the sensor unit and the two tensiometer shafts measure the water tensions with time as water in the initially saturated sample evaporates. Also, the scale records the weight of the sample to determine the weight of water evaporated for each time steps. After obtaining the draining curve of the sample, the Hyprop Fit software automatically fits the data points to determine unsaturated properties of the sample.

Due to different sizes of sample rings for the Hyprop device and the soil samples collected, a feasible adaptor for attaching the collected samples to the device was manufactured by Matt Lowe (Machine Shop Supervisor, School of Engineering, University of Mississippi) (Fig. 15). Since there are physical limitations to obtaining a draining curve for fine-grained clay soil samples by using the hanging water column method (clay samples require significant amount of negative pressures to drain the water out of the sample), the Hyprop device was used to test sample A-3 in order to determine the unsaturated hydraulic properties representative of the confining clay layer at the field site.

Hanging Water Column Method

The hanging water column method is designed to determine the wetting/draining curve of a soil sample. This method is performed in a system consisting of a Buchner funnel, burette, and connecting tubing, also referred to as a Haines apparatus. In the hanging water column method, a fully saturated soil sample is placed on the porous plate inside the Buchner funnel

using a silica flour slurry to ensure the sample is in hydraulic contact with water in the porous plate and with bulk water in the system (Fig. 16). The tubing from the funnel is connected to the burette where a specific water level is maintained upon hydraulic equilibrium of the system. Also, rubber stoppers and tubing are used to connect the burette back to the Buchner funnel where the sample is placed, in order to have a closed system throughout the funnel, porous plate, burette, and tubing. All connections are sealed with electrical tape to ensure no evaporation occurs from the system.

After obtaining equilibrium of the system with the burette water level positioned at the base of the soil sample, a defined negative pressure is applied to the saturated sample by lowering the burette, which results in drainage of moisture in the sample. Then, the displacement of increased water level in the burette is recorded to determine the amount of water drained per established negative pressure. This procedure is repeated, each time lowering the burette to a new level until the moisture content of the sample reaches residual moisture content of the soil sample (i.e. until there is no increased water level in the burette even with higher negative pressure). The moisture wetting curve can be obtained by reversing the procedure, starting with the residually saturated sample and incrementally raising the burette until it reaches equilibrium at each level. The porosity of the sample is calculated by comparing the mass of the fully saturated soil sample and the mass of fully dried soil sample after 24 hours of oven drying.

After obtaining both draining and wetting curve data, the van Genuchten (1980) model is applied to determine unsaturated hydraulic properties.

The formula of this model is:

$$S = \left[1 + \left(\alpha\psi\right)^{n}\right]^{(1/n)-1}$$

where, S is the saturation, ψ is the suction head (m), α is the scaling parameter inversely related

to the air-entry head and *n* is the slope parameter inversely related to the width of the pore-size distribution. The saturation, *S*, is calculated as:

$$S = \frac{\theta - \theta_r}{\theta_s - \theta_r}$$

where, θ is the volumetric moisture content, θ_r is the residual moisture content and θ_s is the saturated moisture content.

Moisture wetting and draining curves were determined for the only the sandy sample (SL-1-11) using this method, as stated before, since this method will not work for the fine-grained samples because it takes too long to reach equilibrium and requires very high negative pressures

.

Computer Simulations

2D Numerical Model using VS2DTi

In order to better understand the effects of various saturated/unsaturated hydraulic parameters on vadose-zone well hydraulics, a two-dimensional (2D) axisymmetric variably saturated model was developed using the VS2DTI software from USGS (Fig. 17) to predict vadose-zone well hydraulics. This model is constructed based on the function developed by Brooks and Corey (1964). This model consists of the following three layers: clayey layer (gray) with saturated hydraulic conductivity (K_{sat}) of 3.7×10^{-5}m/day and porosity (n) of 0.43, sand layer (green) with K_{sat} of 2.23 m/day and n of 0.28, and gravel layer (yellow) with K_{sat} of 2.15 m/day and n of 0.27. The clayey layer is at the depth from ground level (0 m) to 9.76 m, sand layer is at the depth from 9.76 m to 27.43 m, and the gravel layer is at the depth from 27.43 m to 42.67 m. This model assumes that the elevation of ground surface is the elevation-head datum, so that a

negative total head represents a water level that is below the ground surface. The initial water table is at the depth of 14.6 m below the ground surface.

The vadose-zone well is screened over depth of 9.11 to 12.19 m at the field site, however, we have excluded the screened section in the clay layer because flow into or out of the clay is negligible given the small K_{sat} and there was convergence failure while running the model if we included the screened clay part; the well is screened from 9.76 m to 12.20 m in our model. The value of 200 m^3/day was given for specified volumetric flow into the domain at the red line on the left side of the model as a boundary condition. For the following models, we have varied both K_{sat} and porosity and ran all combinations of K_{sat} and n as shown in Table 2. In addition, we varied Brooks& Corey parameters (h_b and λ) and ran all combinations of h_b and λ as shown in Table 2.

Since the model is axisymmetric and uses radial coordinates, it cannot simulate more than one recharging boundary condition (e.g. multiple vadose-zone wells). Also, the production well is very near the vadose-zone wells. Since withdrawal from the production well is not radially symmetric in relation to the vadose-zone well, the model also cannot simulate the drawdown effect. Thus, for this research, a 3D variably saturated numerical flow model is required to successfully simulate our field site situation.

3D Numerical Model using HYDRUS-3D

The HYDRUS-3D software is a finite element model for simulating three-dimensional movement of water in variably saturated media (Šimůnek et al. 2013). This program numerically

solves the Richards equation for saturated-unsaturated water flow (Sejna et al., 2011). Since the Richards equation is highly nonlinear, its numerical approximation requires much finer spatial and temporal discretization than saturated flow models in order to obtain accurate simulation results.

Using a domain size for the 3D model in HYDRUS-3D similar in lateral extent as the VS2DTi axisymmetric model required a very fine mesh size with a computationally prohibitive number of nodes. Therefore, in order to reduce the domain size and number of nodes, a domain with a lateral extent of 20 by 20 m and a vertical extent of 32.91m (extending from the bottom of the upper clayey layer to the bottom of the MRVAA) was developed for the 3D model (Fig. 18). The origin of the coordinate system is located at the center of the bottom surface of the model. The upper clay confining layer was omitted, because flow exchange between the clay and sand is negligible given the very large contrast in hydraulic conductivity. The targeted finite element size of the domain was 0.5 m; at points representing the vadose-zone wells, the mesh was refined up to a radius of 2 m with inner mesh size of 0.005 m (at the well) and outer mesh size of 0.05 m (at the 2-m radial distance). The total number of finite element mesh nodes was 234,025 (Figures 19 and 20). The model consists of a sand layer with saturated hydraulic conductivity of 200 m/day, residual moisture content of 0.09, and porosity of 0.34. The model is based on the van Genuchten (1980) model. The model parameters are: α of 4.54 m^{-1} and n of 2.98.

An equilibrium initial condition was specified with a water table at the depth of 4.84 m from the top boundary of the model with a linear distribution of pressure head with depth. The horizontal boundary conditions were specified as constant head at all four lateral boundaries with the same pressure head distribution as the initial condition. No-flow boundaries were specified at

the upper and lower surfaces of the model, corresponding to the bottom of the upper clay confining unit (top of the MRVAA) and the top of the lower confining unit (bottom of the MRVAA), respectively.

Explicitly representing the physical dimension of each vadose-zone well with a diameter of 0.01 m was unnecessary given the project objectives of assessing well impact at a much larger scale of 1 m or more. Therefore, nodal recharge of 22 cubic meter per day (m^3/d) was specified at the nodes corresponding to the position approximately at the mid-point of the screened section of the vadose-zone wells (Fig. 21). Four nodes were specified as nodal recharge to simulate the vadose-zone wells. The production well was omitted because field monitoring indicated an approximately constant drawdown was reached after only 2 hours of pumping, which also allowed reduction of the domain size of the model. The four nodal recharge points were applied to locations [x,y,z coordinates: (0,-5,31.635), (6,2,31.635), (0,6.1,31.635), and (-6,2,31.635)]. The observation points were applied to locations [x,y,z coordinates: N6 (0,0,27.9), N5 (1.5,0.5,27.9), N4 (3,1,27.9), N3 (4.5,1.5,27.9) and N2 (6,2,27.9)] to observe water level response over distance from a vadose-zone well and an observation well (0,0,13.26) representing monitoring well M2. The straight-line distances between the observation points and the vadose zone well are: N6: 6.32 m, N5: 4.74 m, N4: 3.16 m, N3: 1.58 m, and N2: 0.00m. The model was run for 1 day, giving a total volume 88 m^3 of water injected into the domain.

III. RESULTS AND DISCUSSION

Field Pumping Tests

Field tests indicated that each of the two initially tested vadose-zone wells (V1 and V2) could intake 100 to 170 m^3/day by gravity flow. Transducer data and electric water-level meter data collected on October 22, 2018 show that drawdowns ranged from 2 to 5 cm in the observation wells after pumping 5 hours (Fig. 22). We interpreted that the drawdowns are due to pumping effect of the source well since the source well is adjacent to the observation wells. Since there was no increase in the water table, it was concluded that a longer pumping test was required for the final test. The transmissivity was calculated as 7800 m^2/day. Given the thickness of the aquifer as 39.62 m, the hydraulic conductivity is calculated as 220 m/day which is in the range of typical coarse sand. The calculated storativity of the aquifer was 0.22 which is in the range of typical unconfined aquifer (0.1 – 0.3) (Appendix B).

On March 28, 2019, an 8-hour pumping test was conducted in order to further estimate the effect of pumping on the water table. Groundwater was pumped from the production well and discharged only to the pond for 8 hours, starting at 9:00 AM and stopping 5:00 PM. Transducer data and electric water-level meter data collected during the test show that drawdowns approximately ranged from 2 to 5 cm in the observation wells after pumping 3 hours (Fig. 23).

After 3 hours of pumping, groundwater level actually started to increase and seemingly reached equilibrium at the end of the pumping test. The water-level fluctuations are interpreted

as due to change in barometric pressure. As barometric pressure increased, water level in the well decreased. This inverse correlation in water level and barometer pressure is clearly shown in Figure 23. The transmissivity was calculated as 5800 m^2/day. Given the thickness of the aquifer as 39.624 m, the hydraulic conductivity is calculated as 150 m/day which is in the range of typical coarse sand. The calculated storativity of the aquifer was 0.19 which is in the range of typical unconfined aquifer (0.1 – 0.3).

The final field test was conducted from May 28 to 31, 2019. Transducer data and electric water-level meter data collected show that drawdowns approximately ranged from 6 to 8 cm in the observation wells after pumping of 8.5 hours (Figs. 24 and 25). Transmissivity was calculated as 5700 m^2/day. Given the thickness of the aquifer as 39.62 m, the hydraulic conductivity is calculated as 140 m/day which is in the range of typical coarse sand. The calculated storativity of the aquifer was 0.03 which was much smaller than other tests. This result is due to larger drawdowns during this test. Comparison of the transducer data with the manual tape downs from the electric water-level meter (after applying the appropriate correction factors in Table 1) shows close agreement, indicating that the transducers were providing accurate measurements (Appendix C).

As observed in the pumping test on March 28, 2019, the barometric pressure effects on groundwater levels were also observed in the final test. Figure 26 presents a hydrograph showing this inverse correlation between barometric pressure and water-level. The data was collected for approximately 14 days including 3 days of final test data at the end. The graph is showing there were clear barometric effects on the water table levels, with a magnitude half that of the drawdown from pumping. Comparison of the transducer data with the manual tape downs from

the electric water-level meter (after applying the appropriate correction factors in Table 1) shows close agreement, indicating that the transducers were providing accurate measurements. Also, the flow rate into the vadose zone data from field site indicate that the flow rates taken by vadose-zone wells are generally decreasing over time (Fig 27).

In order to calculate the barometer pressure effects on the water tables during final field test, the correlation between the barometer pressure head and the water table pressures for M2, M4, and M5 were plotted (Appendix D). The barometric efficiency was calculated as 60%, where the slope of the line for the plots represents the barometric efficiency. The barometric efficiency corrected water table data was plotted (Fig. 28). This data show that a slight increase in water levels occurs after injection starts, with the largest increase at M2 (about 4 cm), less at M4 (about 2 cm), and the least at M5 (about 1 cm). Water levels increase quickly at first and then slowly after that, and don't start decreasing until the regional pumping effects from irrigation start the evening of May 30.

Despite approximately 50 hours of injection of water to the vadose-zone wells, small water table rises from well recharge were observed. The water table rises ranged from 1 cm for the well far from vadose zone wells (M5) to 4 cm for the well nearest vadose zone wells (M2). This is much less than what might be estimated by a simple mass balance. Theoretically, given approximately 272m^3/day (49.9 gpm) of injection for 50 hours and porosity of 0.35, this volume of water would give approximately 40 cm rise (1.3 ft) in the water table over an area of about 4,050 m^2 (1 acre).

This result is likely due to high hydraulic conductivity, vertical heterogeneity in hydraulic properties, well placement, or some combination of these factors. High hydraulic

conductivity of the aquifer may allow rapid transport of infiltrated water laterally with little hydraulic gradient, resulting in little mounding of the water table. In the vadose-zone, thin lenses of sediments with lower or higher hydraulic conductivity potentially could intercept infiltrating water spreading it laterally over a larger area. Lateral and vertical locations of the monitoring wells relative to hydraulic property variations also may affect observed water levels. The monitoring wells are all screened in the lower coarse sand and sand and gravel layers of the aquifer, whereas, the water table is located in the upper sand and pea gravel layer. The top of the shallowest monitoring well screen is approximately 10 m below the water table. As a result, the pressure increase from the rise in the water table due to injection of water possibly is substantially dissipated as it moves downward to the depth of the monitoring wells, which results in smaller rises in the water-level data in the monitoring wells. This issue can be addressed for future research by placing monitoring wells closer to the vadose-zone wells or screening the monitoring wells at shallower depths or across the water table.

Laboratory Measurements

From the falling-head permeability test, sample A-3 from depth of 0.94 m had saturated hydraulic conductivity of 2.18×10^{-3} m/day which is in the reasonable range of hydraulic conductivity for fine-grained clay samples. Sample A-8 from depth of 3.01 m had saturated hydraulic conductivity of 0.02 m/day, which is in the reasonable range of hydraulic conductivities for silt and clay samples. Sample SL-1-11 had saturated hydraulic conductivity as 7.97 m/day, which is in the reasonable range of hydraulic conductivities for sand samples (Appendix E).

Sample A -3 was tested using METER Hyprop device to determine unsaturated hydraulic properties. Since the sample is fine-grained clay sample, it takes a lot of time to obtain data. According to the tension and weight graphs from the Hyprop test, the pressure in both tensiometers started to increase 3 days after the test started and decreased slowly for another 3 days (Appendix F). According to the volumetric water content versus tension head graph (θ(pF)) and hydraulic conductivity versus tension head graph (K(pF)), the K(pF) data generally had the right shape, however, the θ(pF) graph was incorrect due to physically unrealistic data (Fig. 29). This error in θ graph is likely due to using a different sample ring size than the standard Hyprop ring. In contrast, the Ksat of 0.2 cm/day from falling head test is close to 0.1 cm/day from k(pF) curve at pF = 0, likely because Hyprop calculates K from tension-head difference and flux from weight change. Therefore, it appears that only θ data was influenced by the different soil sample ring size. Further analysis of the data is required to obtain reliable data for the sample, which would involve calculations outside of the Hyprop Fit software.

Sample SL-1-11 was tested using the hanging water column method to determine unsaturated hydraulic properties. Both draining curve and wetting curve data for the sample were plotted (Fig. 30), and the van Genuchten model was applied to each dataset (Fig. 31). Based on the curve fitting method using the root-mean-square error and the Excel Solver Add-in, the parameters are calculated as $\theta_r = 0.097;\ \theta_s = 0.34;\ \alpha = 2.99\frac{1}{m};\ n = 7.082$ from draining curve fitting, and $\theta_r = 0.092;\ \theta_s = 0.335;\ \alpha = 4.54\frac{1}{m};\ n = 3.91$ from wetting curve.After 24 hours of oven drying, the porosity of the sample was calculated as 0.33 (Appendix G).

Computer Simulations

2D Numerical Model using VS2DTi

Figures 32-40 depict color-shaded simulated saturation after 1 day of injection with varying combinations of hydraulic conductivity and porosity. These results show that the groundwater mound was higher in vertical extent and smaller in horizontal extent for lower K_{sat} or higher porosity, whereas the mound was lower in vertical extent but larger in horizontal extent for higher K_{sat} or lower porosity after same period of time. The different heights of groundwater mounds for different K_{sat} values and porosity are due to an increase/decrease in K_{sat} that makes it easy/difficult for water to flow, whereas, given the same K_{sat} value, an increase/decrease in porosity provides more/less volume for water to be stored given the same volume of water injected into the system for each cases.

Figure 41 depicts hydrographs of simulated total head versus time at the observation point with varying hydraulic conductivity and porosity. The hydrograph indicates that the greater the ratio of K_{sat}/n, the more quickly the system reaches equilibrium. The total head changes are smaller, but propagate over a longer distance given the same amount of water injected into the system, because a larger K_{sat} or lower porosity makes it easier/faster for water to flow through the system and less likely for water to be stored in the aquifer and propagate further horizontally. In contrast, the smaller the ratio of K_{sat}/n, the more slowly the system reaches equilibrium. The head changes are larger, but propagate over a shorter distance, because a smaller K_{sat} or higher porosity makes it harder/slower for water to flow and more likely for water to be stored in the aquifer and not propagate horizontally. These results are expected given that K_{sat}/n represents the hydraulic diffusivity of the zone around the vadose zone well that is saturated or nearly saturated.

Figure 42 depicts a hydrograph showing vertical total head profile with depth. For a lower hydraulic conductivity value, there was a large increase of total head where the total head exceeds zero while for the higher hydraulic conductivity total heads stayed under zero. This indicates that there is a large vertical head gradient with smaller K_{sat}, because water is more likely to be stored building a groundwater mound in higher vertical extent and smaller in horizontal extent. Since the MRVAA consists of coarse-grained sediment, gravity force dominates over capillary forces in the vadose-zone. Therefore, water being pumped into the vadose-zone well is flowing out the well and moving predominantly downward by gravity, because the top of the well is open and there is a free-water surface in the well. It is due to the above stated reasons that these simulations indicate water tends to build up a higher pressure around the vadose-well where the low K_{sat} makes it harder for water to flow further horizontally and the upper clayey layer acts like a confining layer. This indicates that simulated total head will rise unrealistically if water is injected into the system more than the aquifer can transmit and store in this model.

Lastly, Figure 43 depicts a hydrograph of total head versus time with varying Brooks – Corey parameters (h_b and λ). The graph indicates that the effects of h_b and λ on total head was smaller compared to that of hydraulic conductivity and porosity, because the impact of the injected water on the total head was primarily due to saturated flow where h_b and λ are parameters controlling unsaturated flow.

3D Numerical Model using HYDRUS-3D

Figure 44 – 47 depict vertical views of pressure head distribution at 0, 0.1, 0.4, and 1 day. The model simulated injection of water from nodal recharge over time; however, no apparent rise in water table was observed. Figure 48 – 51 depict horizontal views of pressure head distribution 0.75 m below the water table at 0, 0.1, 0.4, and 1 day. The size of the plume of the injected water is increasing over time. Figure 52 depicts the cumulative constant flux to four lateral boundaries, showing the system was approaching steady state by 0.4 days.

Figure 53 and 54 depict the pressure head changes in six observation nodes (one monitoring node and five observation points). There was no response in pressure head in the monitoring well. This result is likely due to the greater depth of the monitor well (approximately 10 m below the water table) compared to the observation points that are much shallower, which is also one possible explanation why there was only a small response in the monitor wells during the final field test. Pressure head differences in five observation nodes 0.17 m below the water table showed that N2 (6,2,27.9) which is below the vadose-zone well (6,2,31.635) had largest water level increase of 2 cm and N6 (0,0,27.9) which is furthest from the vadose-zone well had smallest water level increase of 0.6 cm.

Based on the water-balance output file from the model, the absolute water balance error was 87.3 m^3 and the relative water balance error was 53.52 percent. However, these high water balance errors are likely due to programmatic setting of the HYDRUS software. It appears that the nodal fluxes are not included in the equation that calculates water-balance error in the software. Therefore, given total nodal recharge of 88 m^3, the new calculated absolute water-balance error is 0.7 m^3 and the revised relative water-balance error is only 0.8 percent of total

nodal recharge, which confirms proper numerical solution of the Richards equation and the reliability of the model results (Appendix G). When using smaller values for nodal recharge, the same error in the HYDRUS water-balance output was found.

IV. SUMMARY AND CONCLUSIONS

The purposes of this study were to perform full-scale field tests of vadose-zone wells and numerical simulations in order to i) determine properties controlling well hydraulics such as saturated hydraulic conductivities and unsaturated hydraulic properties, flow rate, and groundwater storage, and ii) assess feasibility of vadose-zone wells for artificial recharge of the MRVAA.

Two initial field tests indicated each of two vadose-zone wells could intake 100 to 170 m^3/day by gravity flow. Transducer data and electric water-level meter data collected on October 22, 2018 show that drawdowns ranged from 2 to 5 cm in the observation wells after pumping five hours. The transmissivity was calculated as 7800 m^2/day. The hydraulic conductivity is calculated as 220 m/day. The calculated storativity of the aquifer was 0.22. On March 28, 2019, an 8-hour pumping test was conducted in order to further estimate the effect of pumping on the water table. The transmissivity was calculated as 5800 m^2/day. The hydraulic conductivity is calculated as 150 m/day. The calculated storativity of the aquifer was 0.19.

The final field test results indicate that there is an apparent inverse correlation between barometric pressure and water levels in the monitoring wells. The barometric efficiency was calculated as 60%. Despite approximately 50 hours of injection of water to the vadose-zone wells, small water table rises from well recharge were observed. The water table rises ranged from 1 cm for the well far from vadose zone wells (M5) to 4 cm for the well nearest vadose zone

wells (M2). This result is likely due to vertical heterogeneity and high hydraulic conductivity of the aquifer. High hydraulic conductivity would minimize the formation of a water table mound, as a relatively large lateral water flux could be supported by a small hydraulic gradient. The screen location of the monitoring wells also may be a factor. The monitoring wells are all screened over the lower coarse sand/sand & gravel part of the aquifer, however, the water table is located in the upper sand & pea gravel layer. This issue can be addressed by placing monitoring well screens at a shallower depth or across the water table for future research.

From falling-head permeability test, Sample A-3, which represents the clay layer at the field site at a depth of 0.94 m had saturated hydraulic conductivity of 2.18×10^{-3} m/day. Sample A-8 from depth of 3.01 m had saturated hydraulic conductivity of 0.02 m/day. Sample SL-1-11, which represents sand layer in vadose zone, had saturated hydraulic conductivity of 7.97 m/day. Sample SL-1-11 was tested using hanging water column method to determine unsaturated hydraulic properties. Based on the curve fitting method, the parameters are calculated as $\theta_r = 0.097;\ \theta_s = 0.34;\ \alpha = 2.99\frac{1}{m},;\ n = 7.082$ from draining curve fitting, and $\theta_r = 0.092;\ \theta_s = 0.335;\ \alpha = 4.54\frac{1}{m};\ n = 3.91$ from wetting curve.

The results of the 2D axisymmetric numerical simulations using VS2DTi show that head changes at the nearest monitor well are likely to be smaller with a greater ratio of K_{sat}/n and vice versa, and the simulated total head will rise unrealistically if water is injected into the system at a rate more than an aquifer can transmit and store in this model. Also, it was indicated that the effects of h_b and λ on total head was smaller compared to that of hydraulic conductivity and porosity, since the impact of the injected water on the total head was primarily dominated by saturated flow where h_b and λ are parameters for unsaturated flow.

The results of the 3D numerical model using HYDRUS-3D show that it was able to simulate injection of water from nodal recharge over time. There was no response in pressure head in the monitoring well. This result is likely due to the same reason that caused no response in the final field test. However, pressure head differences in five observation nodes 0.17 m below the water table showed that N2 (6,2,27.9) which is below the vadose-zone well (6,2,31.635) had largest water level increase and N6 (0,0,27.9) which is furthest from the vadose-zone well had smallest water level increase.

The final pumping test result showed that the water table rises ranged from 1 cm for the well far from vadose zone wells (M5) to 4 cm for the well nearest vadose zone wells (M2). It took about 6 hours after start of injection to reach highest water rise in the monitoring wells. According to HYDRUS simulation results, the water table rises ranged from 0.6 cm for the observation point far from the vadose-zone well (N2) to 2 cm for the point nearest the vadose zone well (N6). Also, it took approximately 4 hours after start of injection to reach the highest water table rise at the observation points. These differences are likely due to the differences in the amount of water injected into the system and the positions of the monitor wells. A total of 272 m^3/day of water was injected during the field test whereas only 88 m^3/day of water was injected during the HYDRUS simulation, and the field monitor wells were screened deeper than the depths of the observation points in HYDRUS.

REFERENCES

Ackerman, D.J., 1996. Hydrology of the Mississippi River Valley alluvial aquifer, South-central United States. US Geol. Surv. Prof. Pap. D1–D46. https://doi.org/1416-D

Arthur, J.K., 2001. Hydrogeology, model description, and flow analysis of the Mississippi River alluvial aquifer in northwestern Mississippi: U.S. Geological Survey Water Resources Investigations Report, 2001-4035, 47 p.

Arthur, J.K., 1994. Thickness of the upper and lower confining units of the Mississippi River Alluvial Aquifer in northwestern Mississippi: U.S. Geological Survey Water Resources Investigation Report, 1994

Barlow, J.R.B., Clark, B.R., 2011. Simulation of water-use conservation scenarios for the Mississippi Delta using an existing regional groundwater flow model. U.S. Geol. Surv. Sci. Investig. Rep. 14. https://doi.org/10.1086/344999

Bouwer, H., 2002. Artificial recharge of groundwater: Hydrogeology and engineering. Hydrogeol. J. 10, 121–142. https://doi.org/10.1007/s10040-001-0182-4

Brandon, H, 2015. Declining aquifer an economic challenge for the Delta: Delta Farm Press, March 13, 2015 [http://deltafarmpress.com/management/declining-aquifer economic-challenge-delta]

Cooper, H.H. and C.E. Jacob, 1946. A generalized graphical method for evaluating formation constants and summarizing well field history, Am. Geophys. Union Trans., vol. 27, pp. 526-534.

Händel, F., Liu, G., Dietrich, P., Liedl, R., Butler, J.J. Jr., 2014. Numerical assessment of ASR recharge using small-diameter wells and surface basins, Journal of Hydrology, doi: http://dx.doi.org/10.1016/ j.jhydrol.2014.05.003

Händel, F., Liu, G., Fank, J., Friedl, F., Liedl, R., Dietrich, P., 2016. Assessment of small-diameter shallow wells for managed aquifer recharge at a site in southern Styria , Austria. https://doi.org/10.1007/s10040-016-1442-7

Jenkins, J.L., 2017. Assessment of vadose-zone wells for enhancing groundwater recharge in the Mississippi Delta [Honors College thesis]: University of Mississippi, 52 p., 3 electronic appendixes

Konikow, L.F., 2013. Groundwater depletion in the United States (1900−2008). U.S. Geological Survey Scientific Investigations Report 2013−5079, 75 p.16

Kram, M., Lorenzana, D., Michaelsen, J., Lory, E., 2001. Performance comparison: direct-push wells versus drilled wells. TR-2120-ENV, Naval Facilities Engineering Service Center.

Liu, G., Butler Jr., J.J., Reboulet, E., Knobbe, S., 2012. Hydraulic conductivity profiling with direct push methods. Grundwasser 17, no. 1: 19–29.

Lowry, C.S., Anderson, M.P., 2006. An assessment of aquifer storage recovery using ground water flow models. Ground Water 44, no. 5: 661–667.

Maupin, M.A., Barber, N.L., 2005. Estimated withdrawals from principal aquifers in the United States, 2000, US Geological Survey Circular 1279.

Miller, J.A., 1994. “Ground Water Atlas of the United States.” Appl. Hydrogeol. 2, 59–62. https://doi.org/10.1007/s10040-994-0003-7

Minsley, B.J., Ajo-Franklin, J., Mukhopadhyay, A., Morgan, F.D., 2011. Hydrogeophysical methods for analyzing aquifer storage and recovery systems. Ground Water 49, no. 2: 250–269.

Moore, T.G., 2017. Comparing field and laboratory measurements of hydraulic conductivity in the Mississippi Delta [Honors College thesis]: University of Mississippi, 87 p., 1 electronic appendix

Parker, L., McCall, W., Mulherin, N., Bigl, S., Williams, D., 2011. Comparison of hydraulic conductivity determinations in co-located conventional and direct-push monitoring wells. No. ERDC/CRREL-TR-11-6, Engineer Research and Development Center Hannover NhCold Regions Research and Engineering Lab.

Pyne, D.G., 1995, Groundwater recharge and wells: A guide to aquifer storage recovery, 375 p.

Rigby, J.R., 2015. Research Proposal: A small-scale pilot study to examine the use of vadose-zone recharge wells in the lower Mississippi River Alluvial Aquifer as a viable recharge

enhancement technology, MS Department of Environmental Quality, Office of Land and Water.

Šejna, M., Šimůnek, J., van Genuchten, M. Th., 2011. The Hydrus Software Package for Simulating the Two- and Three-Dimensional Movement of Water, Heat and Multiple Solutes in Variably Saturated Media. Hydrus User Manual, PC-Progress, Prague.

Šimůnek, J., D. Jacques, G. Langergraber, S. A. Bradford, miroslav-sejna M. Šejna, and M. Th. van Genuchten, 2013.Numerical modeling of contaminant transport with HYDRUS and its specialized modules, Invited paper for the Special Issue "Water Management in Changing Environment", Editor M. S. Mohan Kumar, Journal of the Indian Institute of Science, 93(2) 265-284, ISSN: 0970-4140 Coden-JIISAD.

vanGenuchten, M.T., 1980. A closed-form equation for predicting the hydraulic conductivity of unsaturated soils. Soil Sci. Soc. Am. J. 44: 892–898.

Yazoo Mississippi Delta Joint Water Management District, 2010. 2009 Annual work summary, accessed September 10, 2010, at http://www.ymd.org/pdfs/2009annualsummary.pdf.

APPENDIX

Table 1: Well construction information and correction factors to add to transducer measurements to adjust water-level data to elevation above mean sea level.

Well	Well Depth (m), below land surface	Screened Depth (m), below land surface	Well Casing (m), above land surface	Correction Factor (m)
Production Well	28.95	19.8 – 28.95		
Observation Wells				
M1	28.05	21.95 – 28.05	0.83	20.486
M2	30.52	24.42 – 30.52	0.71	20.530
M3	28.55	22.45 – 28.55	0.72	20.161
M4	28.53	22.43 – 28.53	0.73	20.451
M5	27.81	21.71 – 27.81	0.70	20.415
M6	27.38	21.28 – 27.38	0.78	20.333
Vadose-Zone Wells				
V1	12.53	9.05 – 12.53	0.69	
V2	12.08	8.6 – 12.08	0.60	
V3	12.35	8.87 – 12.35	0.67	
V4	13.15	9.67 – 13.15	0.53	

Table 2: Combination of saturated/unsaturated parameter tested in VS2DTi

	Combination of Parameters		
K_{sat} and n simulation high K = 22.3 m/day mid K = 2.23 m/day low K = 0.223 m/day high n = 0.4 mid n = 0.28 low n = 0.1	Low n & Low K	Low n &Mid K	Low n &High K
	Mid n & Low K	Mid n & Mid K	Mid n &High K
	High n & Low K	High n & Mid K	High n & High K
h_b and λ simulation high h_b = -1 m mid h_b = -0.53 low h_b = -2 m high λ = 5 mid λ = 2.25 low λ = 1	Low h_b & Low λ	Low h_b& Mid λ	Low h_b & High λ
	Mid h_b & Low λ	Mid h_b & Mid λ	Mid h_b & High λ
	High h_b & Low λ	High h_b & Mid λ	High h_b & High λ

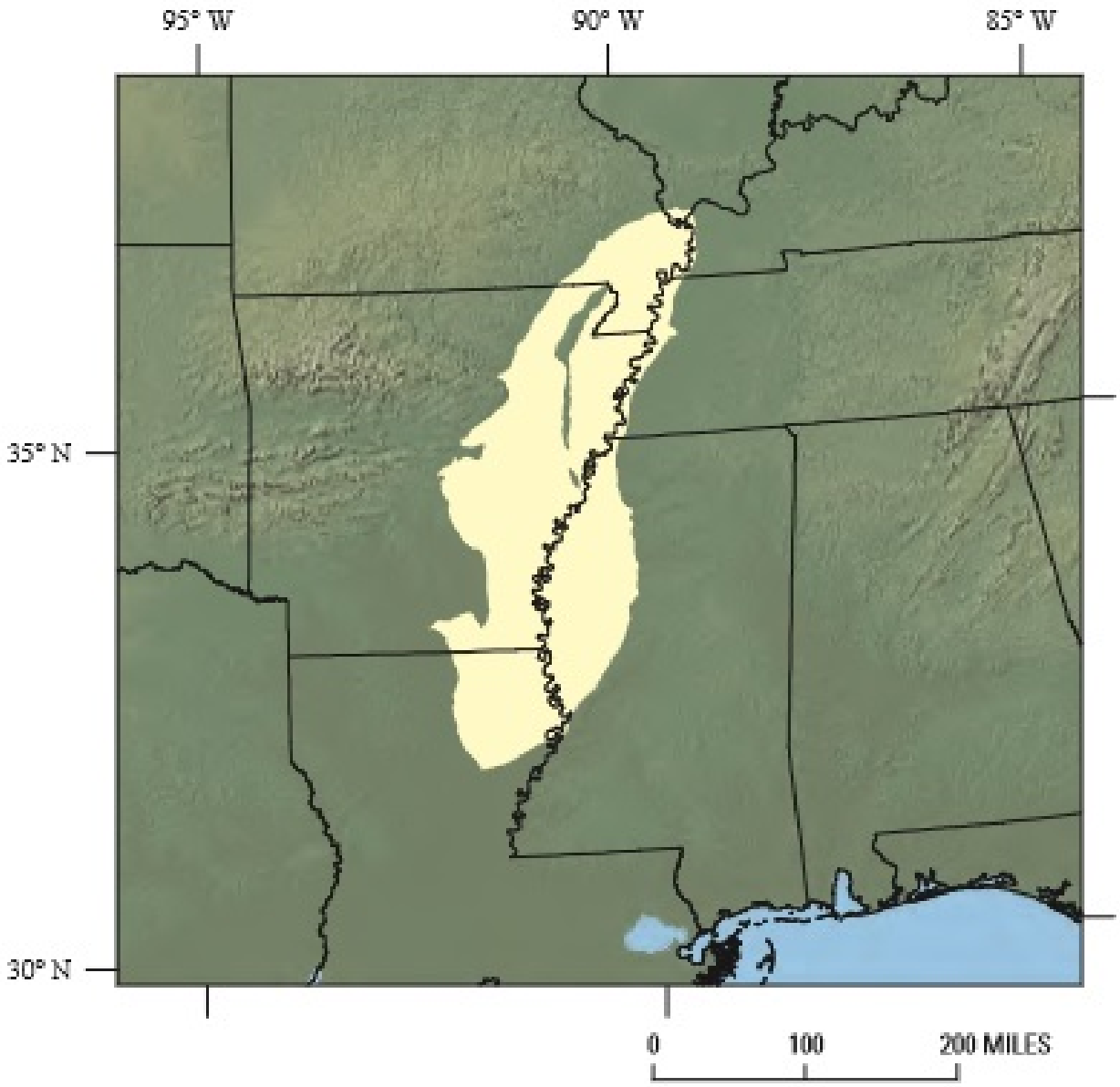

Figure 1: Location of the MRVAA (Maupin and Barber, 2005)

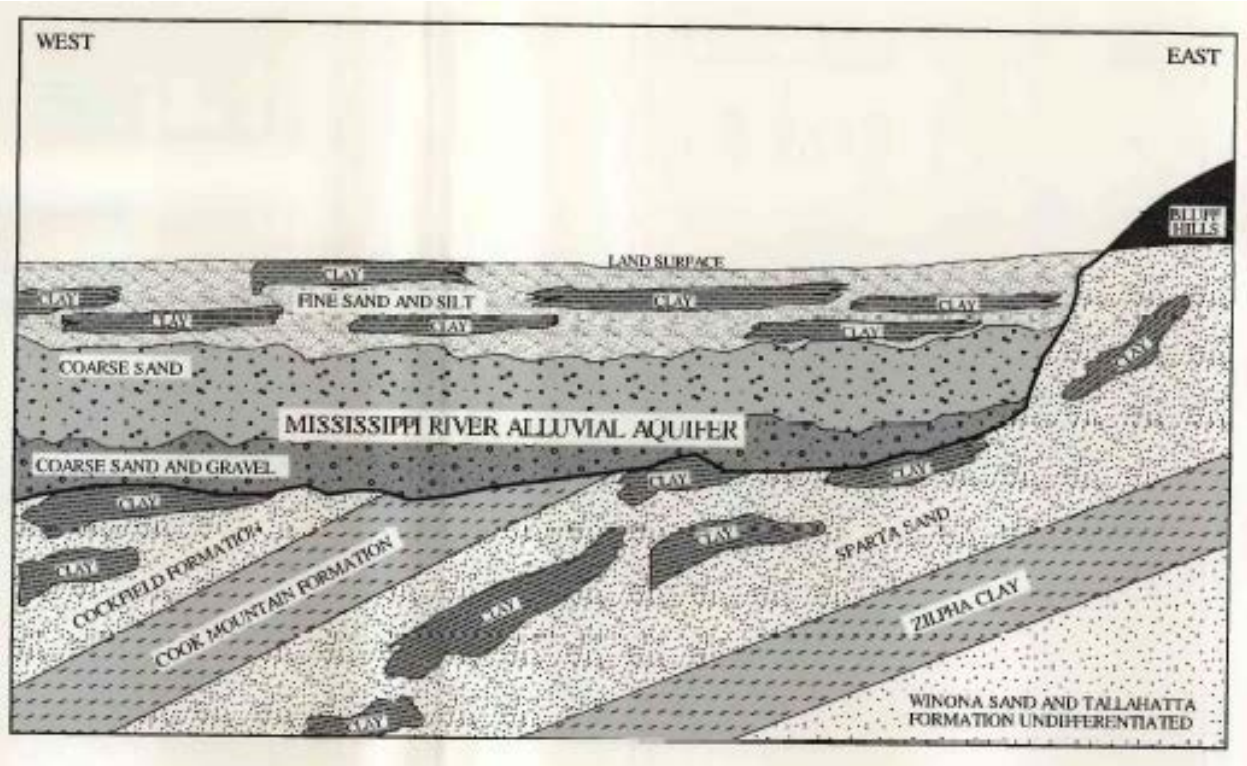

Figure 2: A cross-section view of generalized geologic setting of the MRVAA (Arthur, 1994)

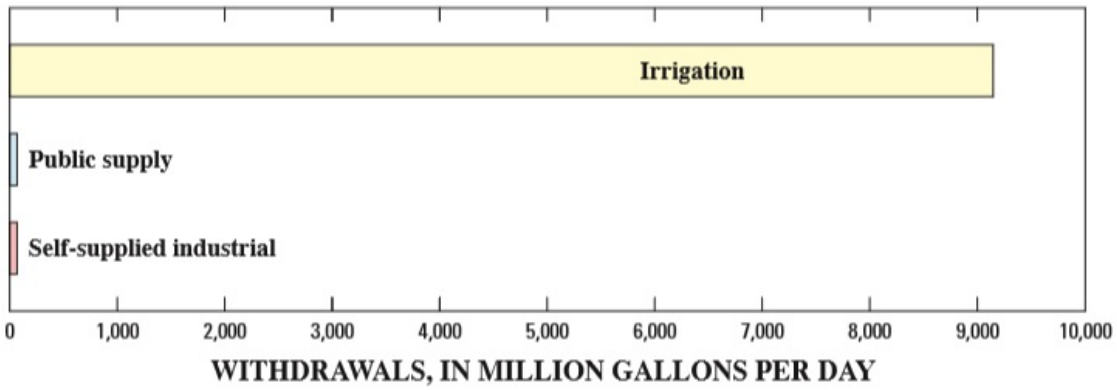

Figure 3: A graph showing percentages of use of groundwater from the MRVAA. More than 98 percent of groundwater from MRVAA was used for irrigation purposes (Maupin and Barber, 2005)

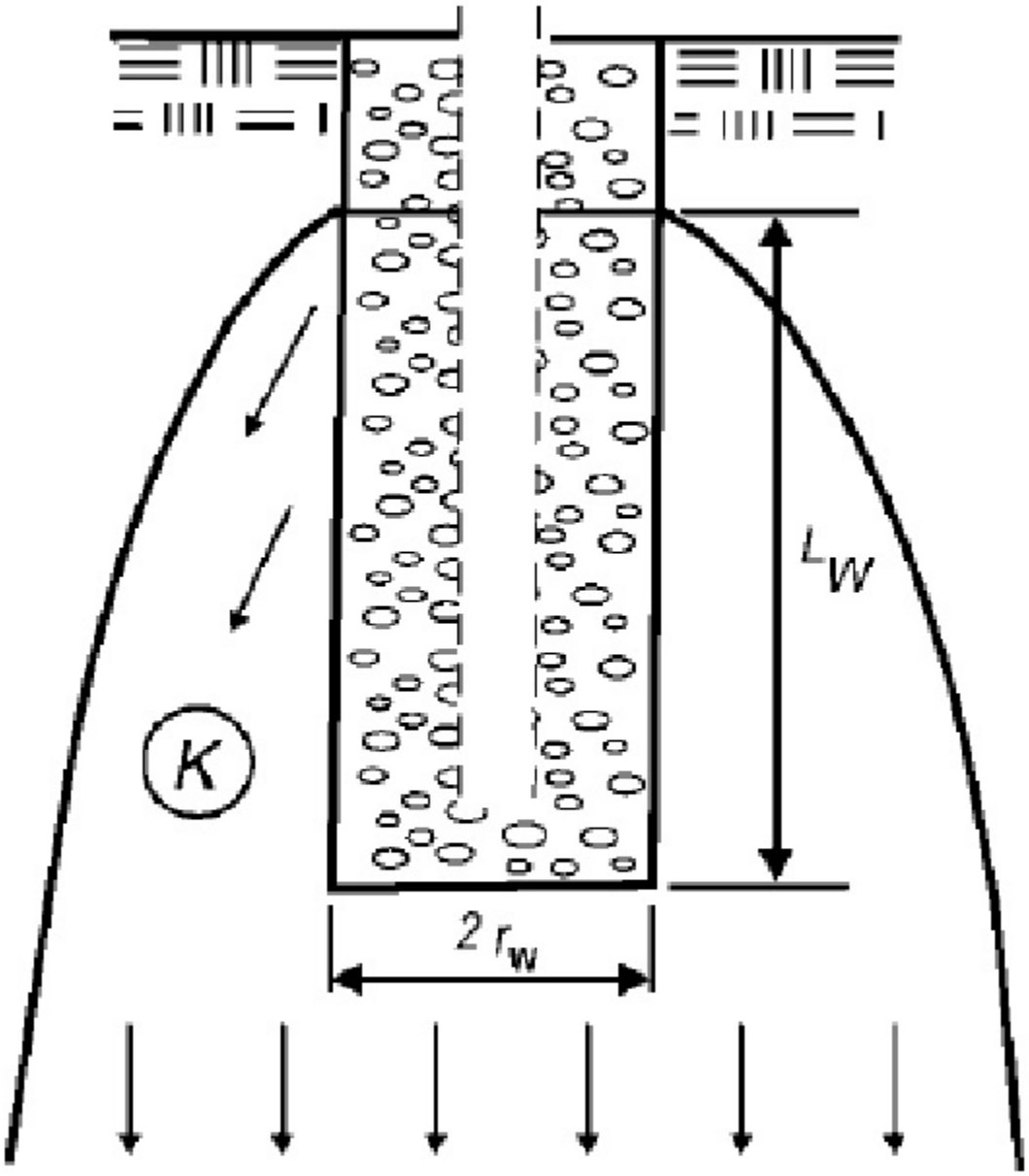

Figure 4: A Cross section of a vadose-zone well (Bower, 2002)

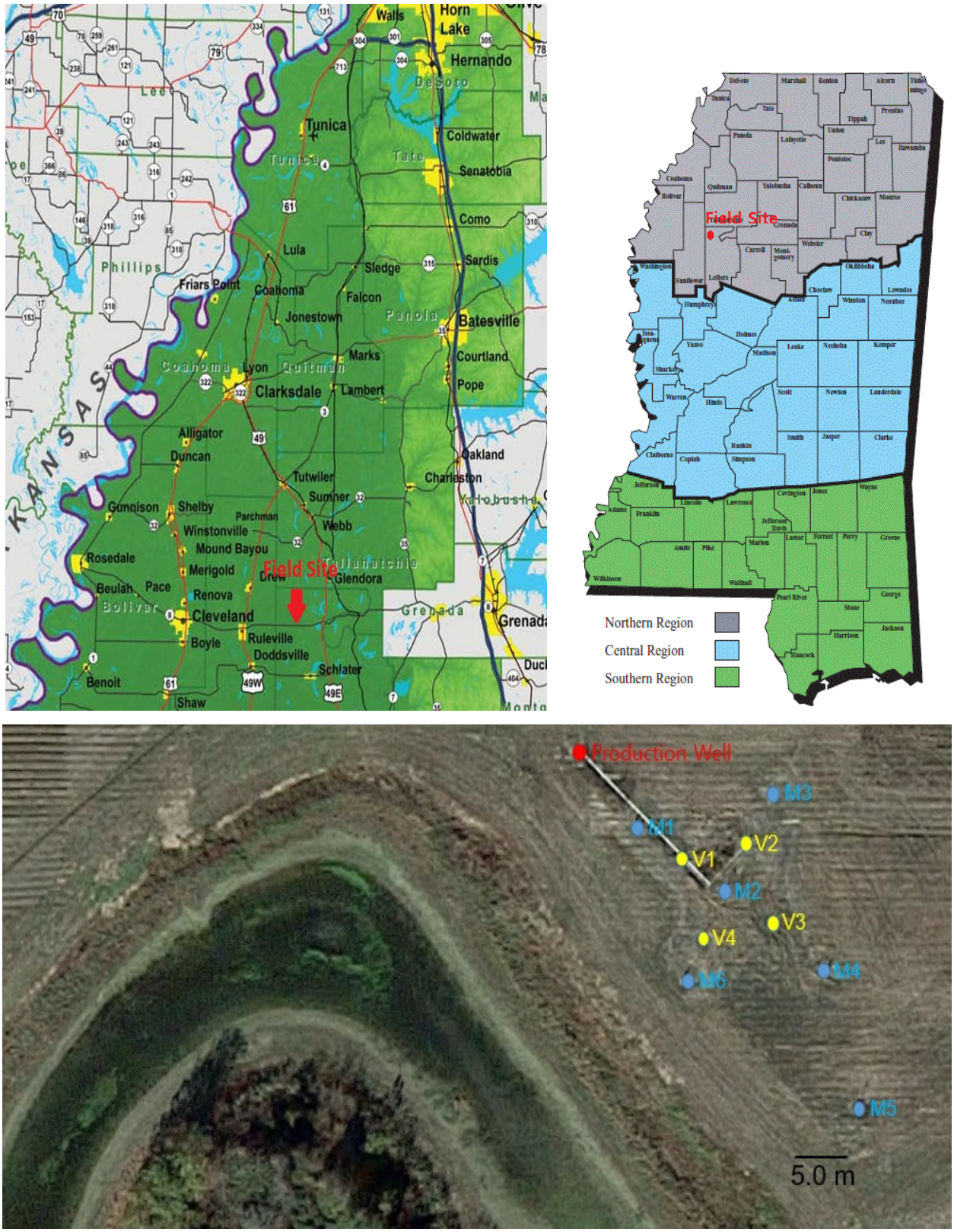

Figure 5: Overview of research sites (Rigby, 2015)

Figure 6: Location of installed wells (looking northeast)

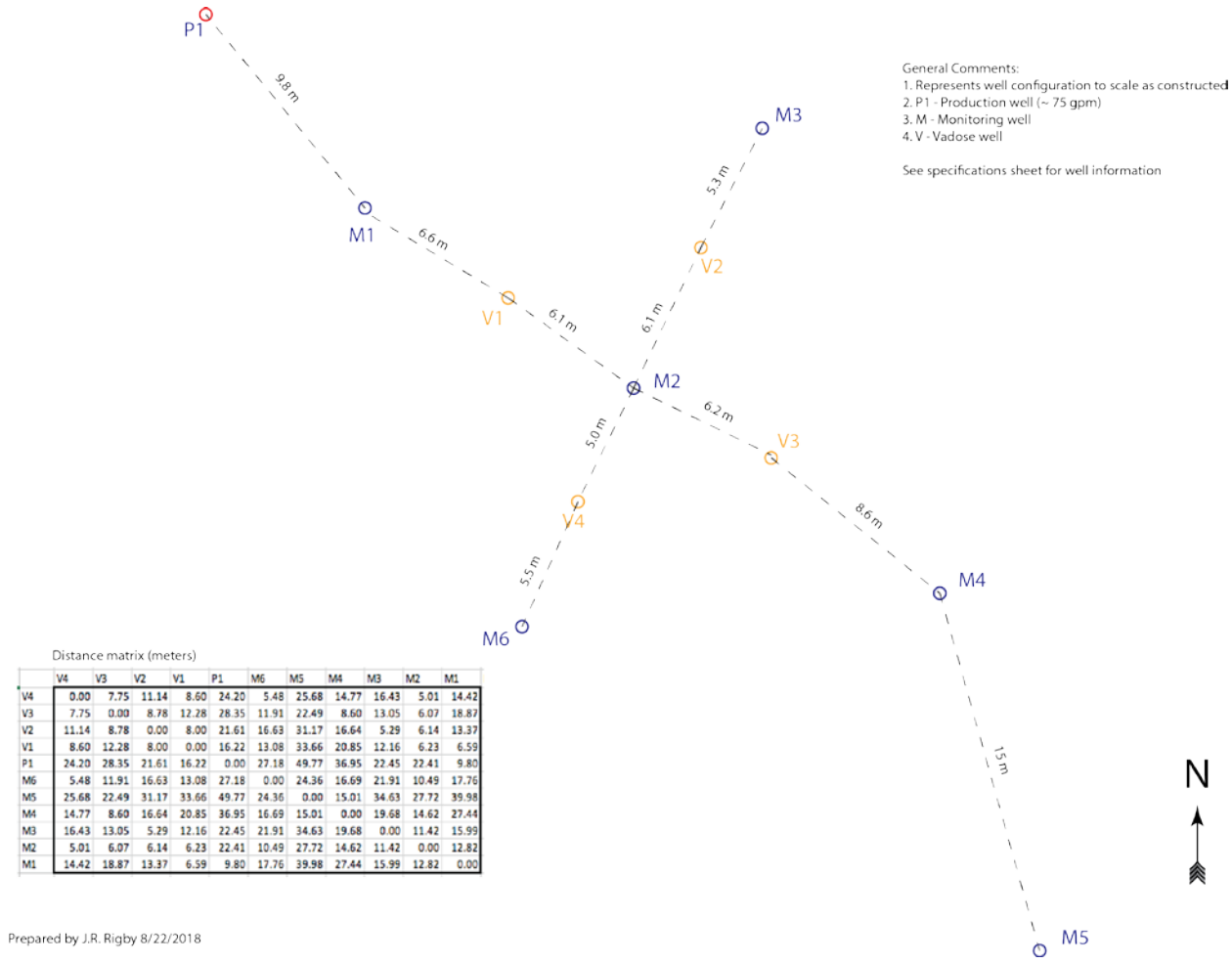

	V4	V3	V2	V1	P1	M6	M5	M4	M3	M2	M1
V4	0.00	7.75	11.14	8.60	24.20	5.48	25.68	14.77	16.43	5.01	14.42
V3	7.75	0.00	8.78	12.28	28.35	11.91	22.49	8.60	13.05	6.07	18.87
V2	11.14	8.78	0.00	8.00	21.61	16.63	31.17	16.64	5.29	6.14	13.37
V1	8.60	12.28	8.00	0.00	16.22	13.08	33.66	20.85	12.16	6.23	6.59
P1	24.20	28.35	21.61	16.22	0.00	27.18	49.77	36.95	22.45	22.41	9.80
M6	5.48	11.91	16.63	13.08	27.18	0.00	24.36	16.69	21.91	10.49	17.76
M5	25.68	22.49	31.17	33.66	49.77	24.36	0.00	15.01	34.63	27.72	39.98
M4	14.77	8.60	16.64	20.85	36.95	16.69	15.01	0.00	19.68	14.62	27.44
M3	16.43	13.05	5.29	12.16	22.45	21.91	34.63	19.68	0.00	11.42	15.99
M2	5.01	6.07	6.14	6.23	22.41	10.49	27.72	14.62	11.42	0.00	12.82
M1	14.42	18.87	13.37	6.59	9.80	17.76	39.98	27.44	15.99	12.82	0.00

Figure 7: Well distance layout including one supply well, six monitoring wells, and four vadose-zone wells (Prepared by J.R. Rigby, 2018)

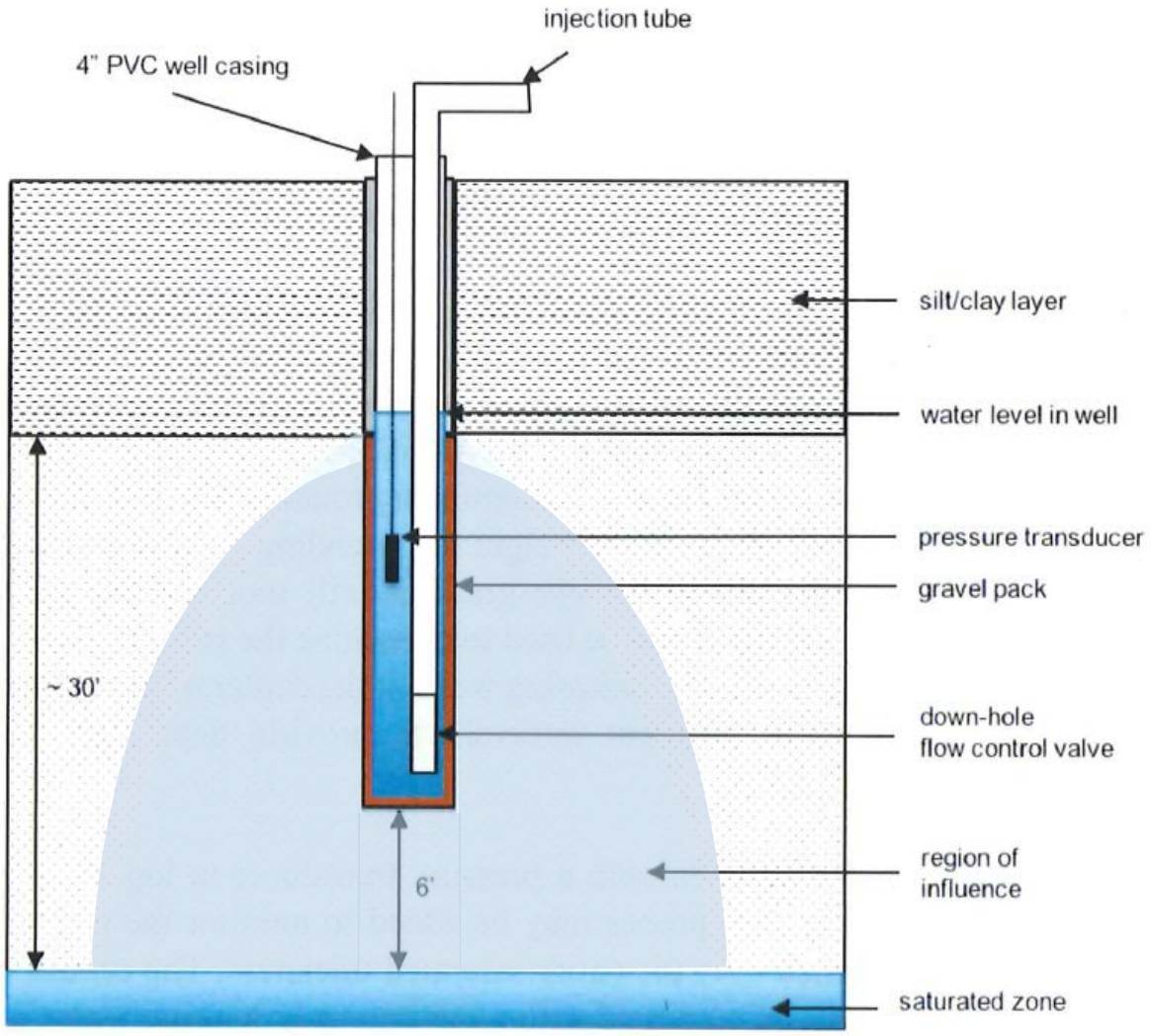

Figure 8: Diagrammatic view of vadose-zone well with injection tube and instrumentation (Rigby, 2015)

Figure 9: A portable generator to run the pump to withdraw water from the supply well

Figure 10: Hyprop sample ring

Figure 11: SoilMositure Equipment Corporation sample ring

Figure 12: Borehole kit from SoilMoisture Equipment Corporation

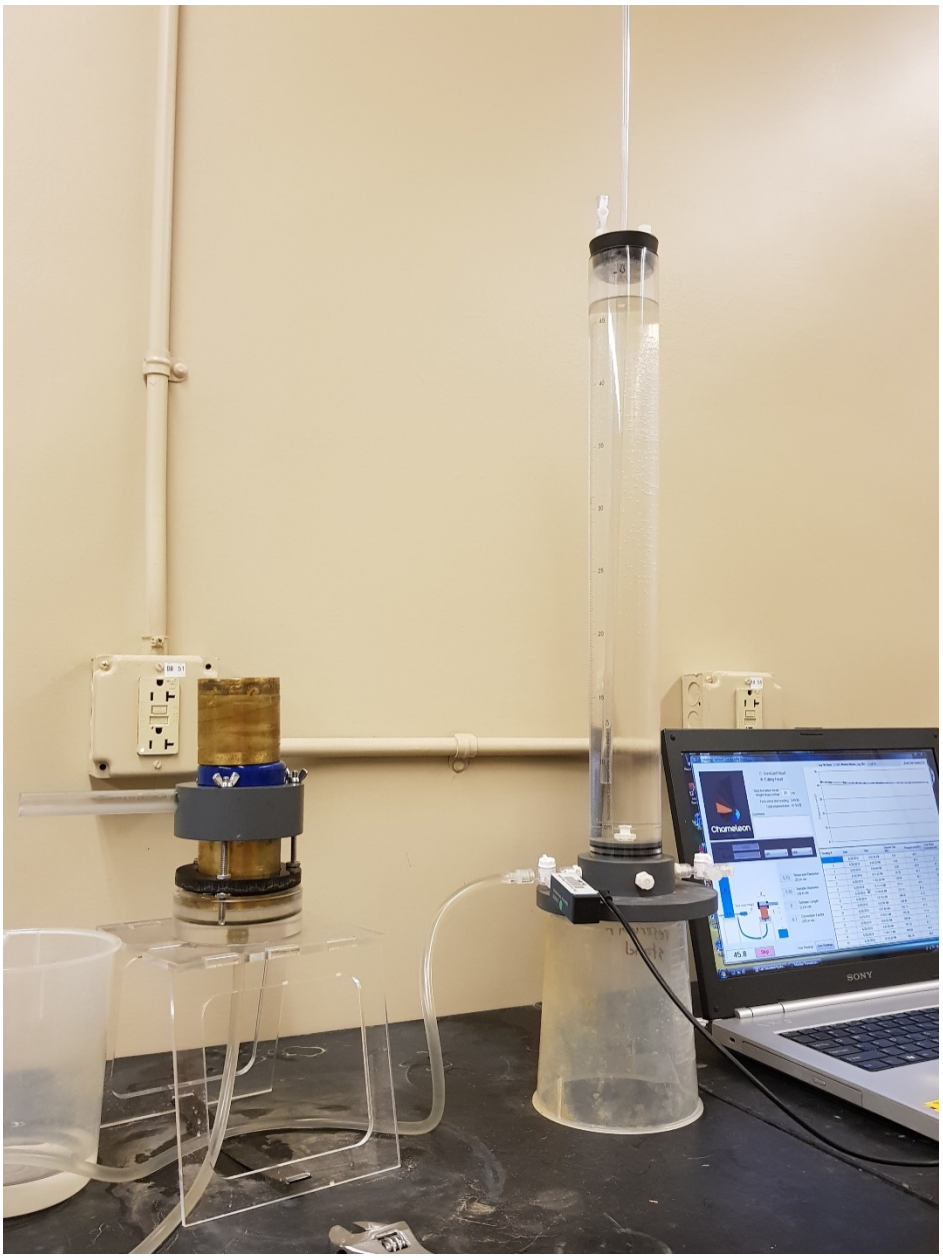

Figure 13: 2816G1 Chameleon Station for falling head permeability test

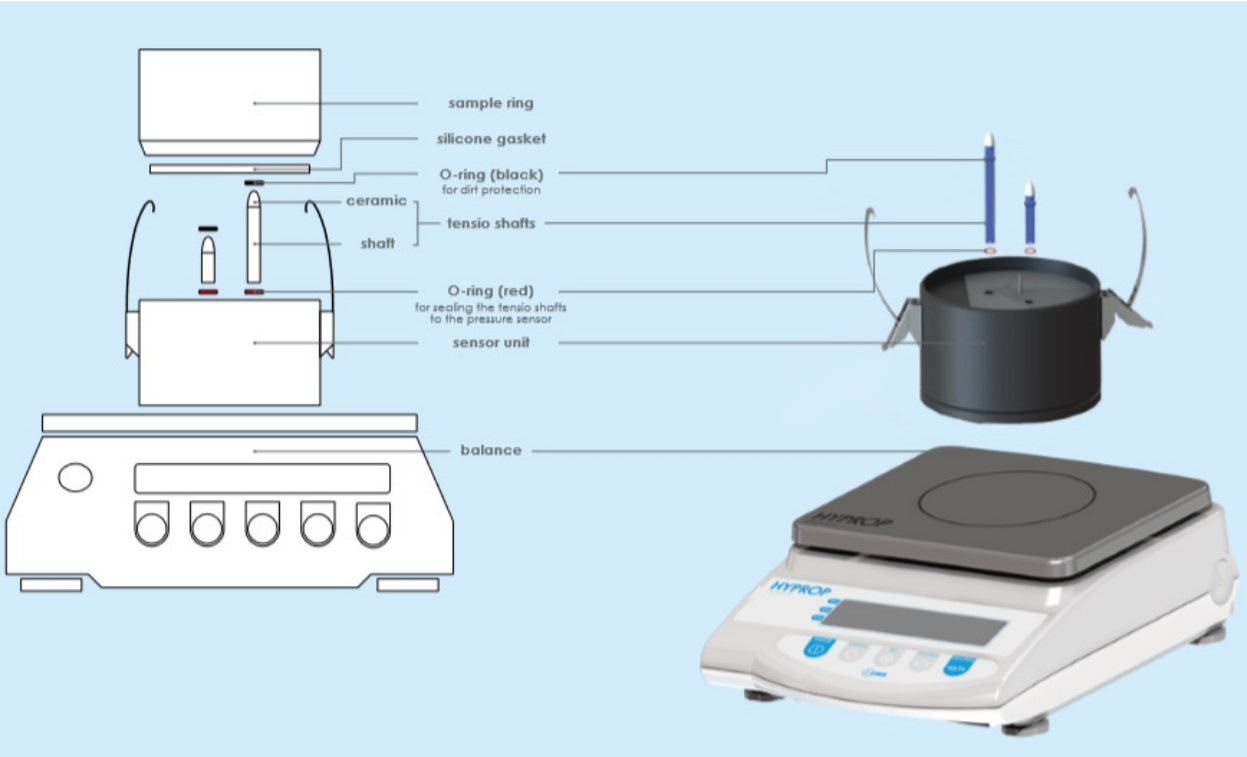

Figure 14: Overview of the parts of Hyprop device

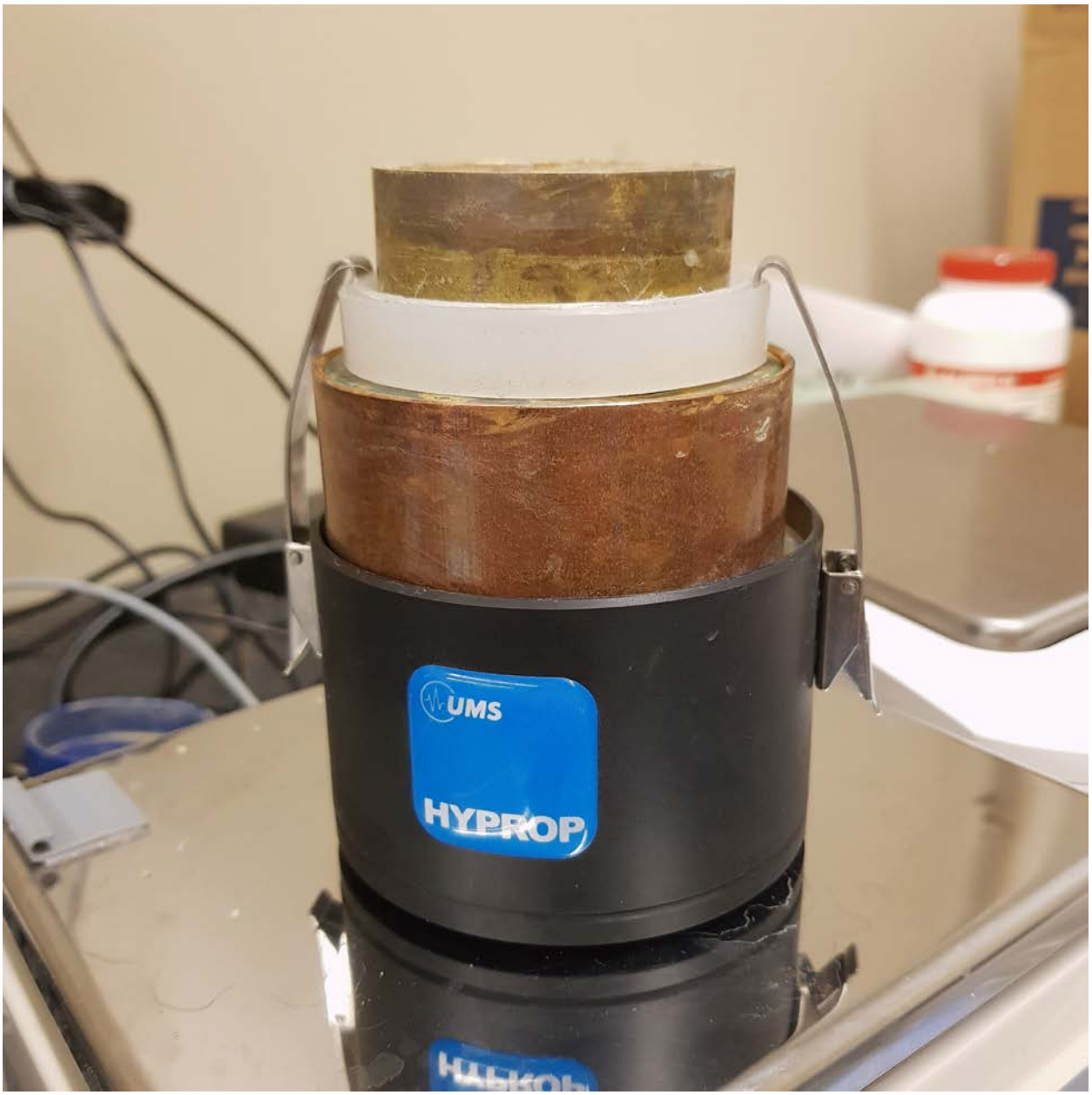

Figure 15: A feasible adaptor for attaching the collected samples to the device was manufactured by Matt Lowe

Figure 16: Overview of the hanging-water column apparatus

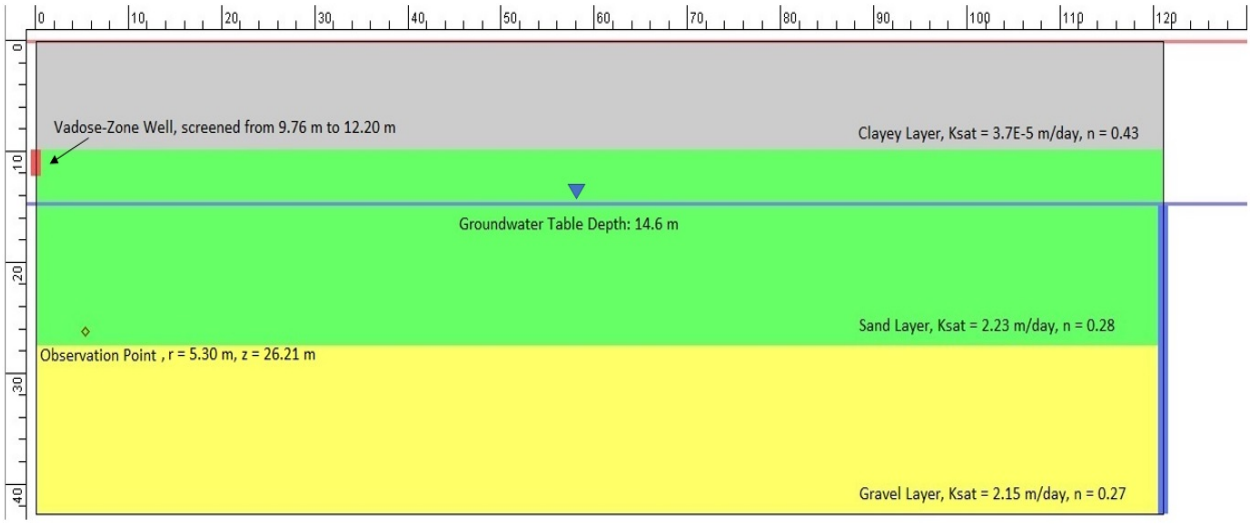

Figure 17: Overview of an axisymmetric model using VS2DTI software from USGS

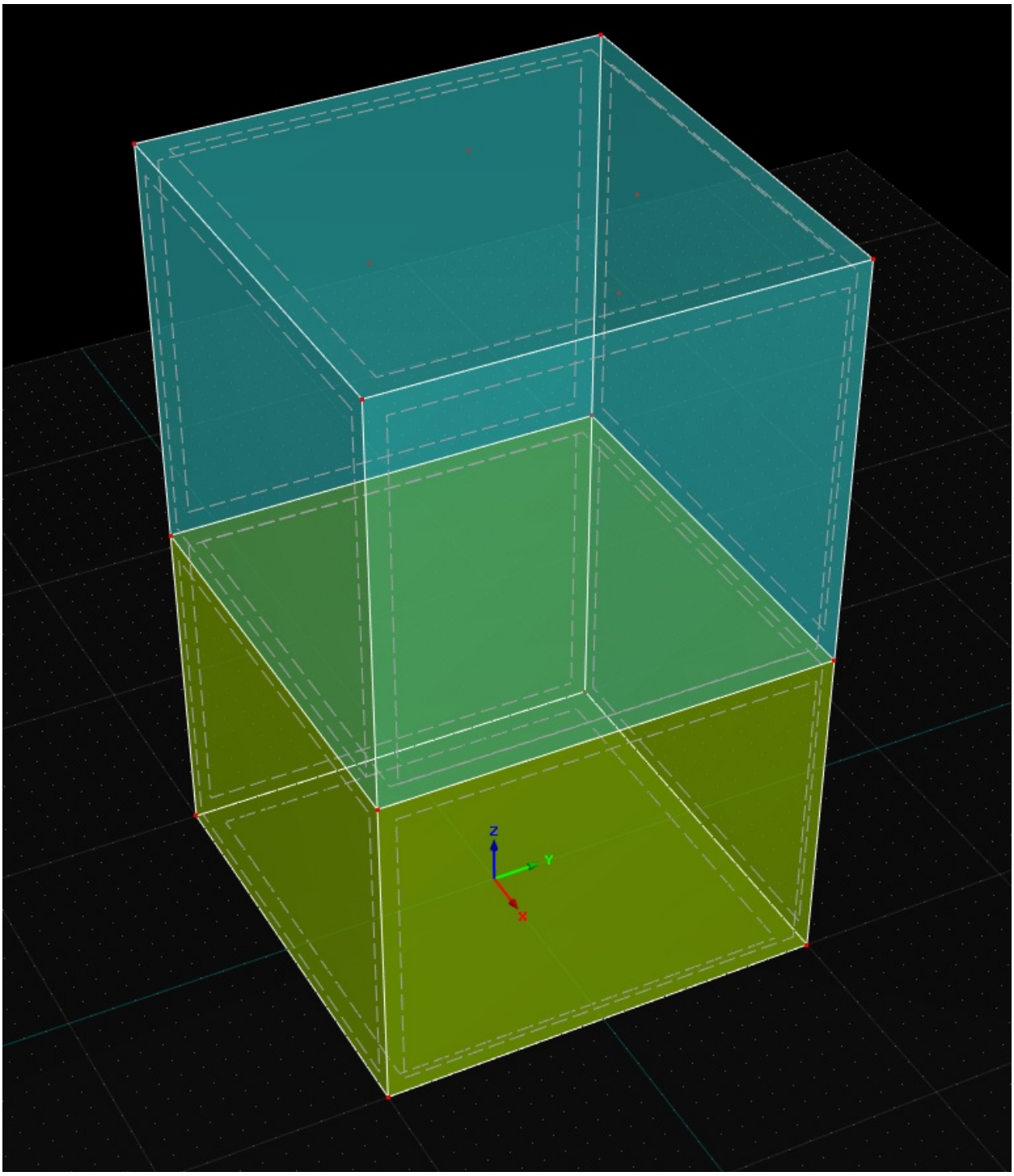

Figure 18: A preview of 3D model domain in HYDRUS-3D

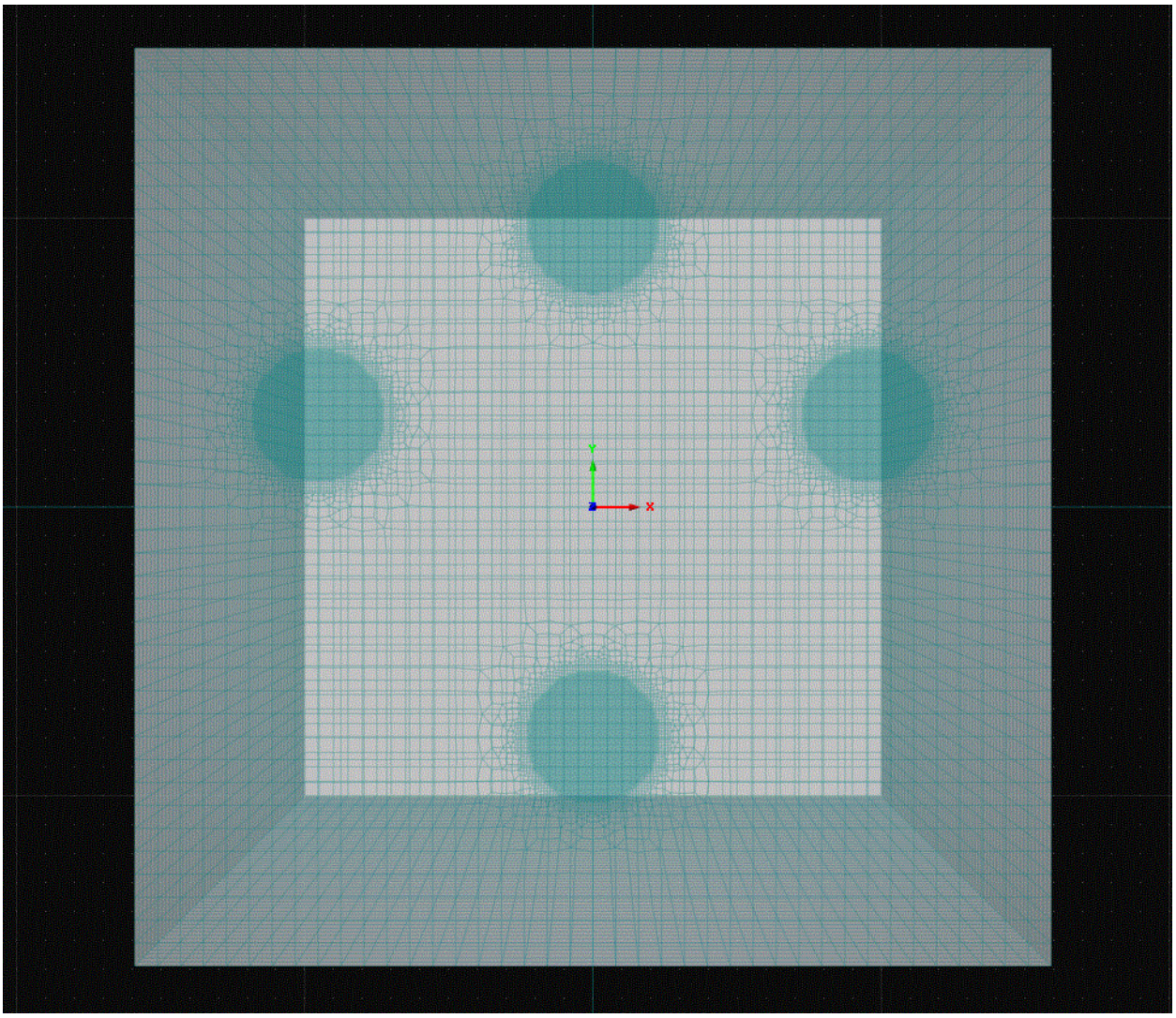

Figure 19: Top view of the model showing mesh distribution in HYDRUS-3D

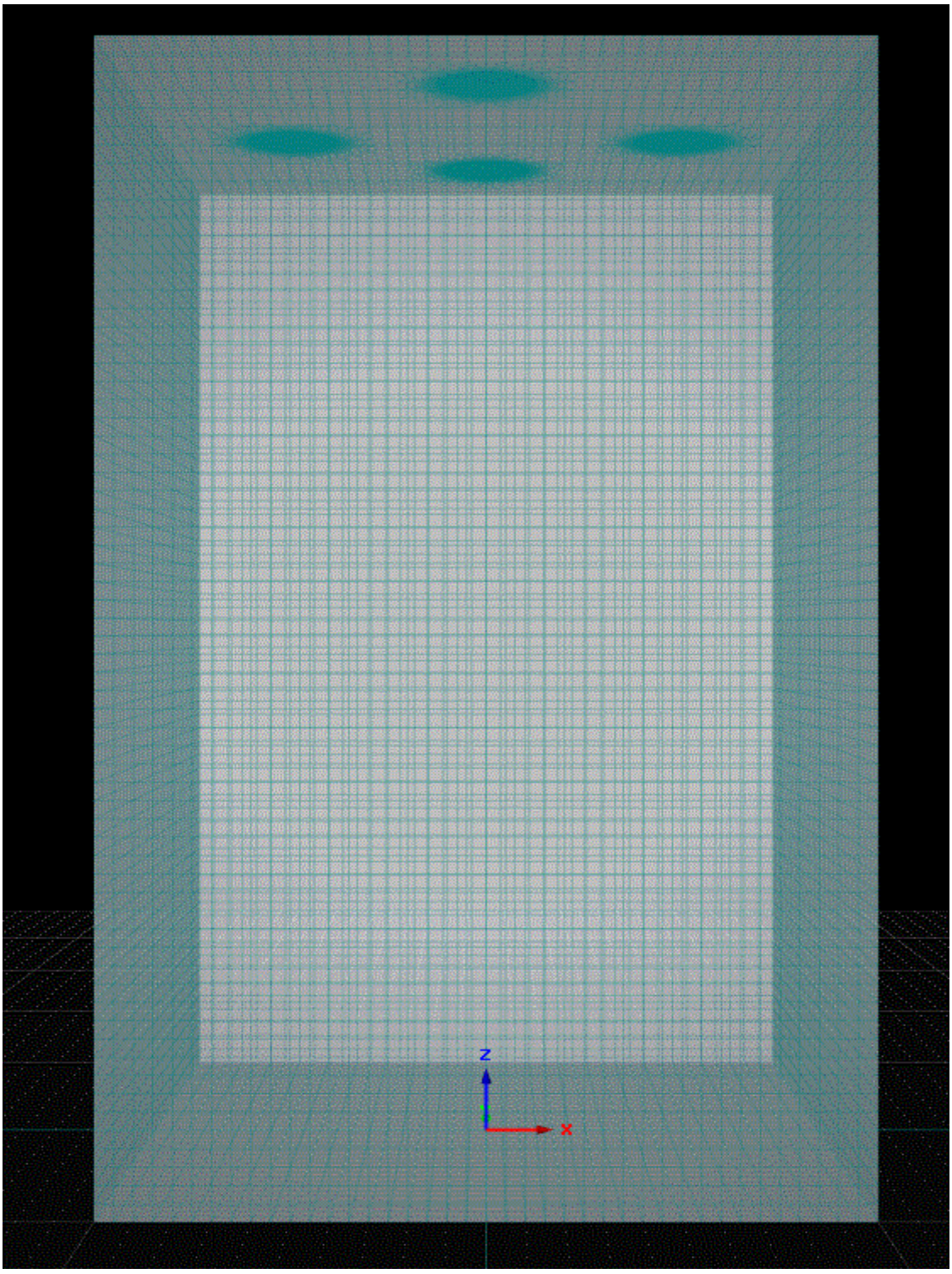

Figure 20: Lateral view of the model showing mesh distribution in HYDRUS-3D

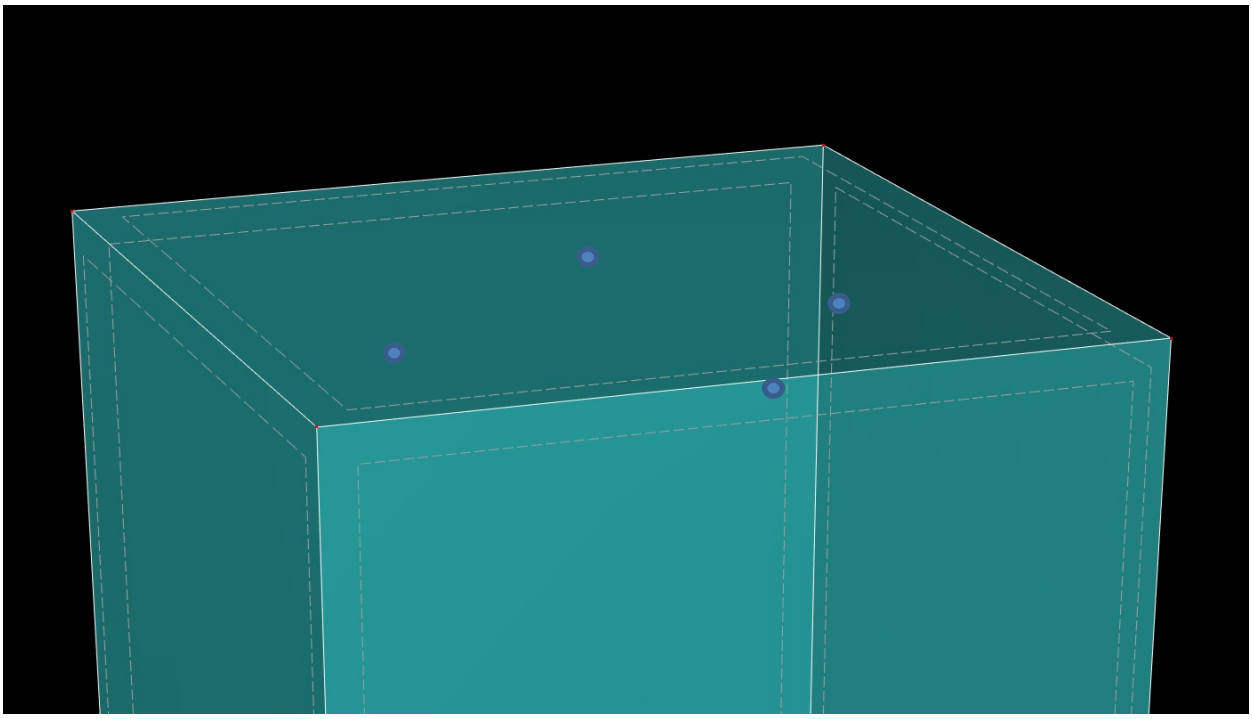

Figure 21: Location of nodal recharge (Vadose-zone wells). Four small blue dots are representing the vadose-zone wells.

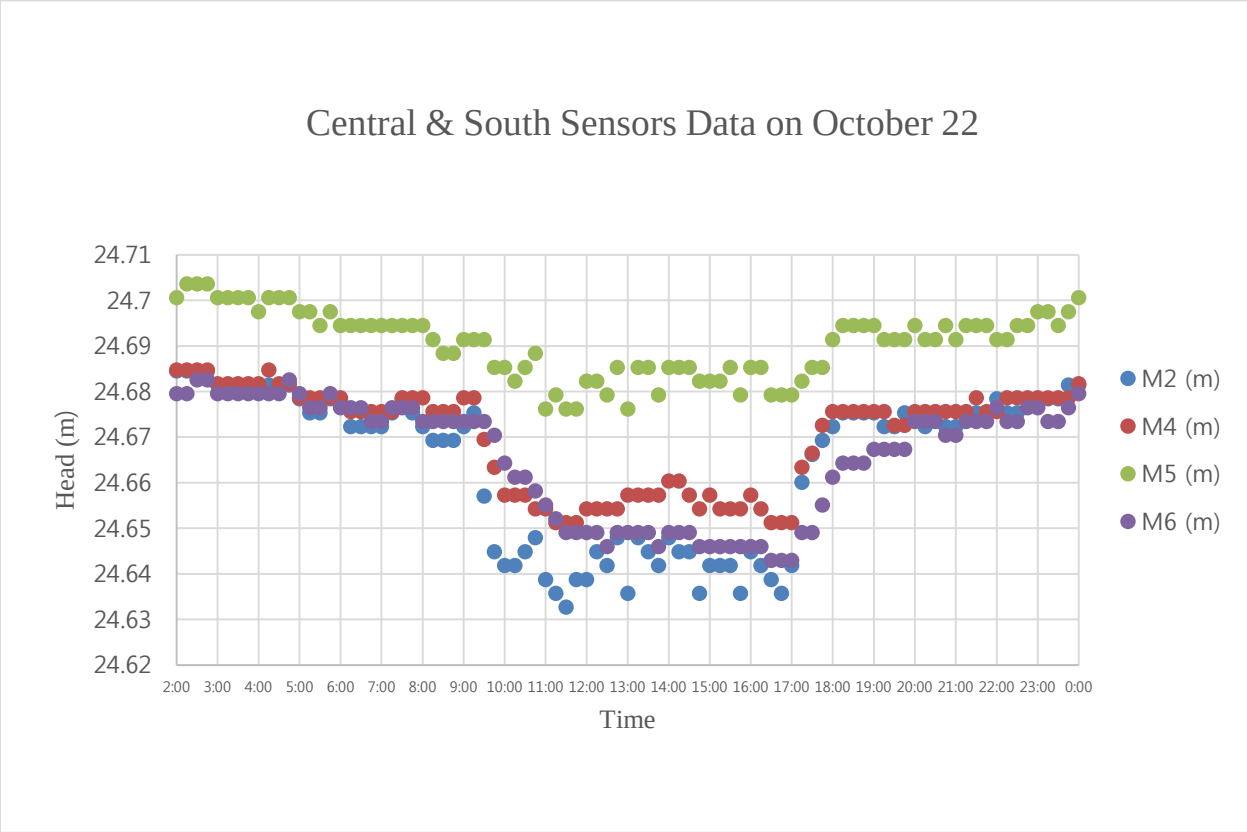

Figure 22: Drawdown data from Central & South transducers on October 22, 2018. The pumping test started at 9:20 am and ended at 5:00 pm

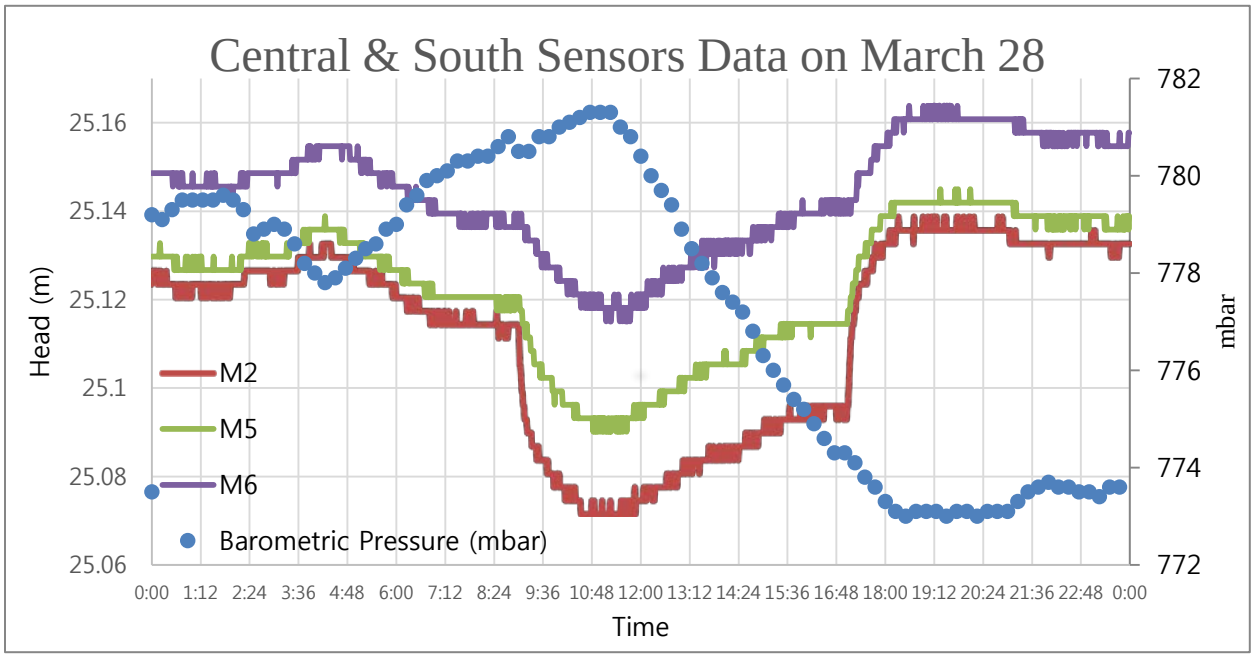

Figure 23: Drawdown data from Central & South transducers on March 28, 2019. The pumping test only to the pond started at 9:00 am and ended at 5:00 pm

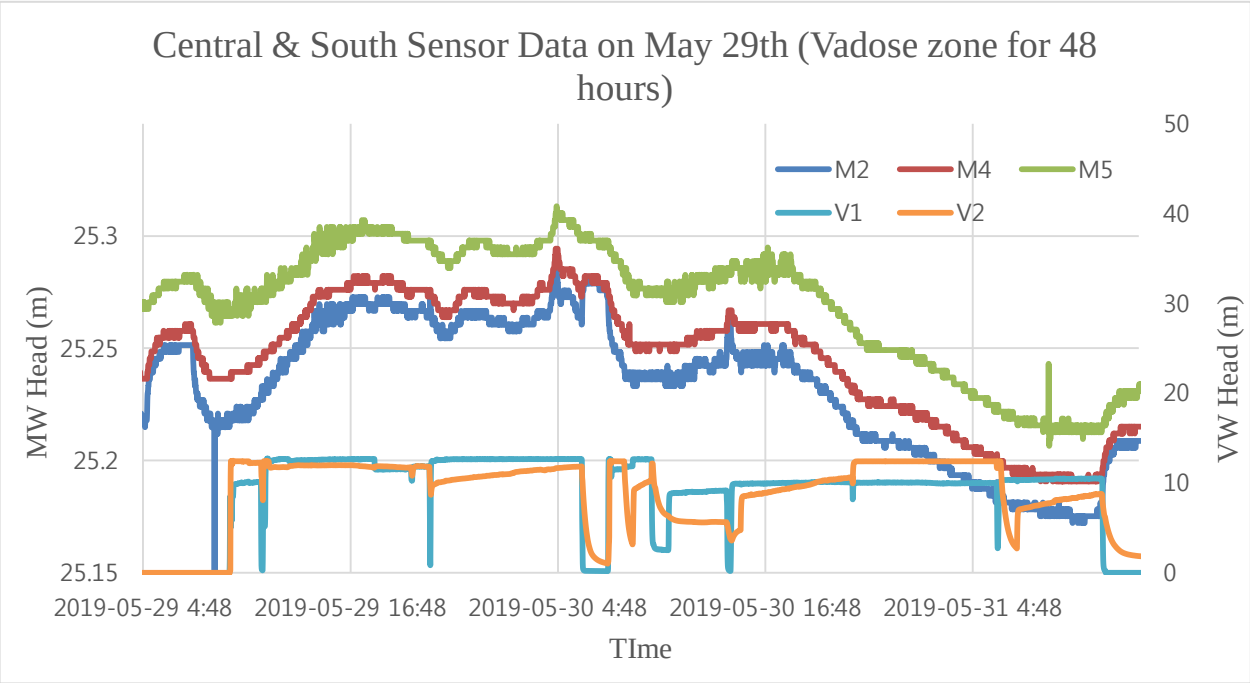

Figure 24: A hydrograph showing Central & South sensor data during 50 hours of final field test

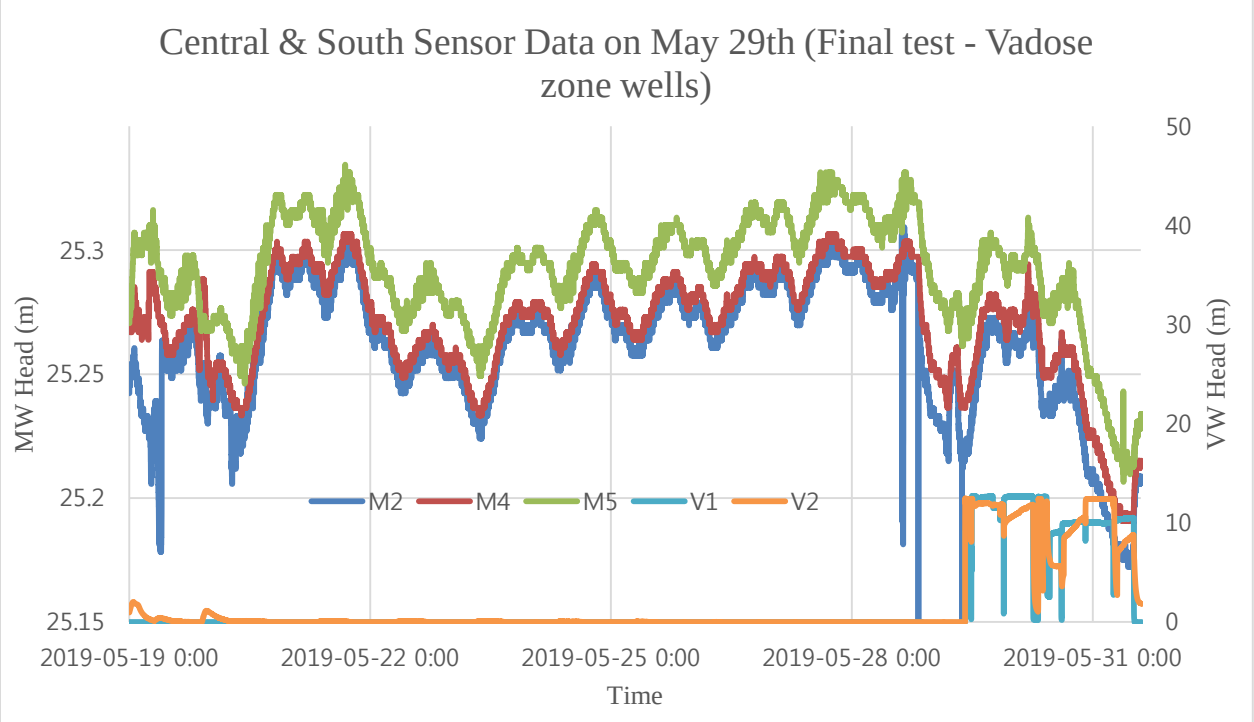

Figure 25: A hydrograph showing Central & South sensor data from May 19th to May 31th. The final field test was conducted from May 28th to May 31th.

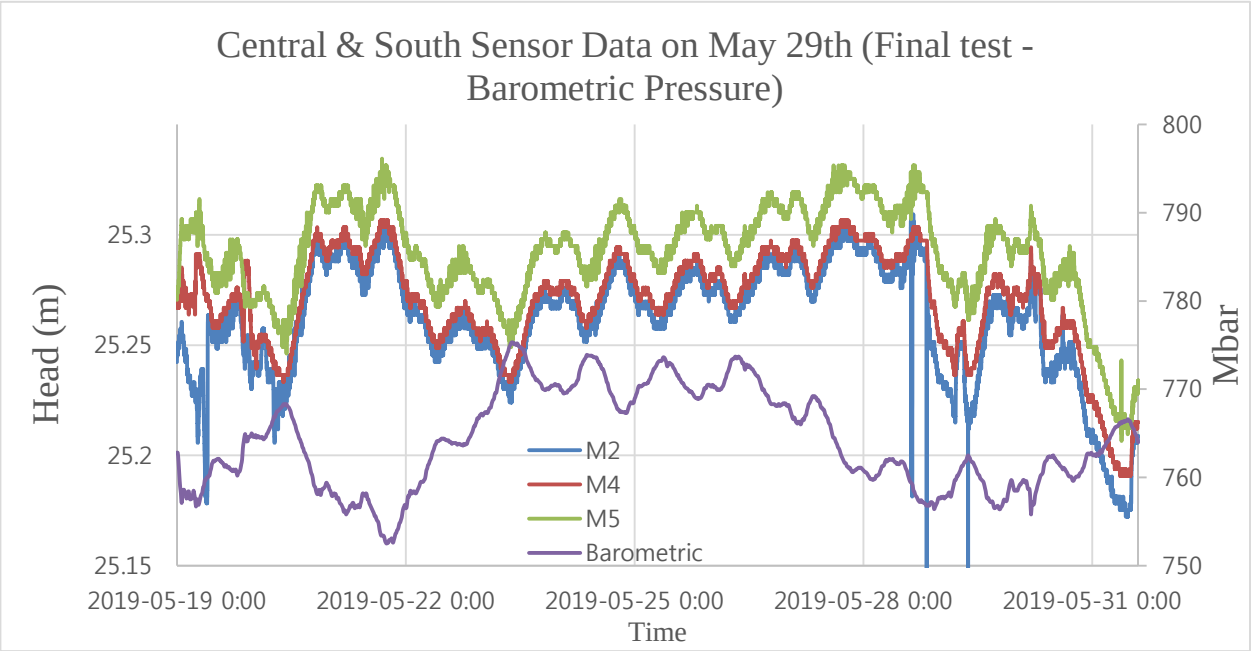

Figure 26: A hydrograph showing Central & South sensor data from May 19th to May 31th, including barometric pressure data. The inverse correlation between barometric pressure and water level is clearly shown on the graph

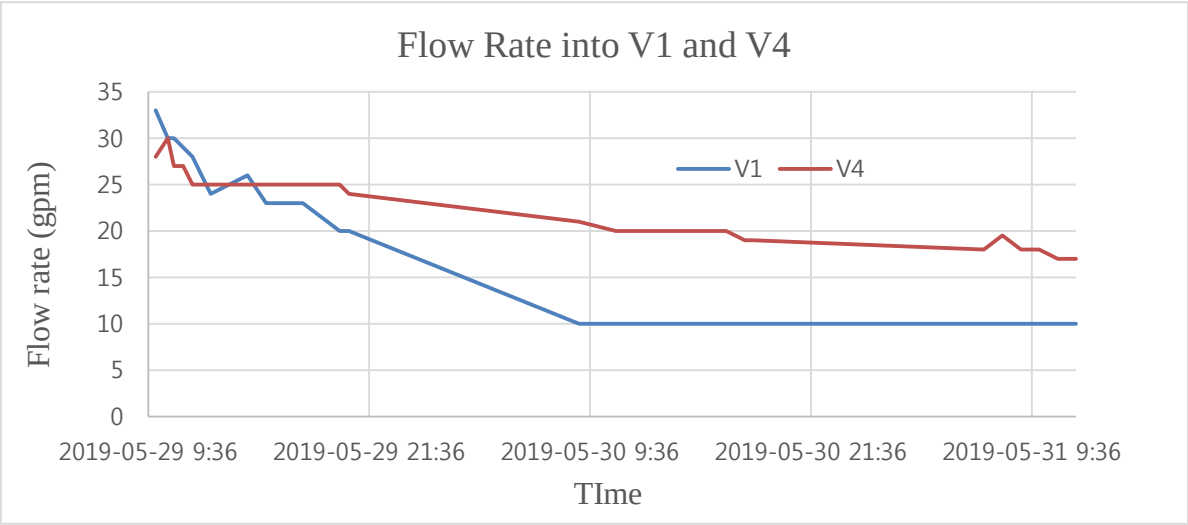

Figure 27: A graph showing flow rates into V1 and V4 over time. Flow rates into the wells are decreasing over time. Values plotted at 10 gpm were below the detection limit of the flow meter, thus actual flow rate may be less than 10 gpm

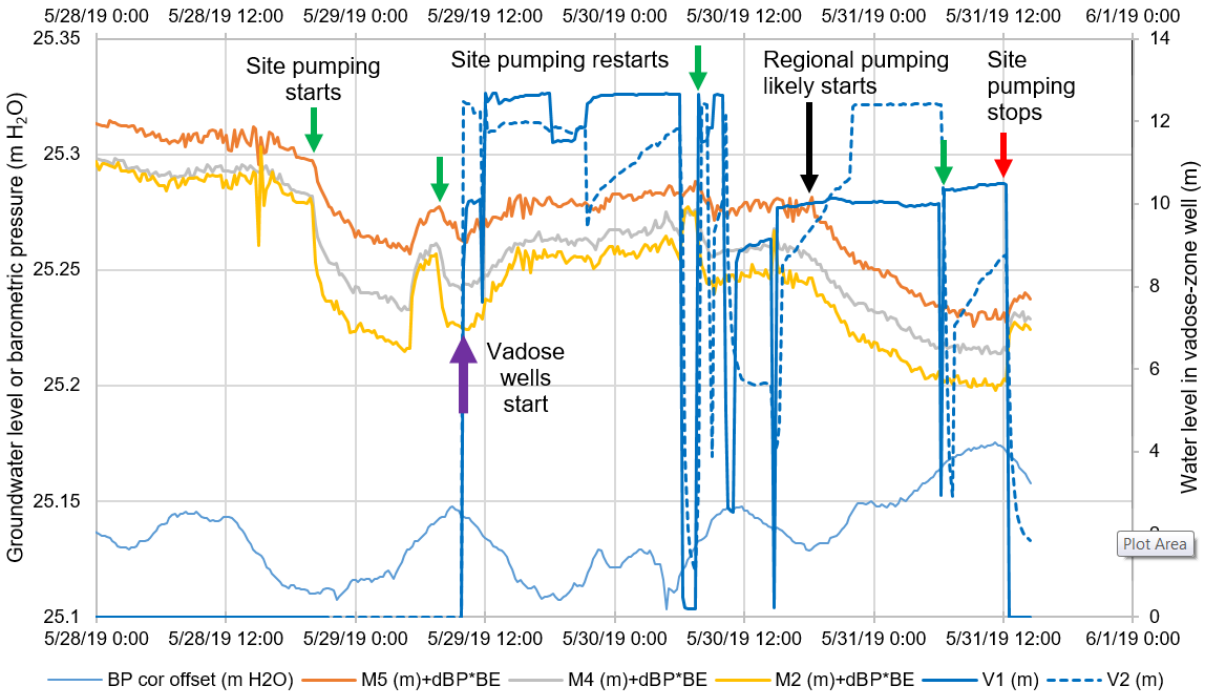

Figure 28: A barometric efficiency corrected graph showing Central & South sensor data from May 19th to May 31th.

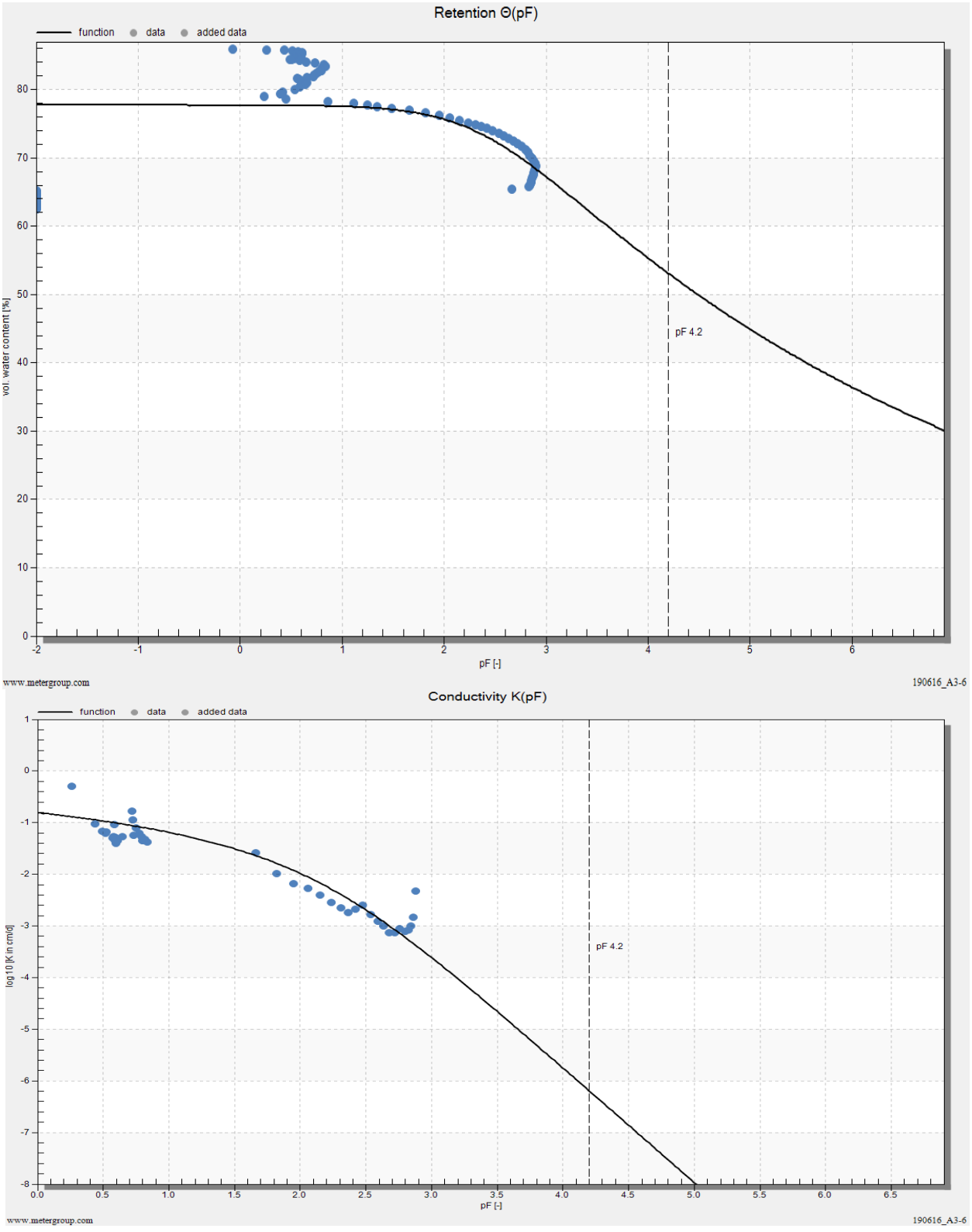

Figure 29: Hyprop Fit calculation

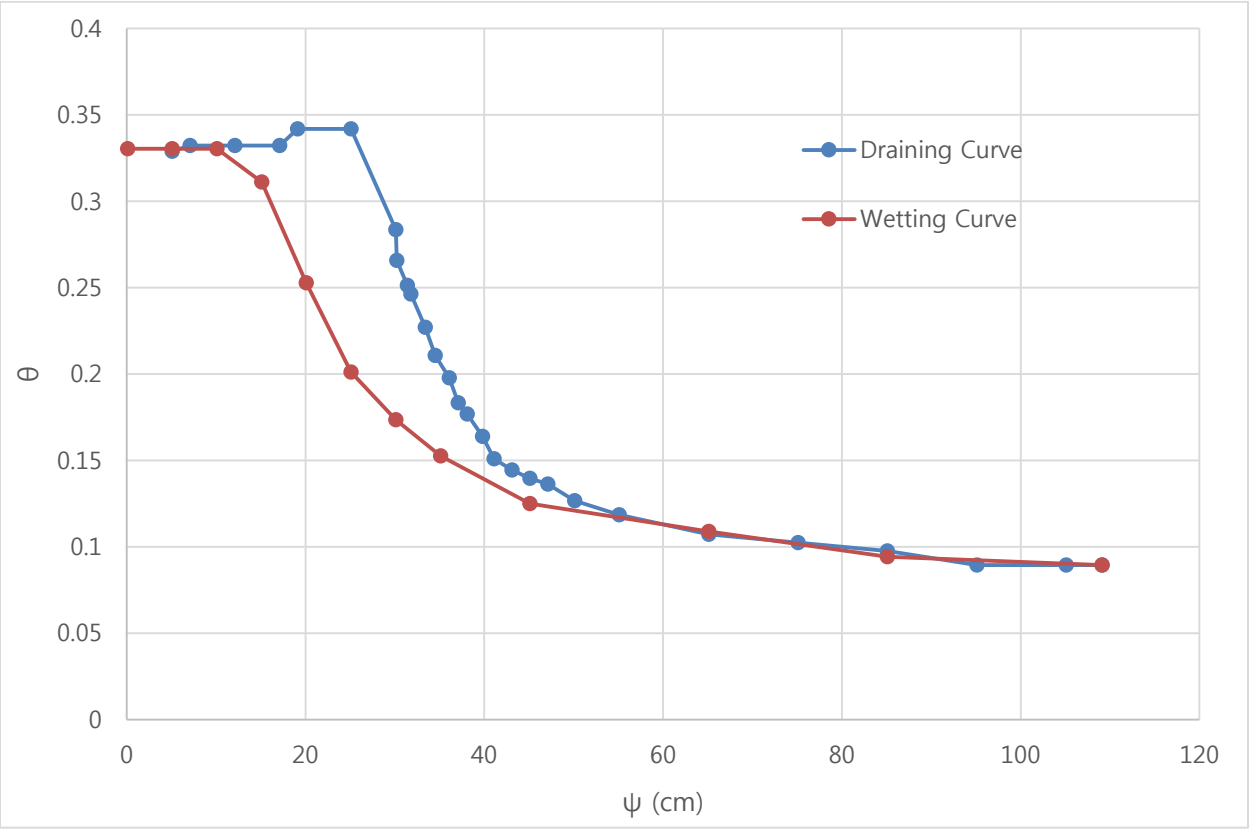

Figure 30: Draining curve and wetting curve of SL-1-11 sample by hanging water column method

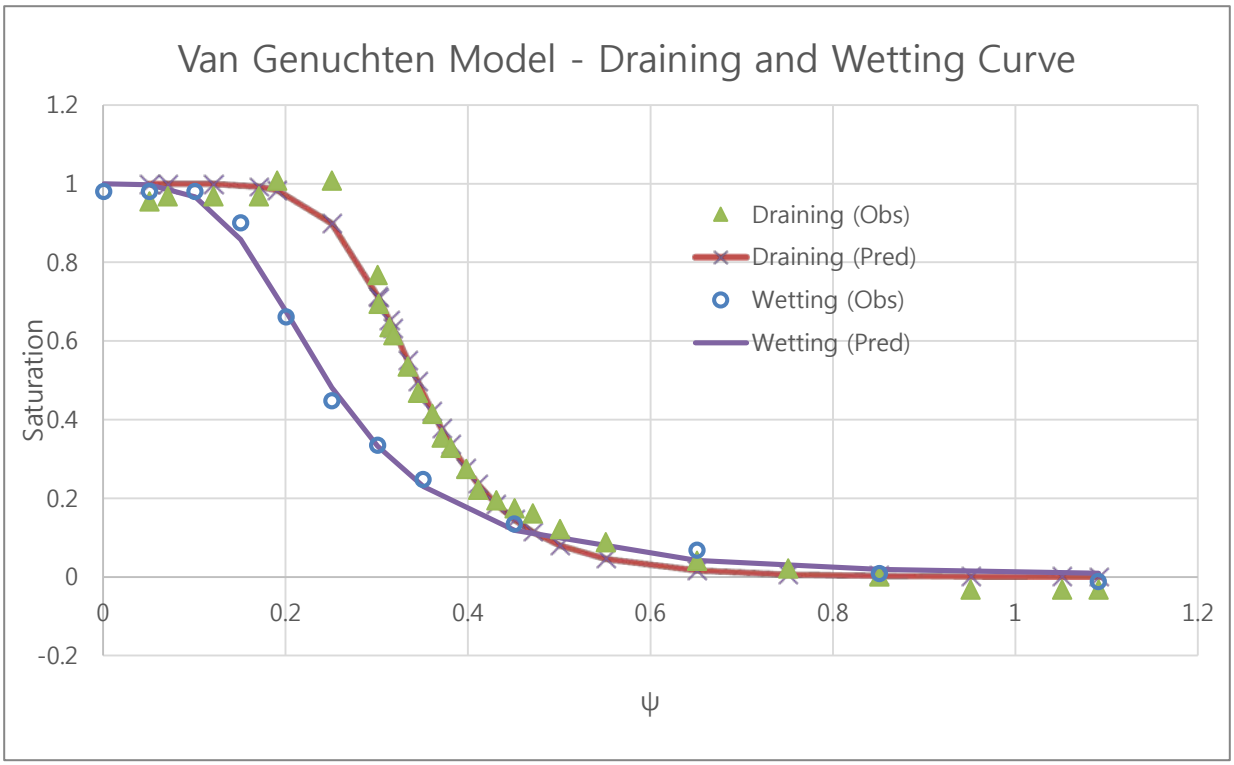

Figure 31: Two curves fitted to the van Genuchten model

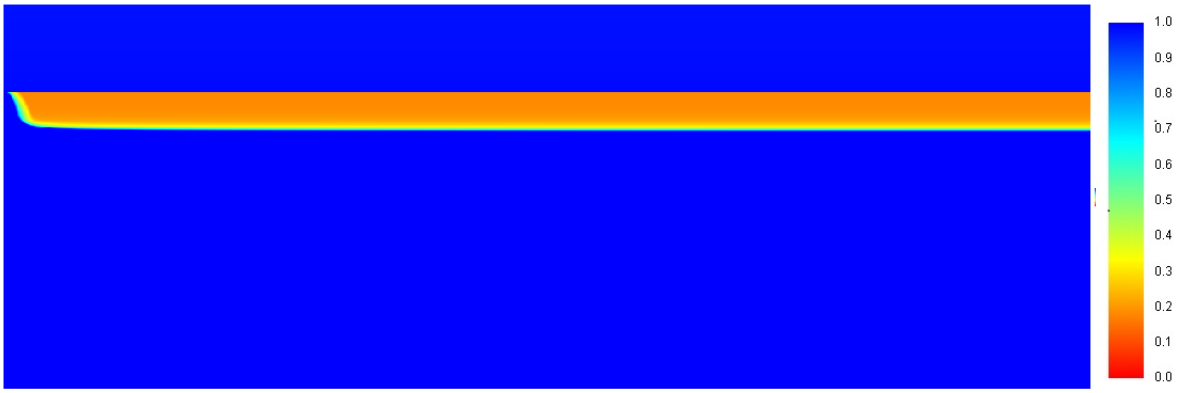

Time = 1.0

Mass Balance Error	Total for Simulation	Rate for this step
Fluid	3.21%	11.71%
Solute	0.00%	0.00%

Figure 32: Simulated saturation for high saturated hydraulic conductivity (22.3 m/day) and high porosity (0.4) for the axisymmetric VS2DTi model

Time = 1.0

Mass Balance Error	Total for Simulation	Rate for this step
Fluid	4.14%	13.05%
Solute	0.00%	0.00%

Figure 33: Simulated saturation for high saturated hydraulic conductivity (22.3 m/day) and mid porosity (0.28) for the axisymmetric VS2DTi model

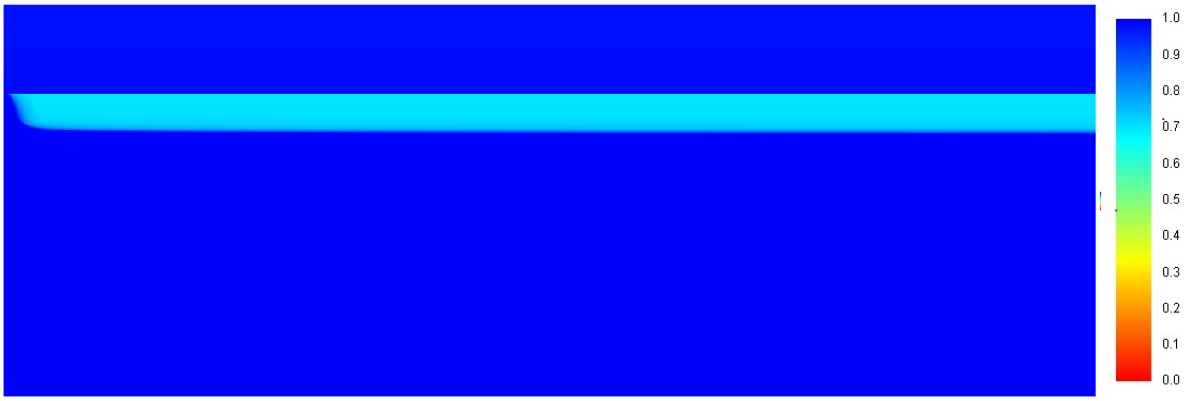

Time = 1.0

Mass Balance Error	Total for Simulation	Rate for this step
Fluid	3.95%	1.73%
Solute	0.00%	0.00%

Figure 34: Simulated saturation for high saturated hydraulic conductivity (22.3 m/day) and low porosity (0.1) for the axisymmetric VS2DTi model

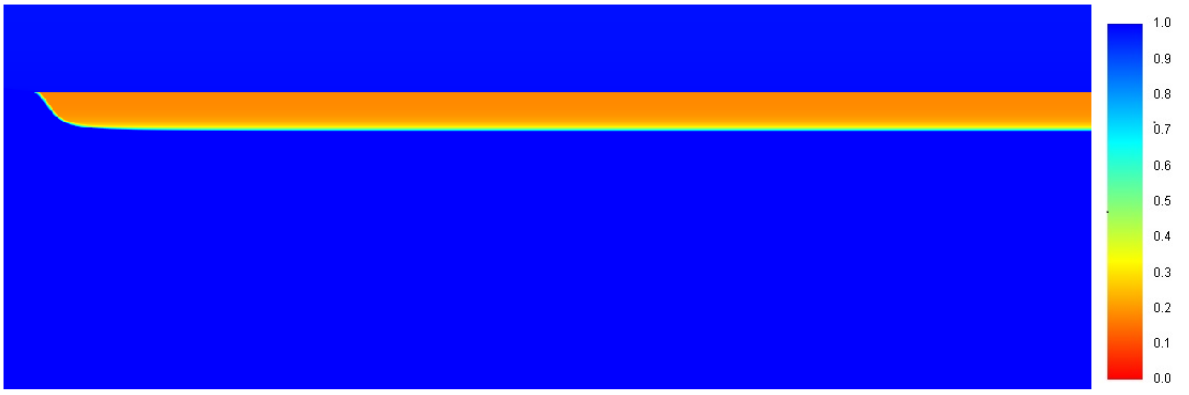

Time = 1.0

Mass Balance Error	Total for Simulation	Rate for this step
Fluid	0.03%	-0.01%
Solute	0.00%	0.00%

Figure 35: Simulated saturation for mid saturated hydraulic conductivity (2.23 m/day) and high porosity (0.4) for the axisymmetric VS2DTi model

Figure 36: Simulated saturation for mid saturated hydraulic conductivity (2.23 m/day) and mid porosity (0.28) for the axisymmetric VS2DTi model

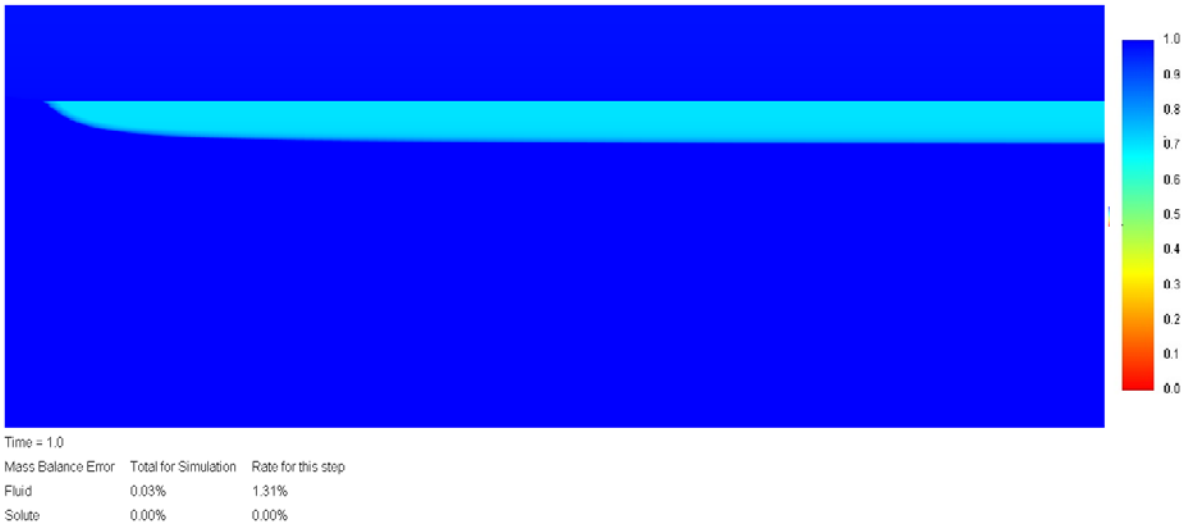

Figure 37: Simulated saturation for mid saturated hydraulic conductivity (2.23 m/day) and low porosity (0.1) for the axisymmetric VS2DTi model

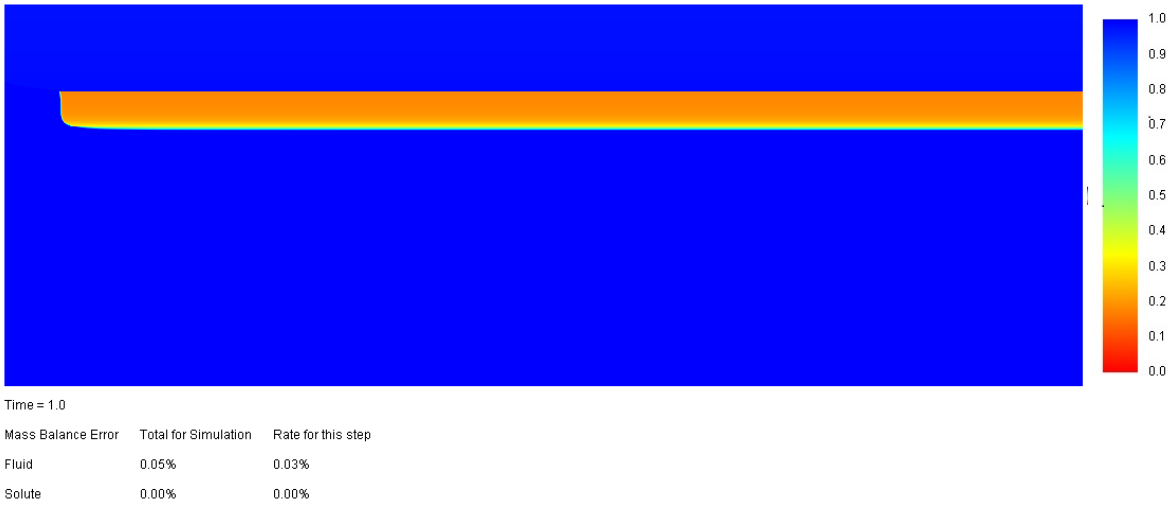

Time = 1.0

Mass Balance Error	Total for Simulation	Rate for this step
Fluid	0.05%	0.03%
Solute	0.00%	0.00%

Figure 38: Simulated saturation for low saturated hydraulic conductivity (0.223 m/day) and high porosity (0.4) for the axisymmetric VS2DTi model

Time = 1.0

Mass Balance Error	Total for Simulation	Rate for this step
Fluid	0.06%	0.07%
Solute	0.00%	0.00%

Figure 39: Simulated saturation for low saturated hydraulic conductivity (0.223 m/day) and mid porosity (0.28) for the axisymmetric VS2DTi model

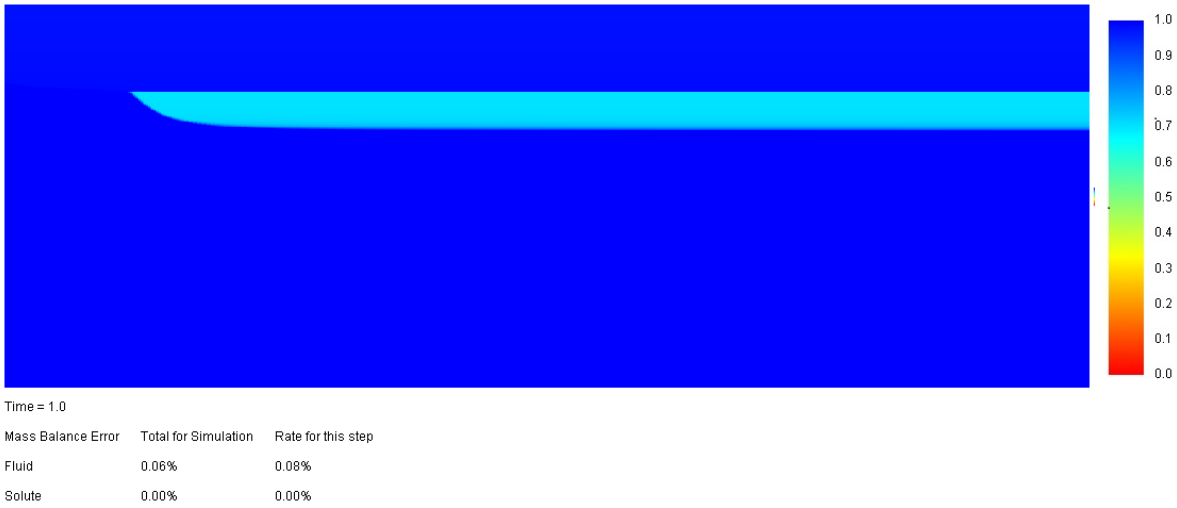

Figure 40: Simulated saturation for low saturated hydraulic conductivity (0.223 m/day) and low porosity (0.1) for the axisymmetric VS2DTi model

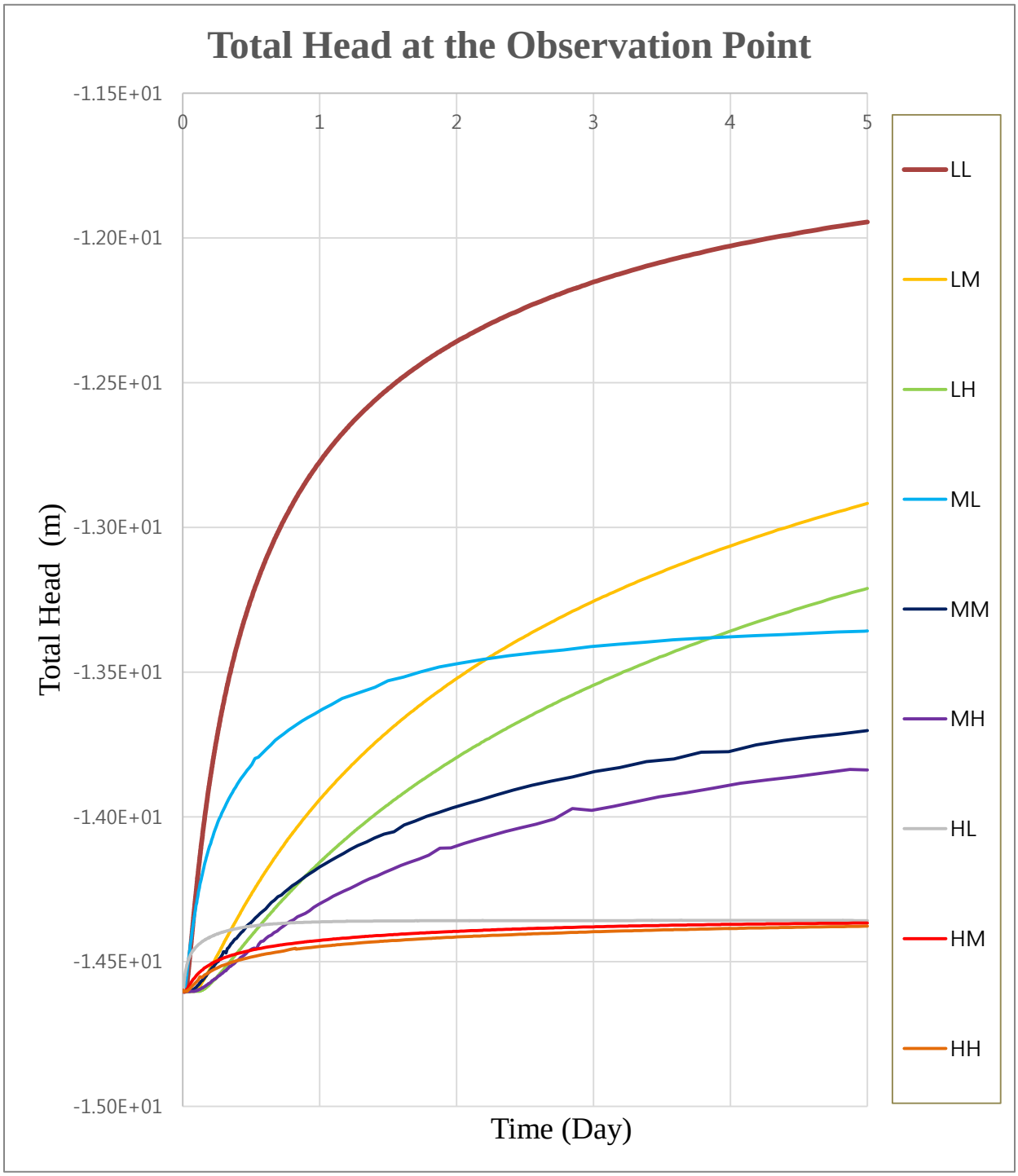

Figure 41: A hydrograph of total head vs time at the observation point with varying hydraulic conductivity (K) and porosity (n) simulated by the axisymmetric VS2DTi model. Two letters stands for hydraulic conductivity and porosity respectively, first letter for K_{sat} and second letter for porosity. For example, LL stands for low K_{sat} and low n and ML stands for mid K_{sat} and low n.

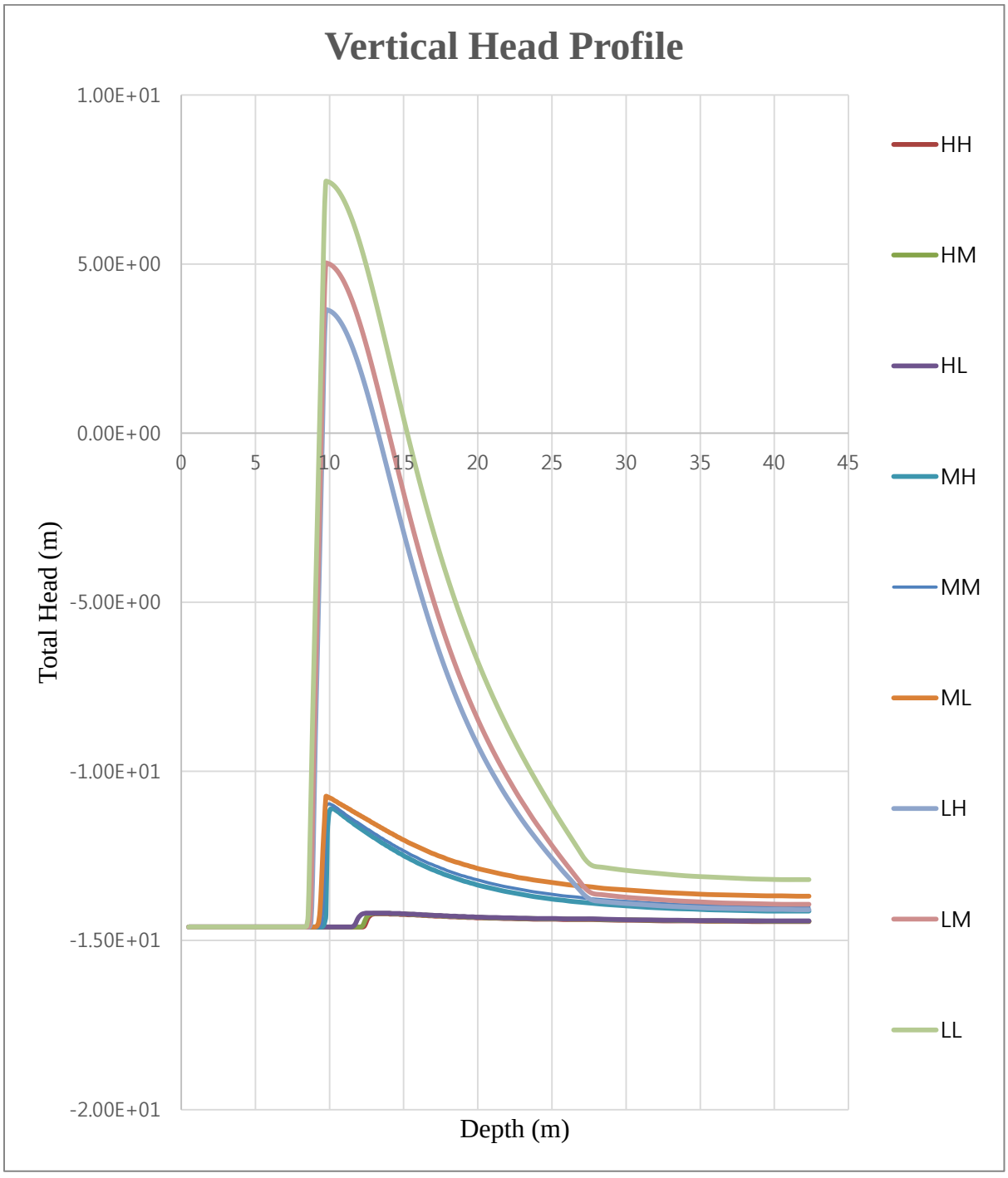

Figure 42: A hydrograph showing vertical total head profile with depth simulated by the axisymmetric VS2DTi model. The radial coordinate for this graph is corresponding to that of observation point. Two letters stands for hydraulic conductivity and porosity respectively, first letter for K_{sat} and second letter for porosity. For example, LL stands for low K_{sat} and low n and ML stands for mid K_{sat} and low n.

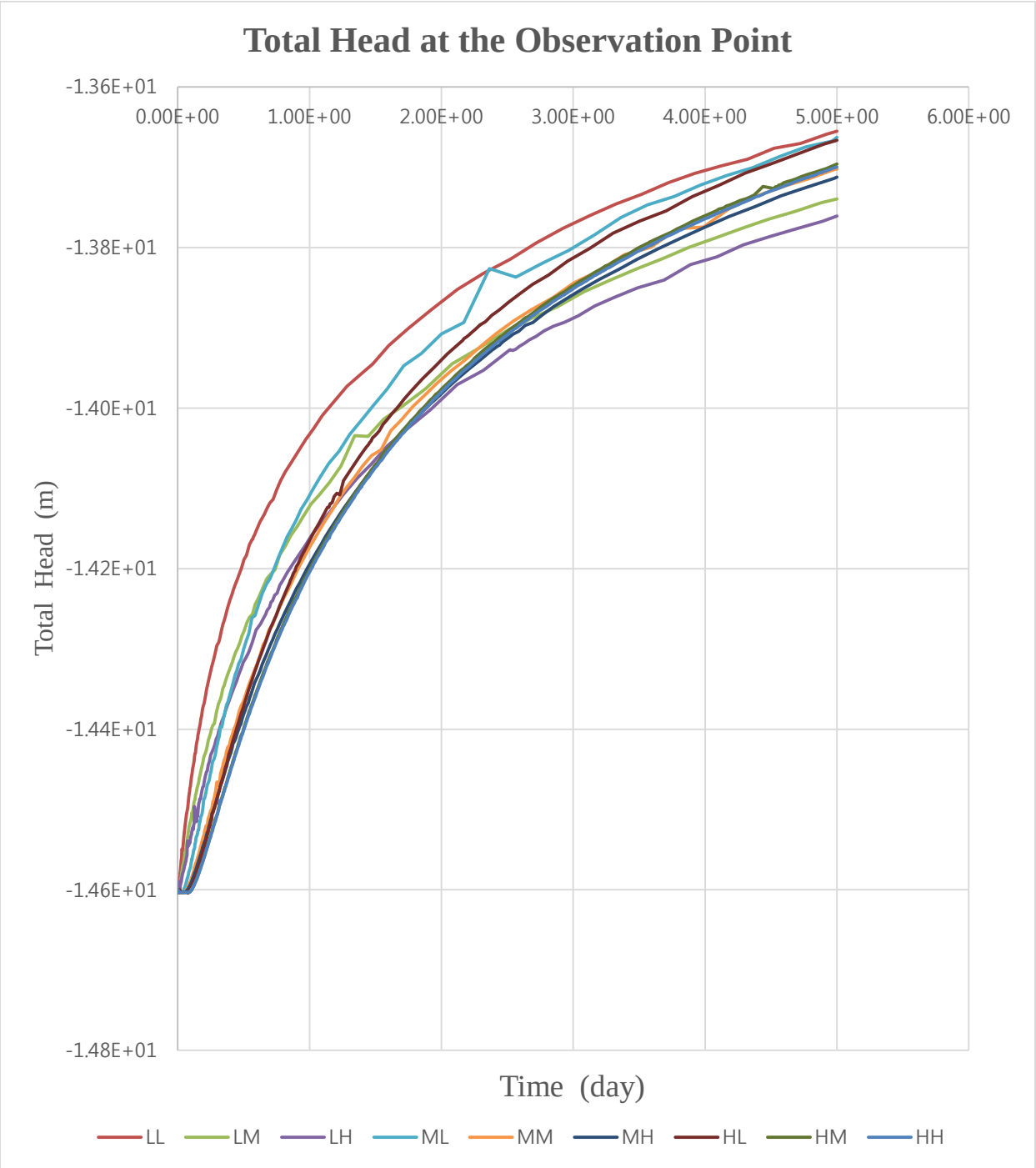

Figure 43: A hydrograph of total head vs time at the observation point with varying h_b and λ simulated by the axisymmetric VS2DTi model. The first letter stands for h_b and second stands for λ. Two letters stands for h_b and λ respectively, first letter for h_b and second letter for λ. For example, LL stands for low h_b and low λ and ML stands for mid h_b and low λ.

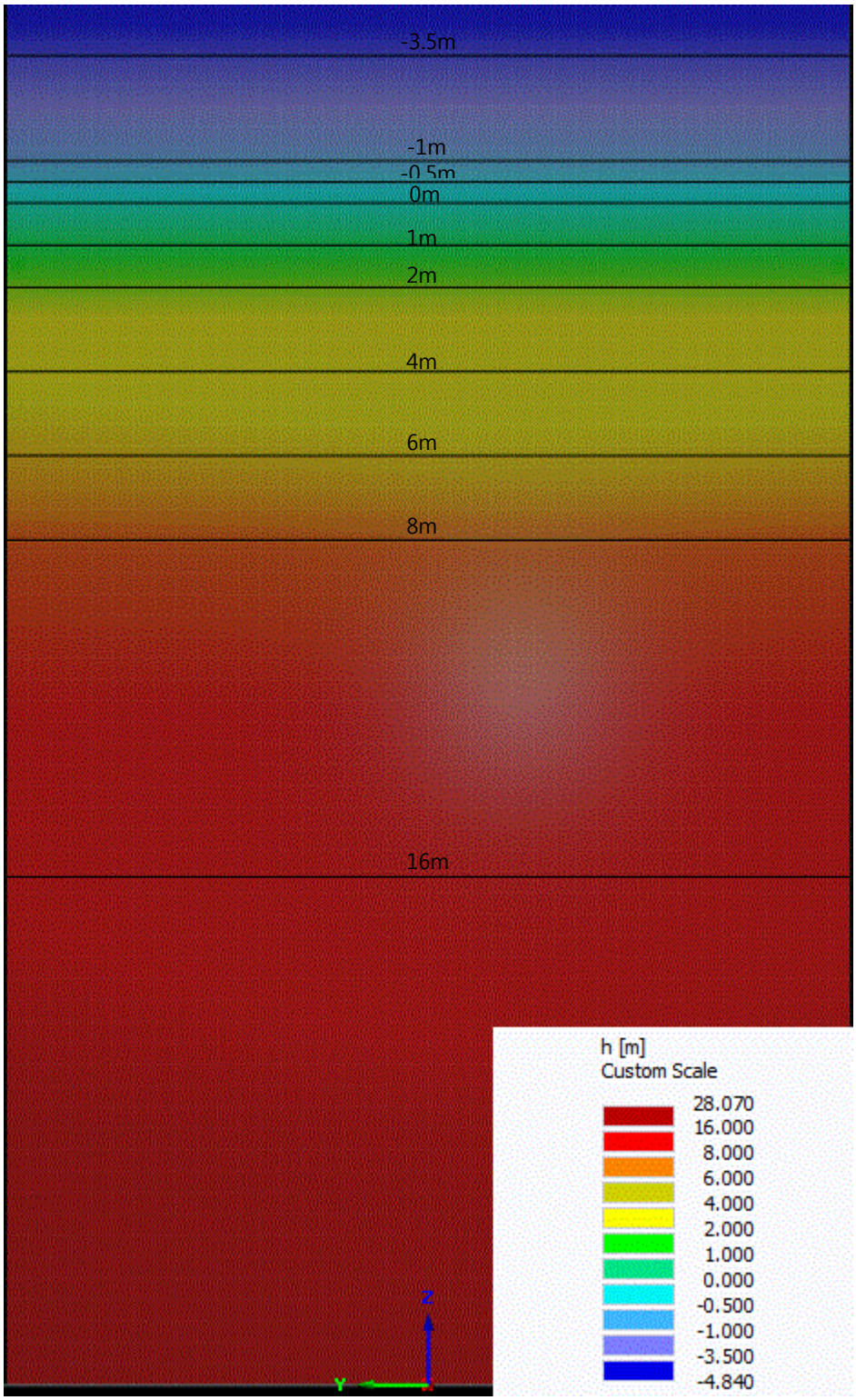

Figure 44: Vertical pressure head distribution after 0 day from 3D HYDRUS model for a cross section at an x-coordinate of 0

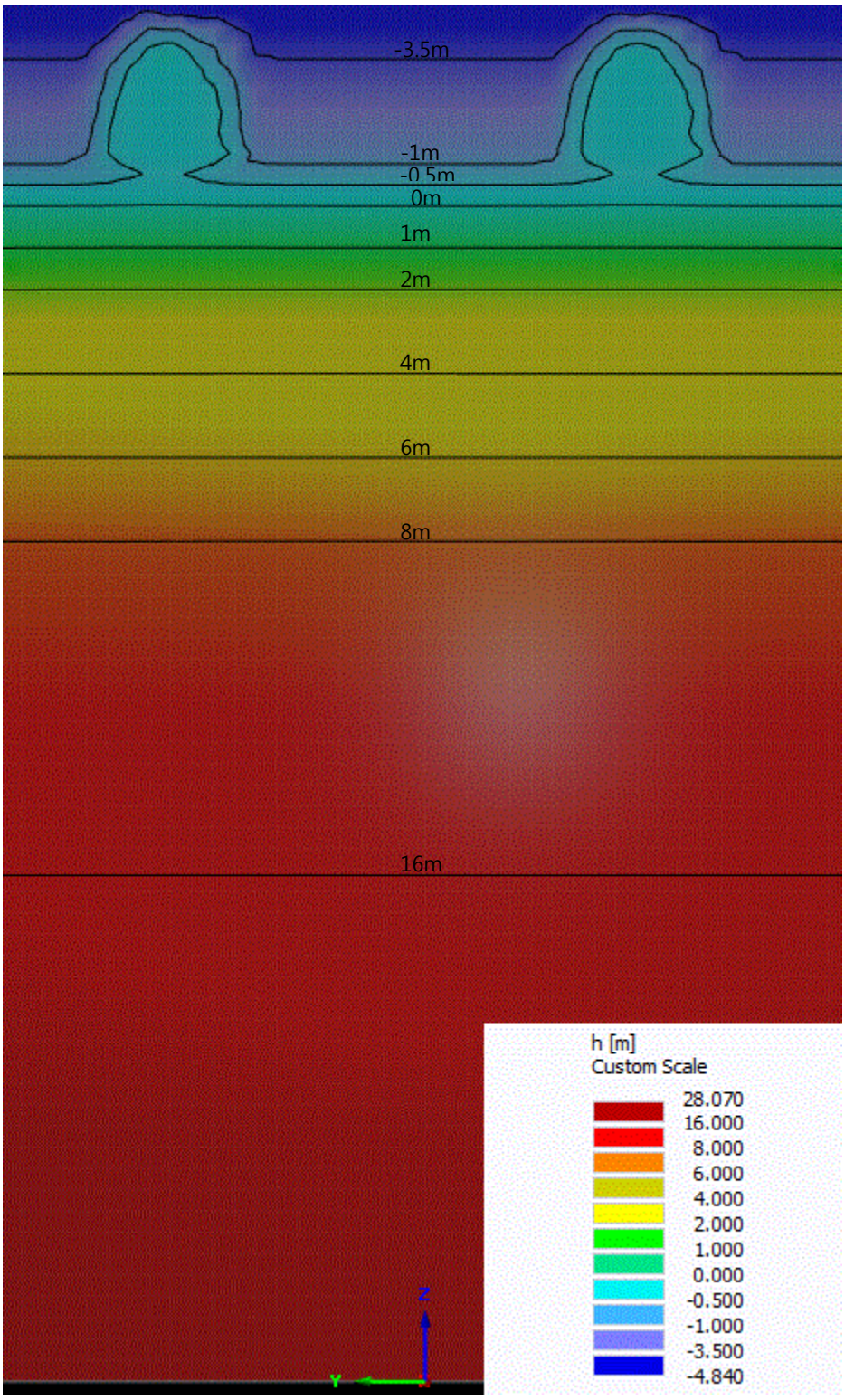

Figure 45: Vertical pressure head distribution after 0.1 day from 3D HYDRUS model for a cross section at an x-coordinate of 0

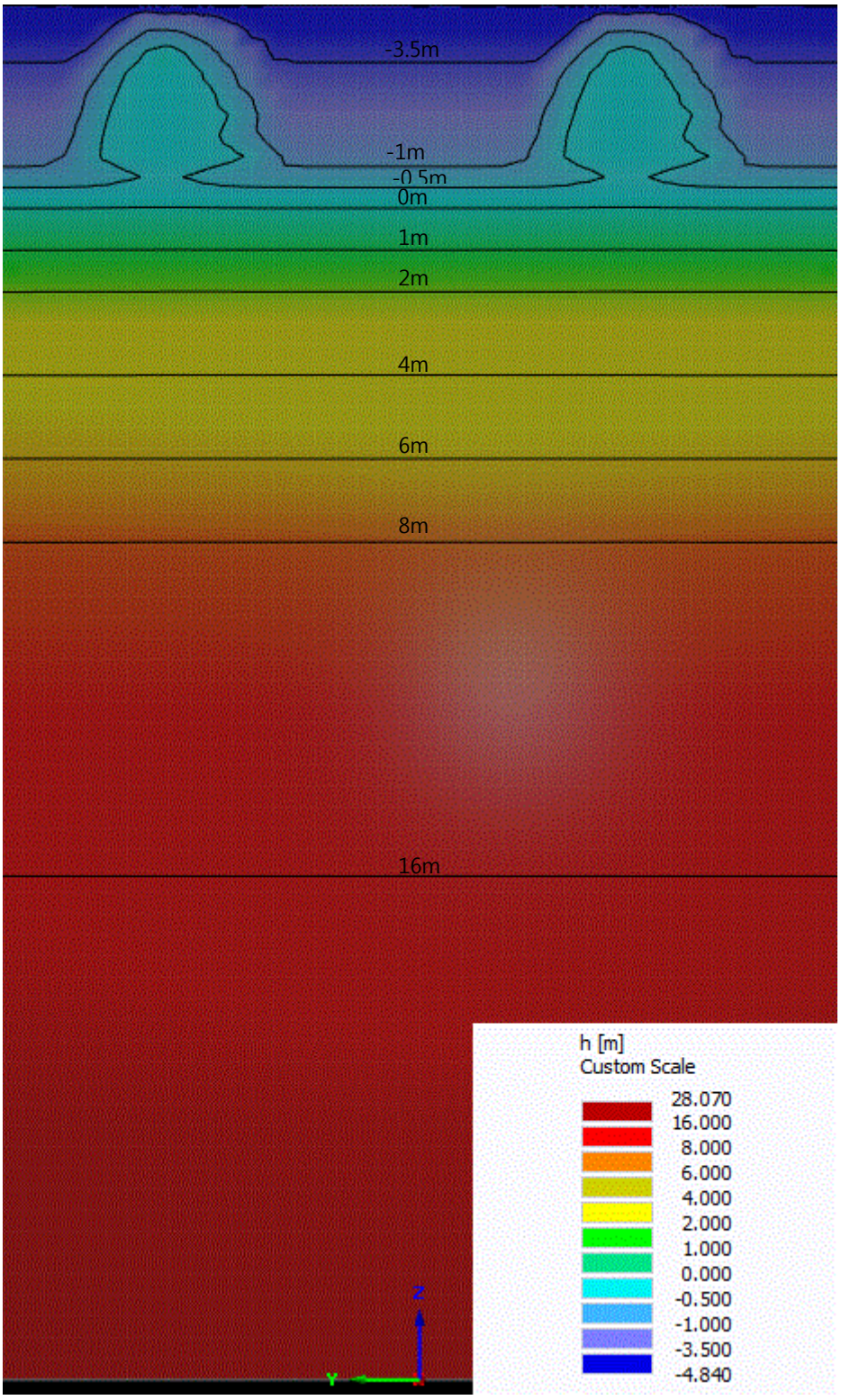

Figure 46: Vertical pressure head distribution after 0.4 day from 3D HYDRUS model for a cross section at an x-coordinate of 0

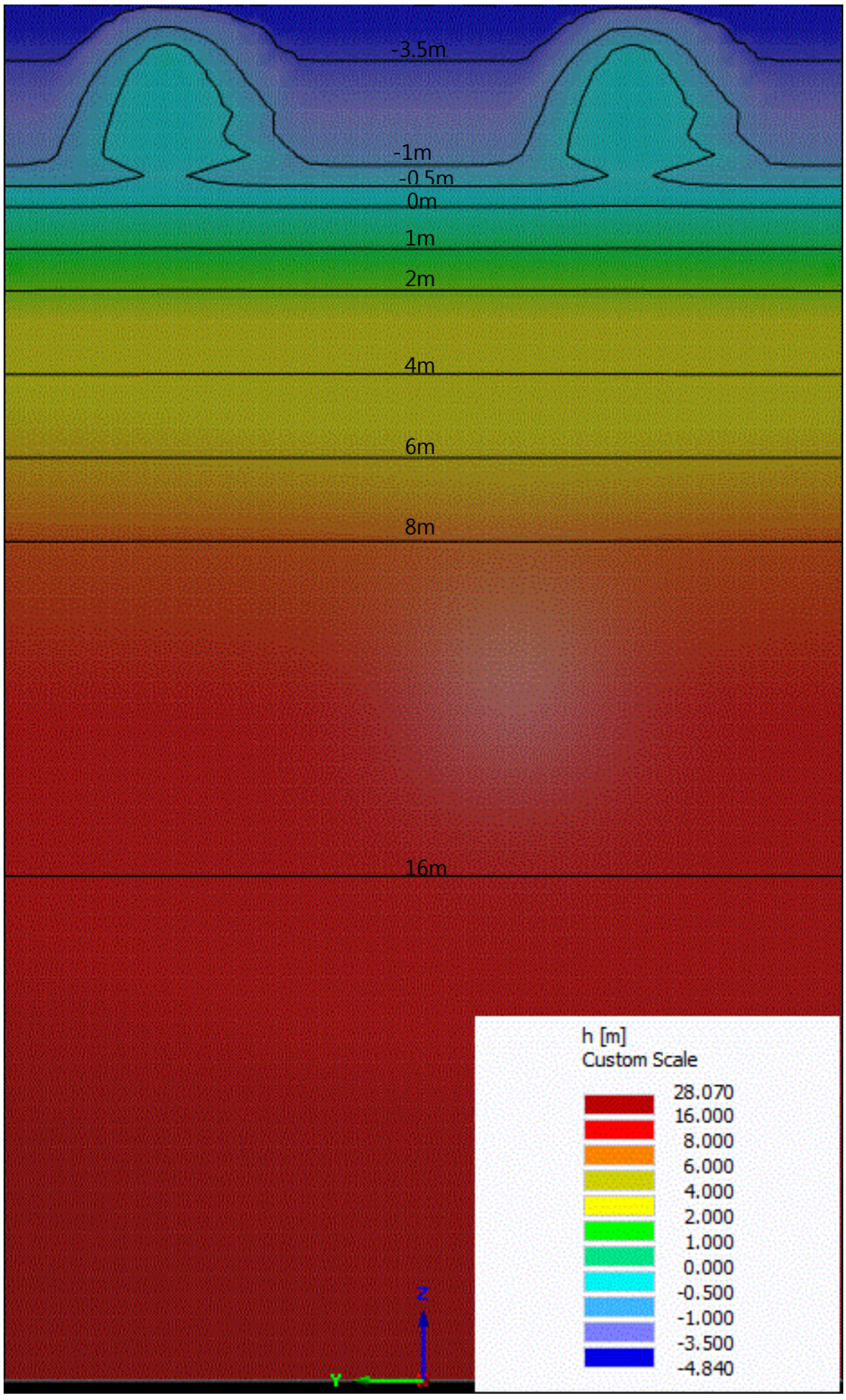

Figure 47: Vertical pressure head distribution after 1 day from 3D HYDRUS modelfor a cross section at an x-coordinate of 0

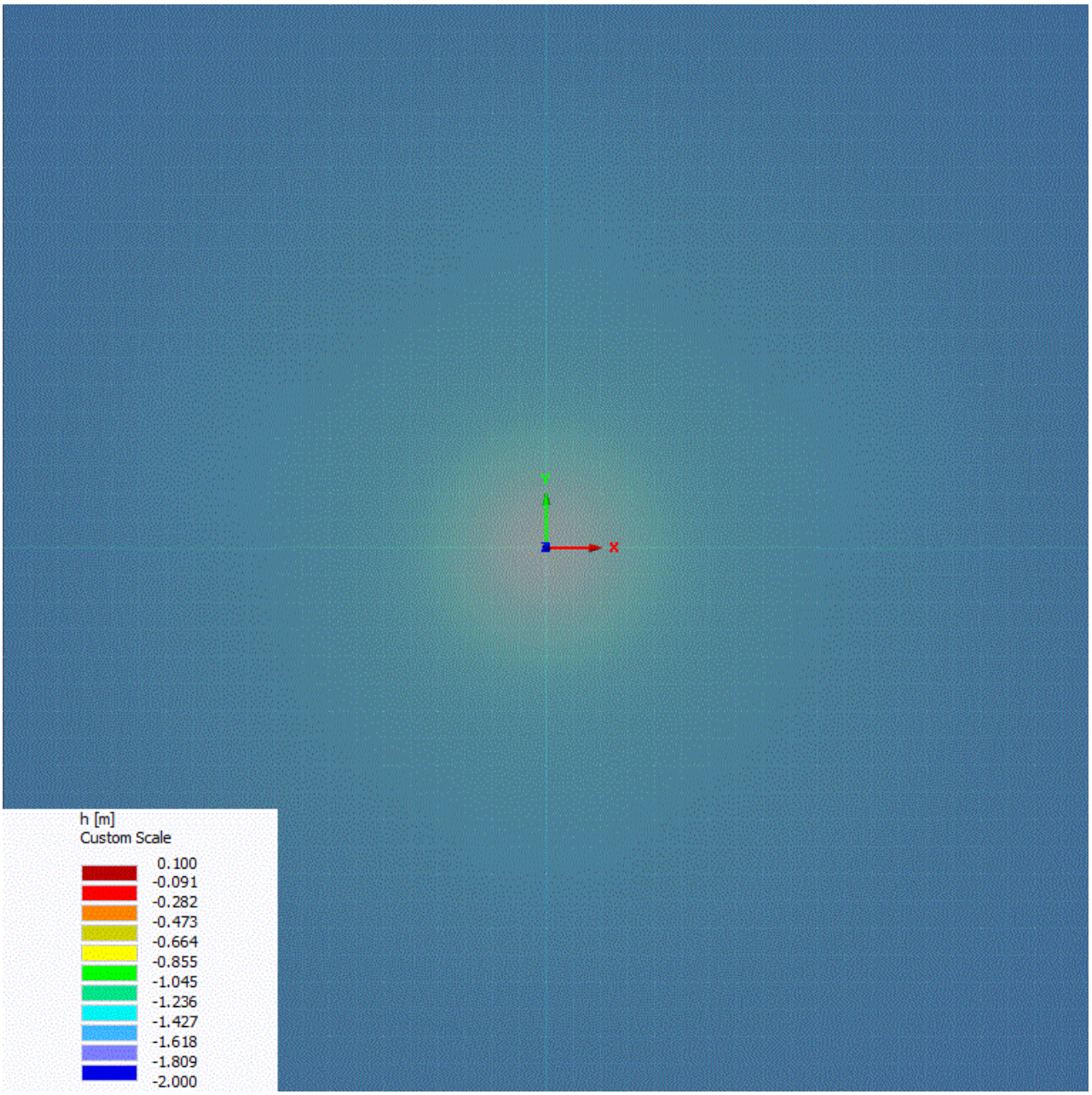

Figure 48: Top view of pressure head distribution after 0 day from 3D HYDRUS model at the depth of 0.75 m below the water table

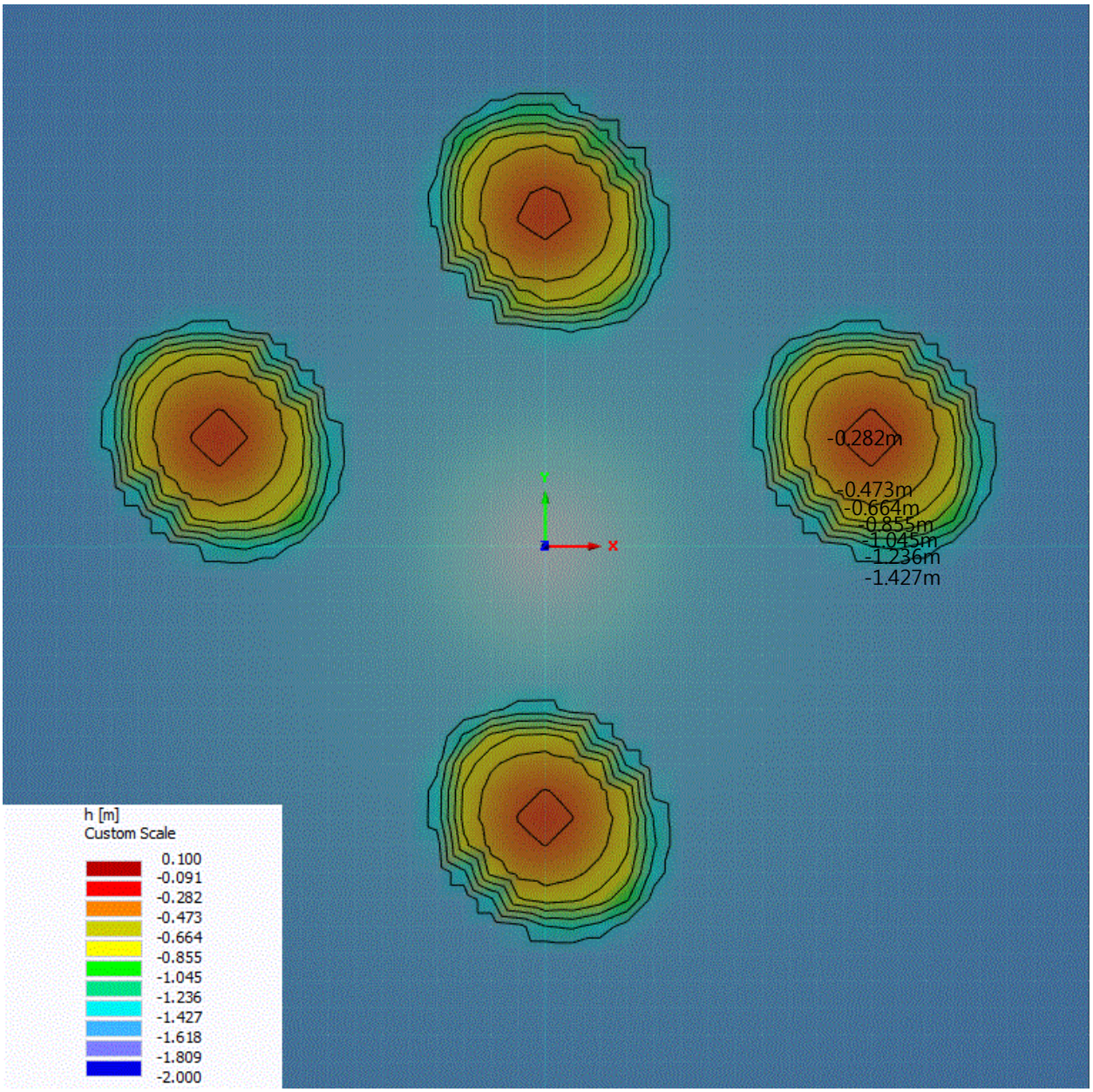

Figure 49: Top view of pressure head distribution after 0.1 day from 3D HYDRUS model at the depth of 0.75 m below the water table

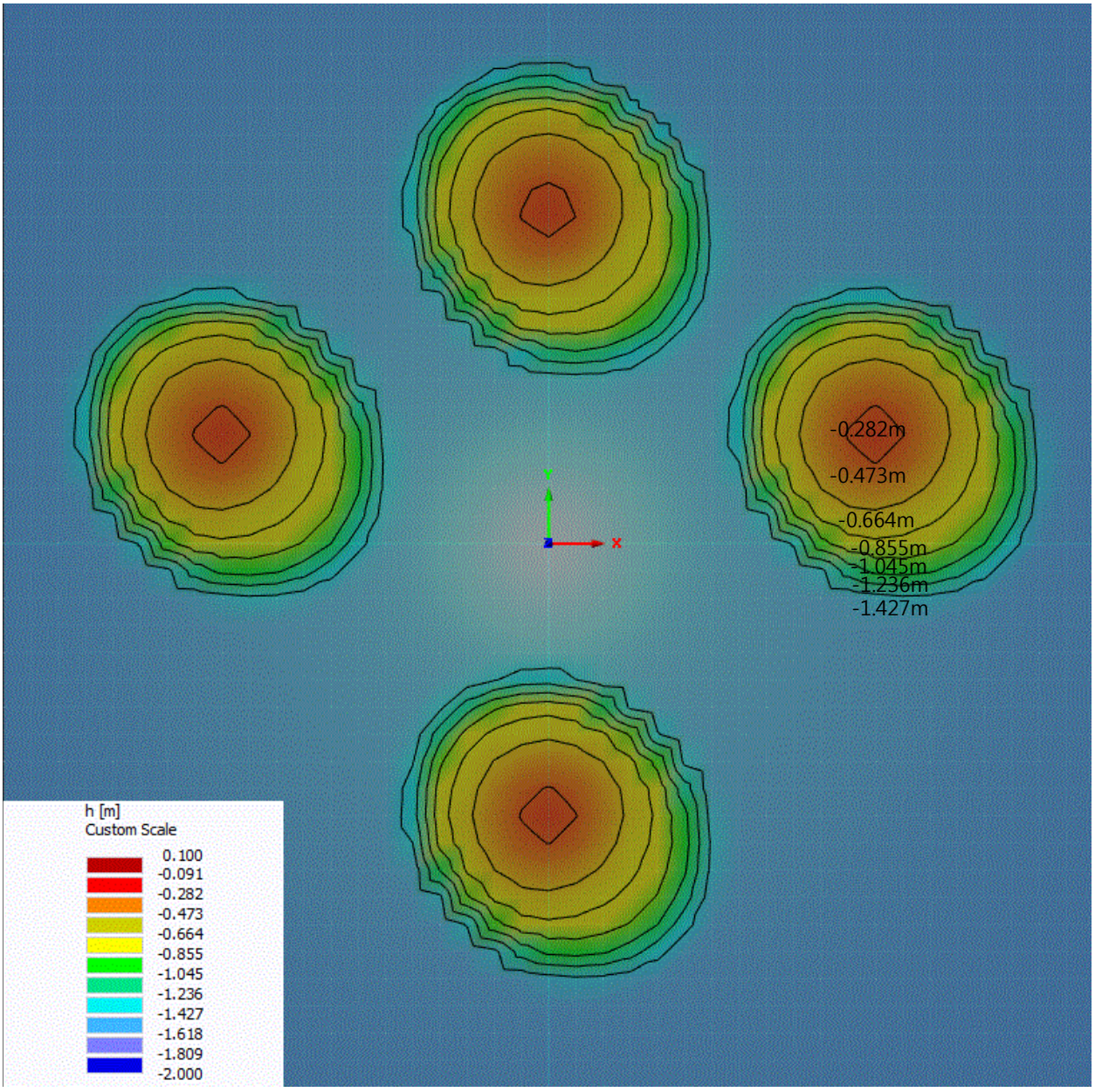

Figure 50: Top view of pressure head distribution after 0.4 day from 3D HYDRUS model at the depth of 0.75 m below the water table

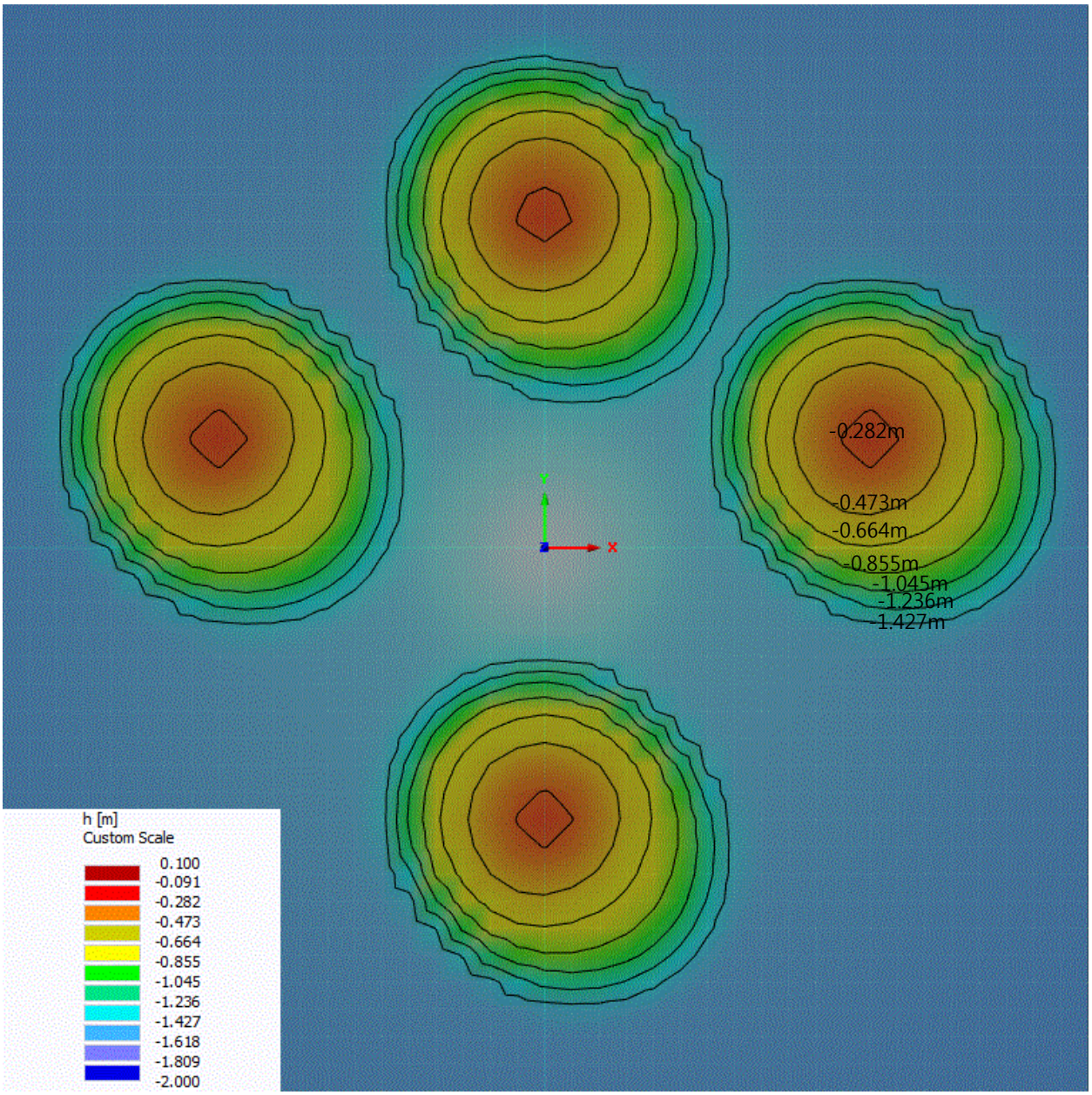

Figure 51: Top view of pressure head distribution after 1 day from 3D HYDRUS model at the depth of 0.75 m below the water table

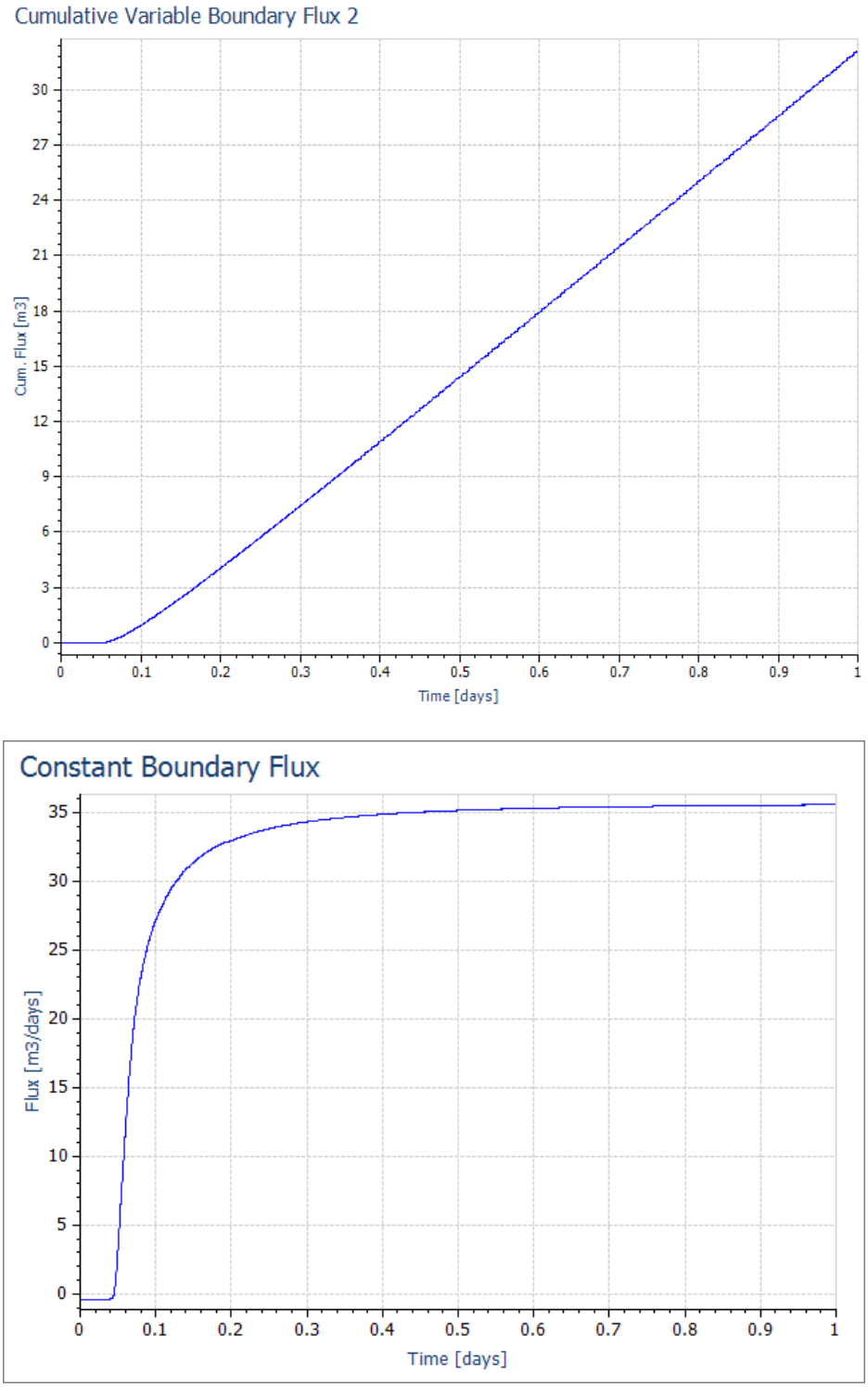

Figure 52: Cumulative flux volume and instantaneous flux to four lateral boundaries from 3D HYDURS model, showing the system approached steady state by 1 day.

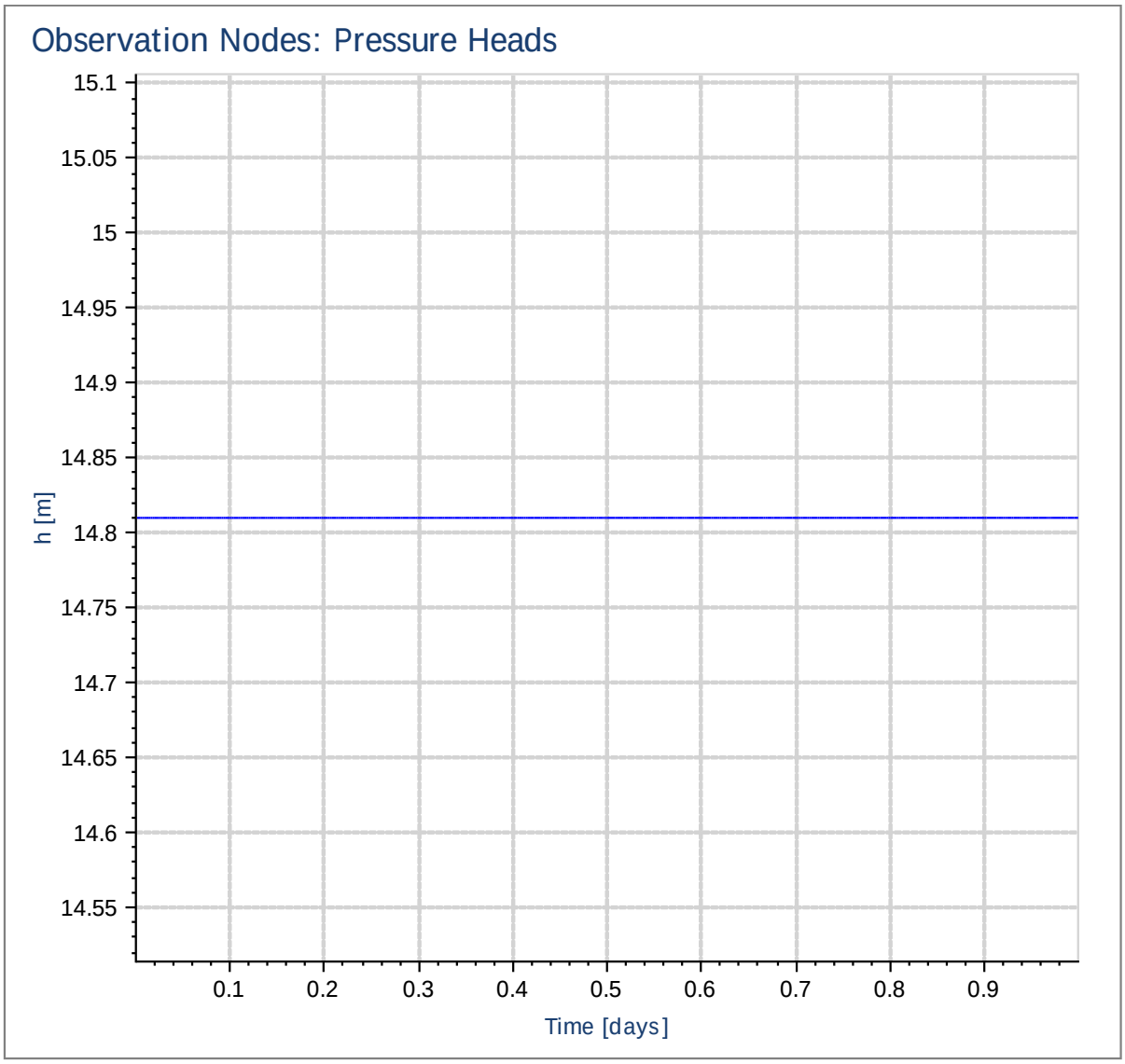

Figure 53: Pressure head changes in the monitoring node from 3D HYDRUS model

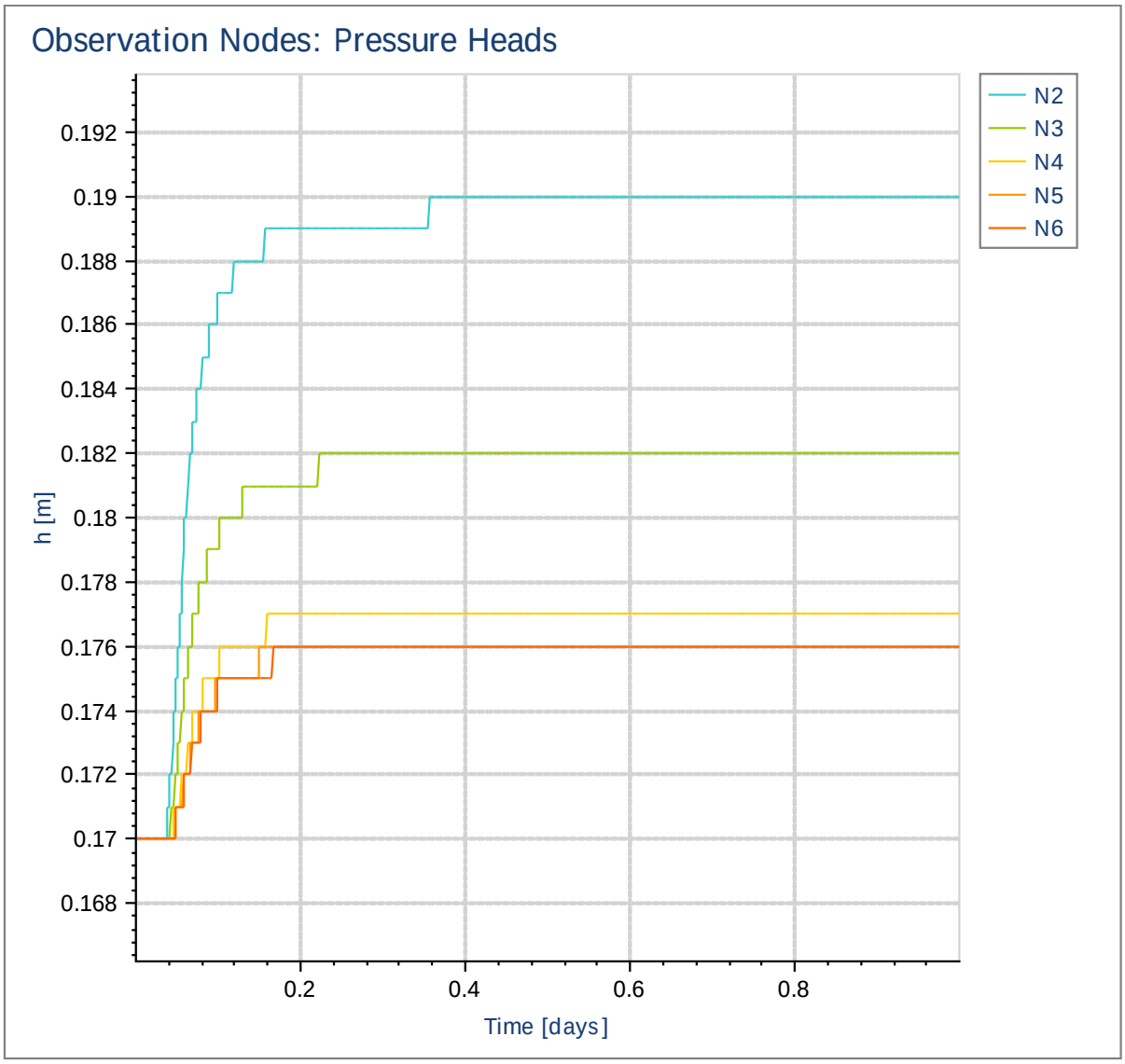

Figure 54: Pressure head changes in the five observation point below the water table from 3D HYDRUS model. N2 is located closest to the vadose-zone well (0 m away in x,y coordinate) and N6 is located furthest from the vadose-zone well (6.32 m away)

APPENDIX A

Geophysical driller's log of the field site

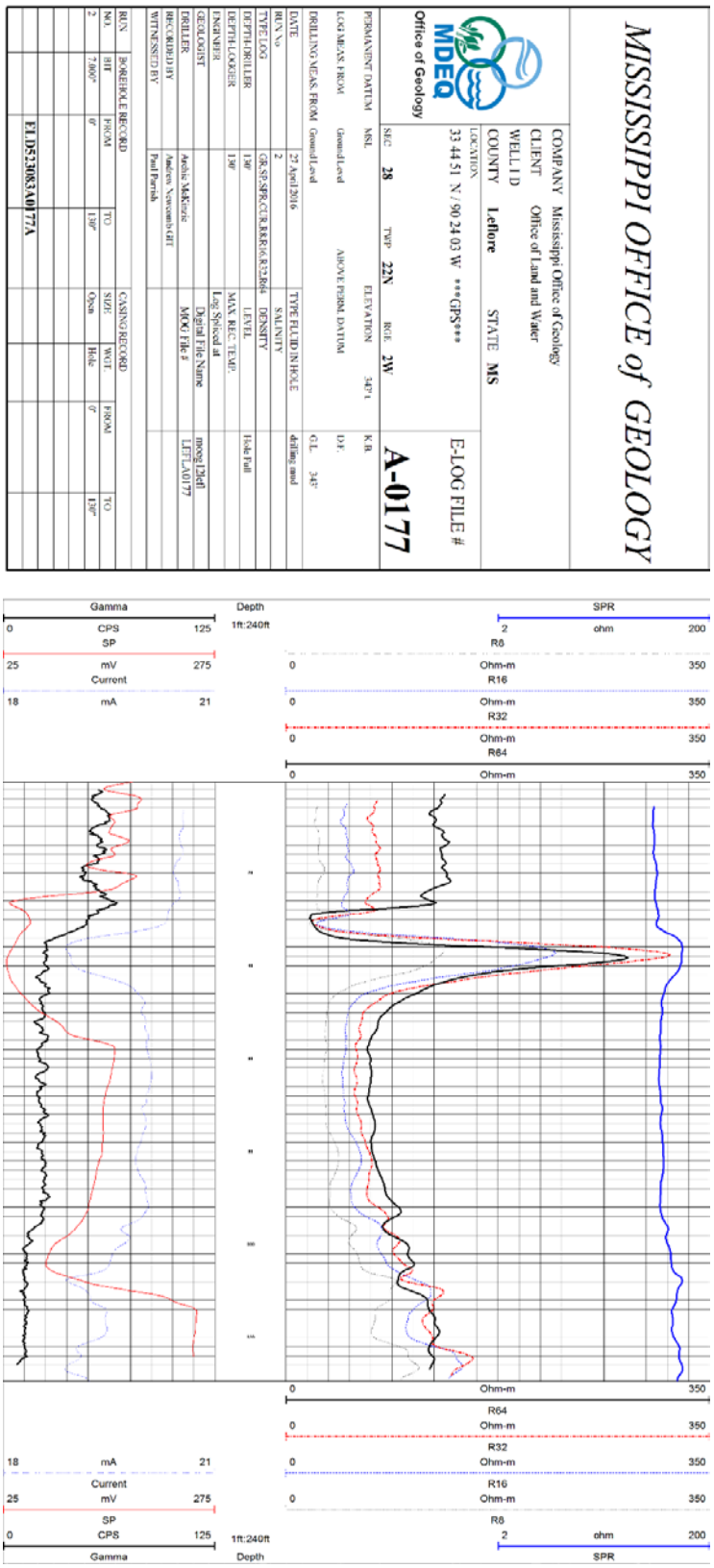

Figure A1: Geophysical driller's log

Table A1: Table of driller's log

Depth	Lithology
Ground level to 9.8 m	Clay
9.8 to 11.9 m	Coarse Sand
11.9 to 17.7 m	Sand and Pea Gravel
17.7 to 18.3 m	Large Gravel
18.3 to 20.7 m	Coarse Sand
20.7 to 29.0 m	Sand and Gravel
29.0 to 39.6 m	Large Gravel

APPENDIX B

Cooper-Jacob Analysis of Pumping Test

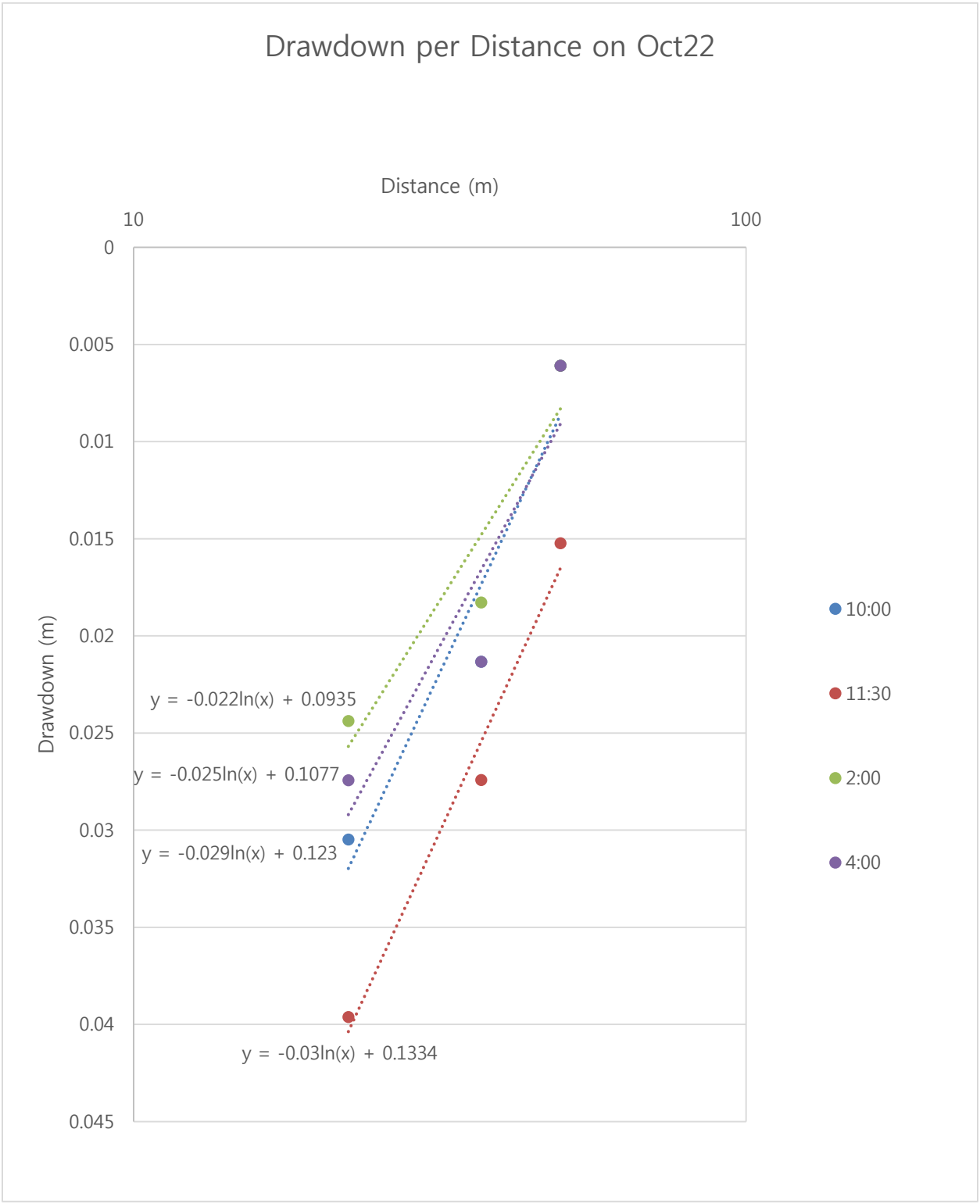

Figure B1: Drawdown per distance Cooper-Jacob method of pumping test on October 22

Table B1: Drawdown data of pumping test on October 22

	M2	M4	M5	M6
Initial H	24.67228	24.67863	24.6914	24.6734
10:00	24.6418	24.65729	24.6853	24.66426
11:30	24.63266	24.6512	24.67616	24.64902
2:00	24.6479	24.66034	24.6853	24.64902
4:00	24.64485	24.65729	24.6853	24.64597
Actual Drawdown				
10:00	0.03048	0.021336	0.006096	0.009144
11:30	0.039622	0.027427	0.015236	0.024385
2:00	0.024384	0.018288	0.006096	0.024384
4:00	0.027432	0.021336	0.006096	0.027432

Initial heads and drawdown at each time at each monitoring wells on October 22 are given in the table above. Using drawdown versus distance method from Copper – Jacob analysis, the transmissivity was calculated as 7800 m^2/day. Given the thickness of the aquifer as 39.62 m, the hydraulic conductivity is calculated as 220 m/day which is in the range of typical coarse sand. The calculated storativity of the aquifer was 0.22 which is in the range of typical unconfined aquifer (0.1 – 0.3)

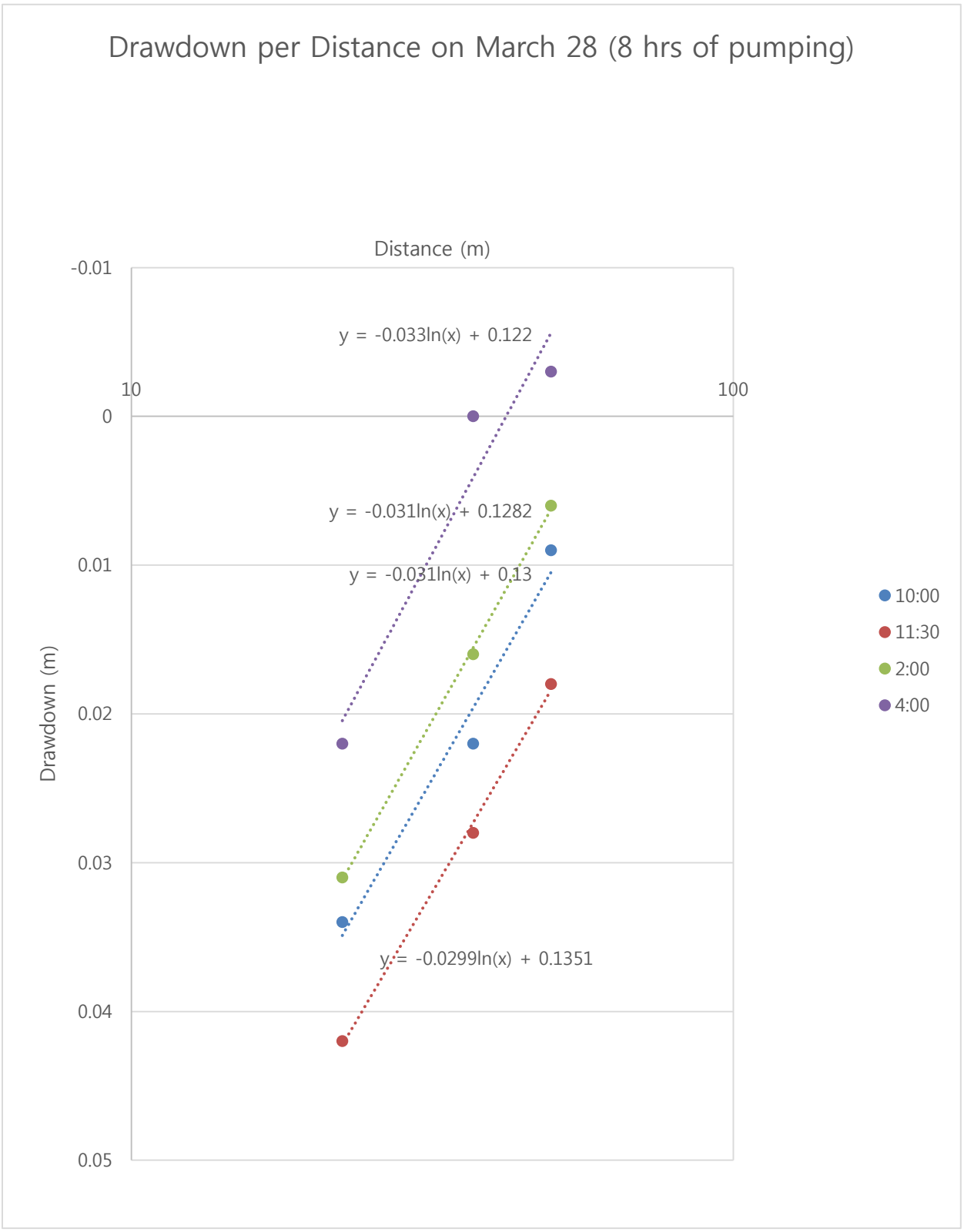

Figure B2: Drawdown per distance Cooper-Jacob method of pumping test on March 28

Table B2: Drawdown data of pumping test on March 28

	M2	M4	M5
Initial H	25.114	25.121	25.136
10:00	25.08	25.099	25.127
11:30	25.072	25.093	25.118
2:00	25.083	25.105	25.13
4:00	25.092	25.114	25.139
Actual Drawdown			
10:00	0.034	0.022	0.009
11:30	0.042	0.028	0.018
2:00	0.031	0.016	0.006
4:00	0.022	0	-0.003

Initial heads and drawdown at each time at each monitoring wells on March 28 are given in the table above. Using drawdown versus distance method from Copper – Jacob analysis, the transmissivity was calculated as 5900 m^2/day. Given the thickness of the aquifer as 39.62 m, the hydraulic conductivity is calculated as 147 m/day which is in the range of typical coarse sand. The calculated storativity of the aquifer was 0.19.

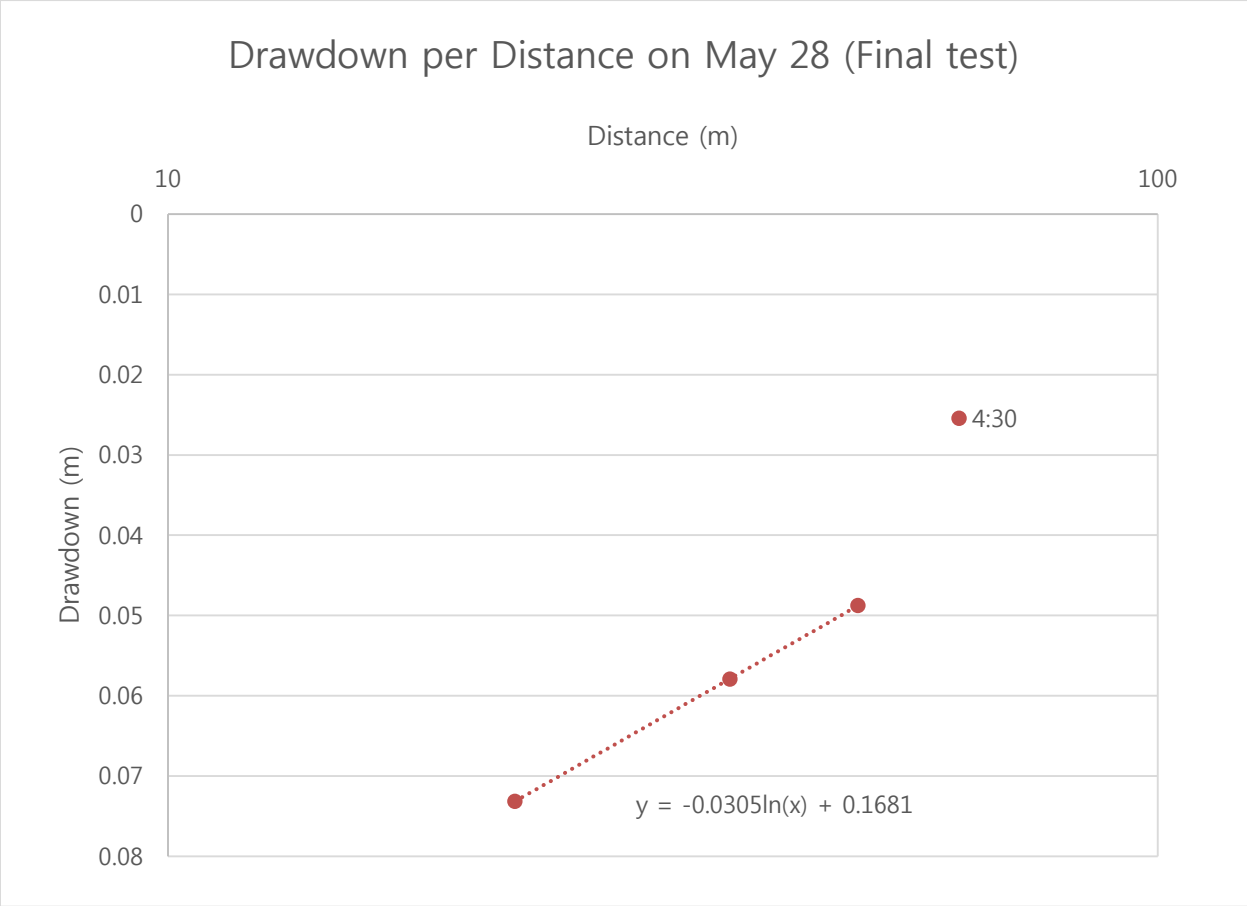

Figure B3: Drawdown per distance Cooper-Jacob method of pumping test on May 28

Table B3: Drawdown data of pumping test on May 28

	M2	M4	M5
Initial H	25.29103	25.29738	25.31929
4:30	25.21788	25.23947	25.27052
Actual Drawdown			
4:30	0.07315	0.05791	0.04877
	Transmissivity (T)		Delta s
4:30		5682.149	0.030547
	Storativity (S)		r0
4:30		0.035582	245.7959

Initial heads and drawdown at each monitoring wells on May 28 are given in the table above. Using drawdown versus distance method from Copper – Jacob analysis, the transmissivity was calculated as 5700 m^2/day. Given the thickness of the aquifer as 39.62 m, the hydraulic conductivity is calculated as 143 m/day which is in the range of typical coarse sand. The calculated storativity of the aquifer was 0.03 which was much smaller than other tests. This result is due to larger drawdowns during this test.

APPENDIX C

Manual Tapedown Data from Final Pumping Test

Table C1: Manual tapedown data of final field test. Water level is above mean sea level.

Time	WL elev–M2(m)	Time	WL elev–M4(m)	Time	WL elev–M5(m)
2019-05-29 8:44	25.227	2019-05-29 8:42	25.245	2019-05-29 8:40	25.273
2019-05-29 9:41	25.229	2019-05-29 9:38	25.247	2019-05-29 9:35	25.269
2019-05-29 10:39	25.231	2019-05-29 10:36	25.251	2019-05-29 13:01	25.281
2019-05-29 13:09	25.254	2019-05-29 13:02	25.265	2019-05-29 15:05	25.298
2019-05-29 15:11	25.273	2019-05-29 15:07	25.283	2019-05-29 17:05	25.299
2019-05-29 17:08	25.279	2019-05-29 17:06	25.287	2019-05-29 20:11	25.296
2019-05-29 20:08	25.274	2019-05-29 20:12	25.281	2019-05-30 8:54	25.282
2019-05-30 8:50	25.255	2019-05-30 8:56	25.262	2019-05-30 11:02	25.275
2019-05-30 11:07	25.248	2019-05-30 11:04	25.26	2019-05-30 13:05	25.281
2019-05-30 13:09	25.254	2019-05-30 13:04	25.266	2019-05-30 15:08	25.288
2019-05-30 15:13	25.257	2019-05-30 15:10	25.27	2019-05-30 17:08	25.289
2019-05-30 17:16	25.255	2019-05-30 17:09	25.269	2019-05-30 18:30	25.282
2019-05-30 18:35	25.249	2019-05-30 18:32	25.26	2019-05-31 7:08	25.221
2019-05-31 7:12	25.19	2019-05-31 7:09	25.204	2019-05-31 9:12	25.209
2019-05-31 9:15	25.185	2019-05-31 9:05	25.204	2019-05-31 10:07	25.22
2019-05-31 10:20	25.187	2019-05-31 10:10	25.203	2019-05-31 12:03	25.218
2019-05-31 12:08	25.19	2019-05-31 12:05	25.202		

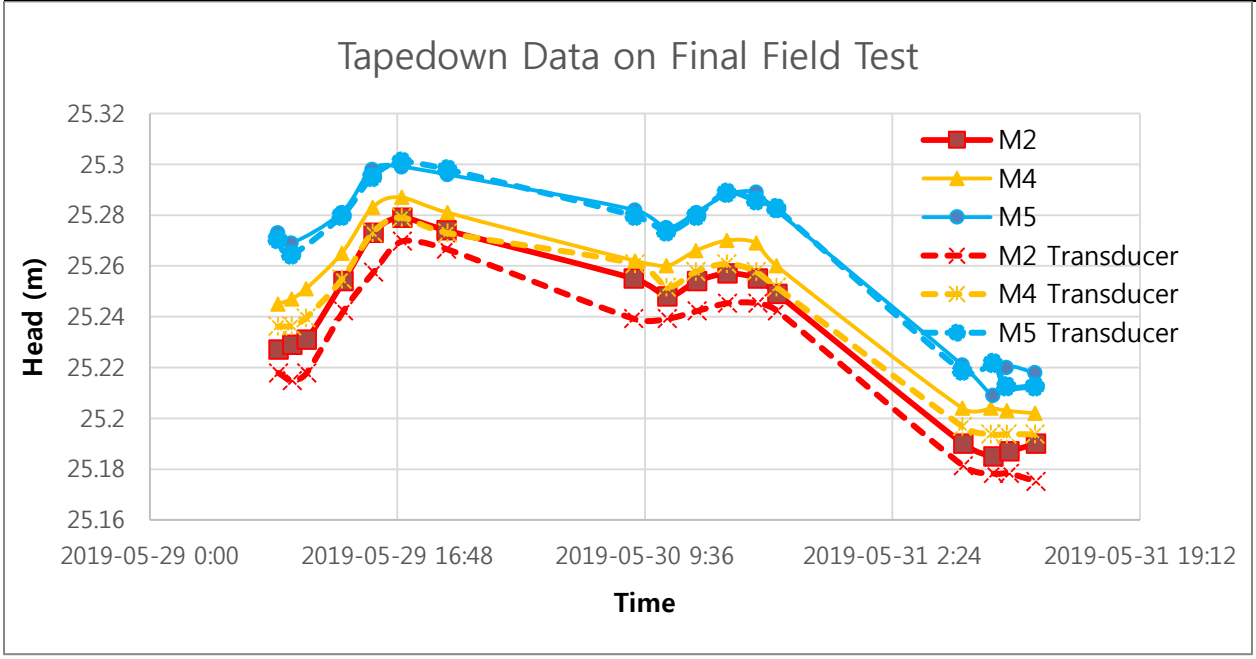

Figure C1: Comparison of manual tapedown data and transducer data

APPENDIX D

Barometric Efficiency Correction

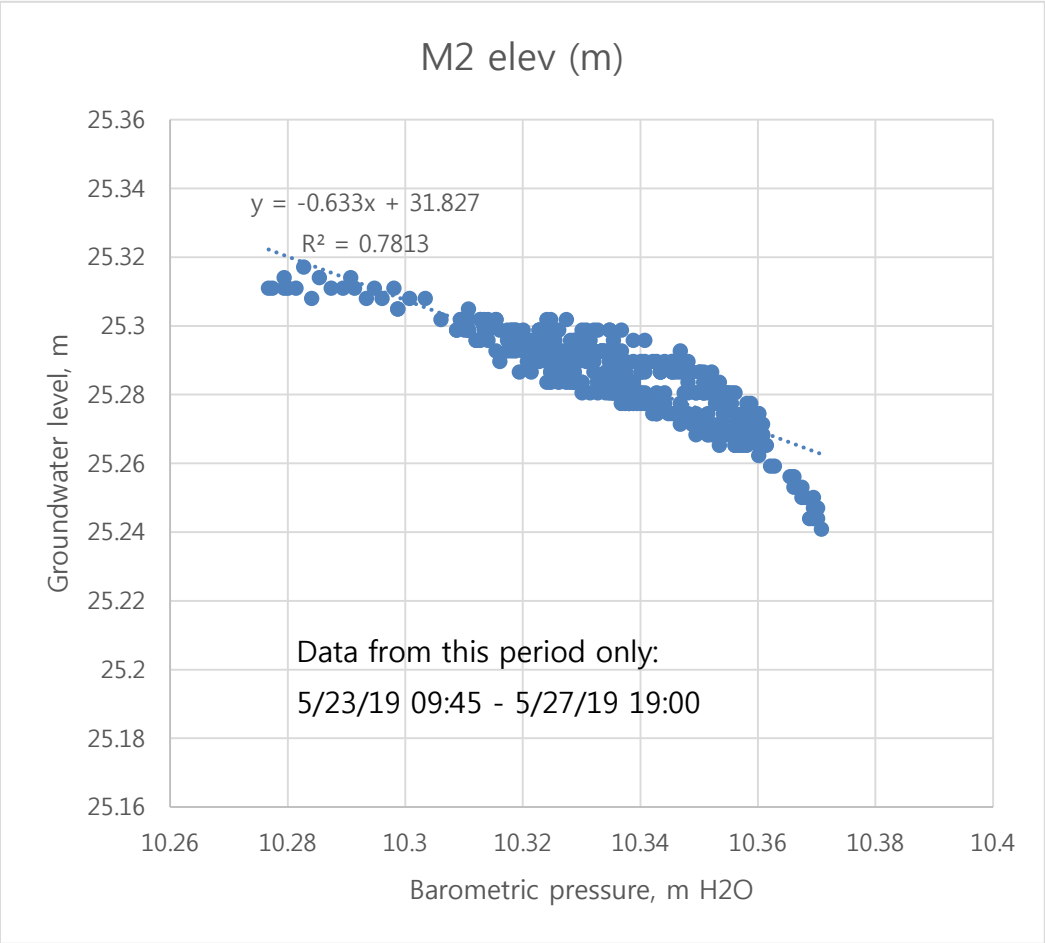

Figure D1: Pearson method of M2 data

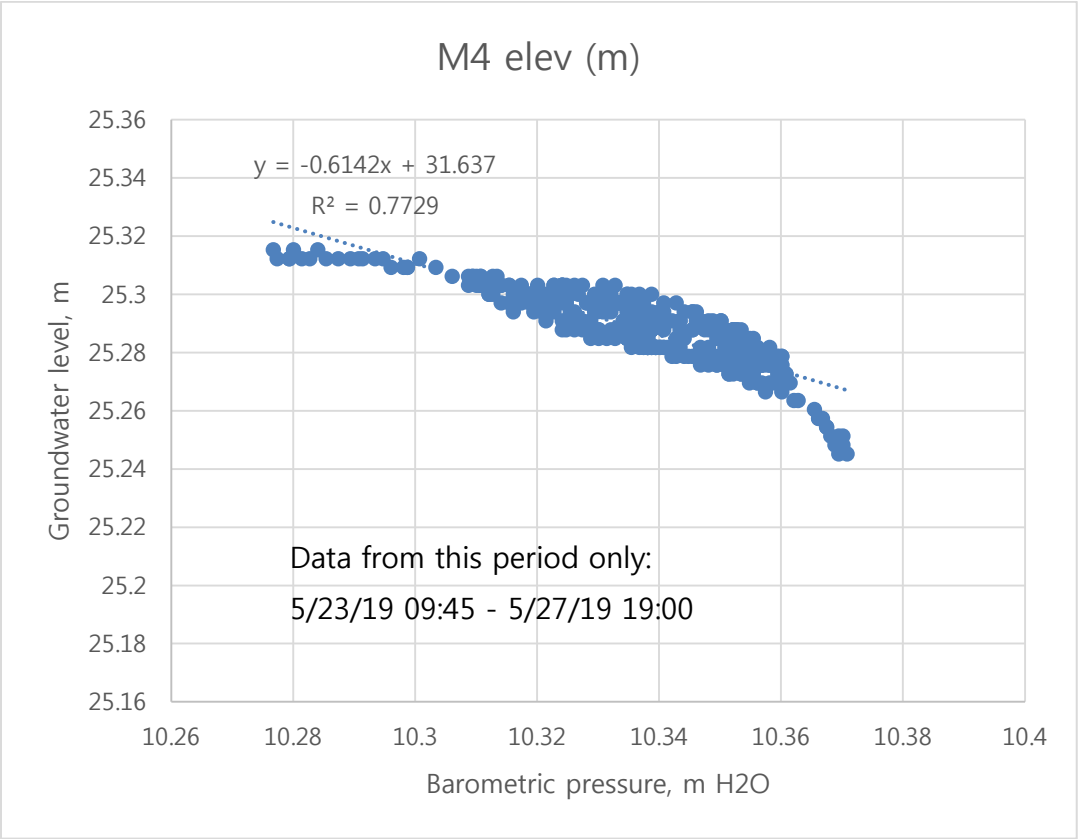

Figure D2: Pearson method of M4 data

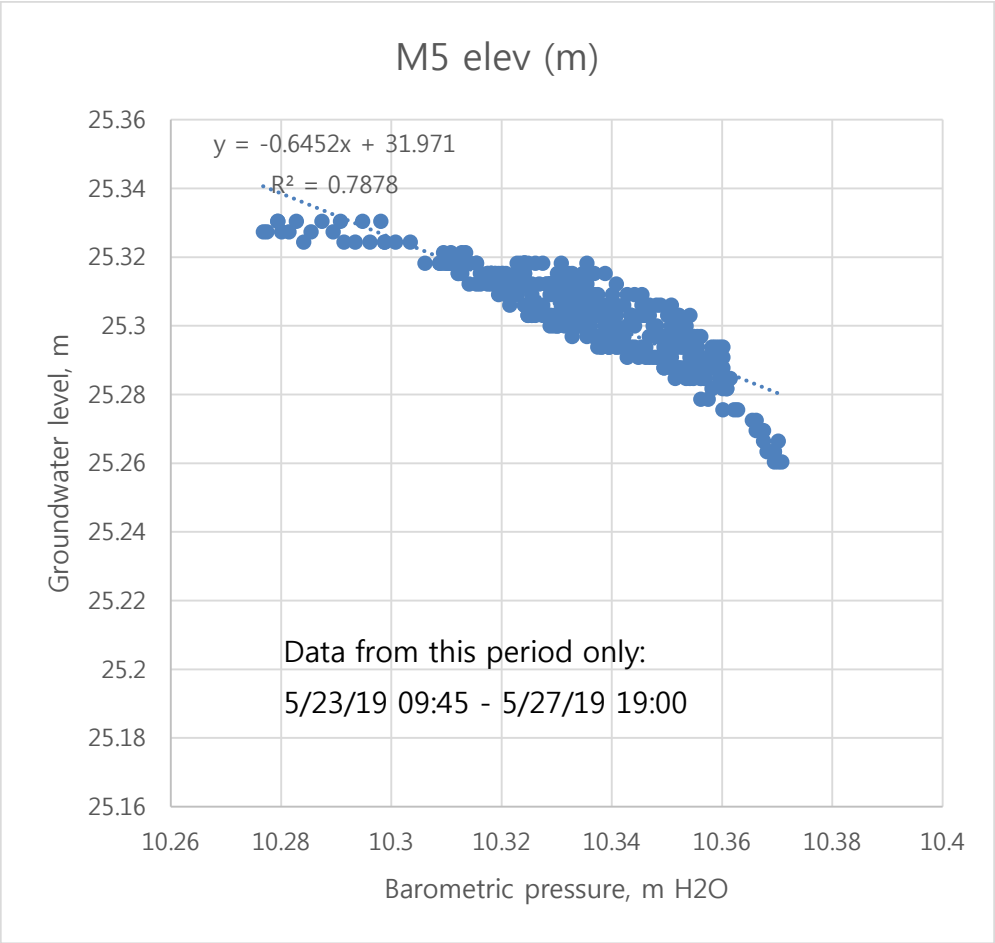

FigureD3: Pearson method of M5 data

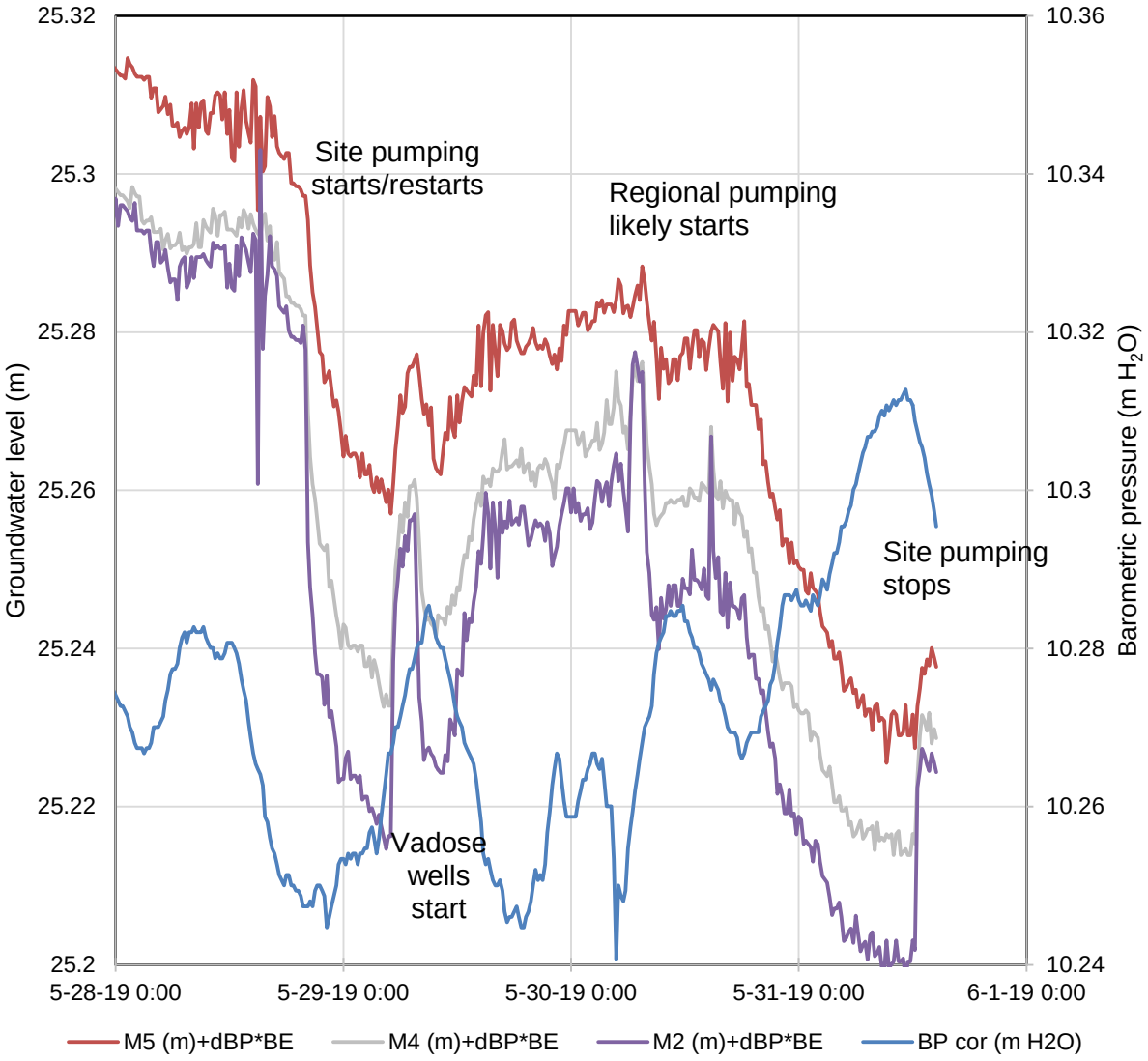

Figure D2: Barometric efficiency corrected water table data

APPENDIX E

Falling Head Permeability Tests

Table E1: Pressure head results of sample A3 from falling head permeability test. Flow rate was calculated as 0.023 ml/min and K_{sat} was 0.0021 meters/day

Date	Time	Elapsed Time (min)	Pressure (cmH2O)	Total Water Consumed (ml)
6/28/2018	8:55:36 PM	0.01	42.6	
6/28/2018	8:56:33 PM	0.95	42.5	2.1
6/28/2018	9:04:48 PM	9.2	42.4	4.1
6/28/2018	9:21:22 PM	25.78	42.3	6.2
6/28/2018	11:03:38 PM	128.05	42.1	10.3
6/29/2018	12:13:12 AM	197.61	42	12.4
6/29/2018	12:34:42 AM	219.1	41.9	14.5
6/29/2018	1:01:53 AM	246.28	41.8	16.5
6/29/2018	5:52:00 AM	536.4	41.6	20.7
6/29/2018	6:07:44 AM	552.13	41.5	22.7
6/29/2018	6:10:51 AM	555.26	41.4	24.8
6/29/2018	6:45:02 AM	589.44	41.3	26.9
6/29/2018	9:42:49 AM	767.22	41.1	31
6/29/2018	11:05:17 AM	849.69	41	33.1
6/29/2018	12:39:20 PM	943.74	40.9	35.1
6/29/2018	2:22:53 PM	1047.3	40.8	37.2
6/29/2018	5:52:53 PM	1257.29	40.6	41.3
6/29/2018	7:26:45 PM	1351.15	40.5	43.4
6/29/2018	9:15:59 PM	1460.38	40.4	45.5
6/29/2018	11:50:08 PM	1614.54	40.3	47.5
6/30/2018	4:19:04 AM	1883.48	40.1	51.7
6/30/2018	5:53:50 AM	1978.24	40	53.7
6/30/2018	7:37:39 AM	2082.05	39.9	55.8
6/30/2018	9:12:17 AM	2176.69	39.8	57.9
6/30/2018	5:04:23 PM	2648.79	39.6	62

Table E2: Pressure head results of Sample A8 from falling head permeability test. Flow rate was calculated as 0.098 ml/min and K_{sat} was 0.02 meters/day

Date	Time	Elapsed Time (min)	Pressure (cmH2O)	Total Water Consumed (ml)
10/17/2018	4:40:06 PM	0	37.5	
10/17/2018	4:40:28 PM	0.38	37.4	2.1
10/17/2018	4:41:10 PM	1.06	37.3	4.1
10/17/2018	4:43:37 PM	3.53	37.1	8.3
10/17/2018	4:43:38 PM	3.54	37	10.3
10/17/2018	4:43:39 PM	3.56	36.8	14.5
10/17/2018	4:43:40 PM	3.58	36.6	18.6
10/17/2018	4:43:49 PM	3.72	36.5	20.7
10/17/2018	4:45:47 PM	5.7	36.4	22.7
10/17/2018	4:47:37 PM	7.53	36.3	24.8
10/17/2018	4:50:52 PM	10.78	36.1	28.9
10/17/2018	4:53:04 PM	12.97	36	31
10/17/2018	4:55:33 PM	15.46	35.9	33.1
10/17/2018	4:56:45 PM	16.66	35.8	35.1
10/17/2018	5:02:56 PM	22.84	35.6	39.3
10/17/2018	5:05:40 PM	25.57	35.5	41.3
10/17/2018	5:08:13 PM	28.13	35.4	43.4
10/17/2018	5:11:18 PM	31.2	35.3	45.5
10/17/2018	5:17:05 PM	36.99	35.1	49.6
10/17/2018	5:21:58 PM	41.87	35	51.7
10/17/2018	5:23:51 PM	43.75	34.9	53.7
10/17/2018	5:29:35 PM	49.49	34.8	55.8
10/17/2018	5:42:38 PM	62.54	34.6	59.9
10/17/2018	5:47:34 PM	67.47	34.5	62
10/17/2018	5:53:31 PM	73.42	34.4	64.1
10/17/2018	5:57:22 PM	77.27	34.3	66.1
10/17/2018	6:04:21 PM	84.26	34.1	70.3
10/17/2018	6:07:52 PM	87.77	34	72.3
10/17/2018	6:12:03 PM	91.95	33.9	74.4

10/17/2018	6:18:30 PM	98.4	33.8	76.5
10/17/2018	6:28:58 PM	108.87	33.6	80.6
10/17/2018	6:36:02 PM	115.95	33.5	82.7
10/17/2018	6:44:01 PM	123.92	33.4	84.7
10/17/2018	6:50:59 PM	130.9	33.3	86.8
10/17/2018	7:08:55 PM	148.83	33.1	90.9
10/17/2018	7:17:08 PM	157.05	33	93
10/17/2018	7:25:54 PM	165.81	32.9	95.1
10/17/2018	7:35:44 PM	175.65	32.8	97.1
10/17/2018	7:50:02 PM	189.93	32.6	101.3
10/17/2018	8:00:38 PM	200.54	32.5	103.3
10/17/2018	8:11:53 PM	211.79	32.4	105.4
10/17/2018	8:17:39 PM	217.56	32.3	107.5
10/17/2018	8:40:42 PM	240.6	32.1	111.6
10/17/2018	8:52:58 PM	252.88	32	113.7
10/17/2018	9:01:13 PM	261.12	31.9	115.7
10/17/2018	9:11:02 PM	270.93	31.8	117.8
10/17/2018	9:30:57 PM	290.85	31.6	121.9
10/17/2018	9:42:43 PM	302.63	31.5	124
10/17/2018	9:55:08 PM	315.05	31.4	126.1
10/17/2018	10:09:42 PM	329.6	31.3	128.1
10/17/2018	10:31:23 PM	351.29	31.1	132.3
10/17/2018	10:42:05 PM	362	31	134.4
10/17/2018	10:54:03 PM	373.96	30.9	136.4
10/17/2018	11:07:51 PM	387.75	30.8	138.5
10/17/2018	11:28:39 PM	408.55	30.6	142.6
10/17/2018	11:42:17 PM	422.19	30.5	144.7
10/17/2018	11:55:51 PM	435.76	30.4	146.8
10/18/2018	12:04:08 AM	444.04	30.3	148.8
10/18/2018	12:35:28 AM	475.38	30.1	153
10/18/2018	12:47:19 AM	487.22	30	155
10/18/2018	1:03:00 AM	502.91	29.9	157.1
10/18/2018	1:15:23 AM	515.29	29.8	159.2
10/18/2018	1:45:40 AM	545.57	29.6	163.3
10/18/2018	1:58:00 AM	557.91	29.5	165.4

10/18/2018	2:13:48 AM	573.7	29.4	167.4
10/18/2018	2:27:55 AM	587.82	29.3	169.5
10/18/2018	2:55:07 AM	615.03	29.1	173.6
10/18/2018	3:07:13 AM	627.12	29	175.7
10/18/2018	3:23:25 AM	643.31	28.9	177.8
10/18/2018	3:34:35 AM	654.48	28.8	179.8
10/18/2018	4:05:05 AM	684.99	28.6	184
10/18/2018	4:17:07 AM	697.02	28.5	186
10/18/2018	4:33:13 AM	713.13	28.4	188.1
10/18/2018	4:42:43 AM	722.62	28.3	190.2
10/18/2018	5:13:33 AM	753.45	28.1	194.3
10/18/2018	5:29:27 AM	769.35	28	196.4
10/18/2018	5:43:29 AM	783.38	27.9	198.4
10/18/2018	5:57:05 AM	796.99	27.8	200.5
10/18/2018	8:00:12 AM	920.11	27.6	204.6
10/18/2018	8:09:39 AM	929.56	27.5	206.7
10/18/2018	8:34:52 AM	954.77	27.4	208.8
10/18/2018	8:38:41 AM	958.58	27.3	210.8
10/18/2018	8:46:23 AM	966.29	27.1	215
10/18/2018	8:57:41 AM	977.59	27	217
10/18/2018	9:11:47 AM	991.7	26.9	219.1
10/18/2018	9:29:27 AM	1009.36	26.8	221.2
10/18/2018	10:03:09 AM	1043.06	26.6	225.3
10/18/2018	10:34:45 AM	1074.65	26.5	227.4
10/18/2018	10:51:03 AM	1090.95	26.4	229.4
10/18/2018	11:07:52 AM	1107.77	26.3	231.5
10/18/2018	11:54:56 AM	1154.84	26.1	235.6
10/18/2018	12:38:25 PM	1198.33	26	237.7
10/18/2018	1:24:59 PM	1244.89	25.9	239.8
10/18/2018	2:21:45 PM	1301.66	25.7	243.9
10/18/2018	2:50:03 PM	1329.95	25.5	248
10/18/2018	3:02:19 PM	1342.22	25.4	250.1
10/18/2018	4:10:34 PM	1410.48	25.2	254.2
10/18/2018	4:48:59 PM	1448.88	25	258.4
10/18/2018	5:05:54 PM	1465.8	24.9	260.4

10/18/2018	5:53:52 PM	1513.76	24.7	264.6
10/18/2018	6:24:48 PM	1544.7	24.5	268.7
10/18/2018	6:50:24 PM	1570.31	24.4	270.8
10/18/2018	7:32:22 PM	1612.27	24.2	274.9
10/18/2018	8:22:03 PM	1661.95	24	279
10/18/2018	9:54:25 PM	1754.33	23.9	281.1
10/18/2018	10:10:17 PM	1770.19	23.7	285.2
10/18/2018	10:27:48 PM	1787.7	23.5	289.4
10/18/2018	10:43:44 PM	1803.65	23.4	291.4
10/18/2018	11:21:20 PM	1841.23	23.2	295.6
10/19/2018	12:05:06 AM	1885.01	23	299.7
10/19/2018	12:25:29 AM	1905.4	22.9	301.8
10/19/2018	1:06:59 AM	1946.89	22.7	305.9
10/19/2018	1:50:39 AM	1990.55	22.5	310
10/19/2018	2:06:12 AM	2006.11	22.4	312.1
10/19/2018	3:00:17 AM	2060.19	22.2	316.2
10/19/2018	3:46:00 AM	2105.91	22	320.4
10/19/2018	4:13:06 AM	2133	21.9	322.4
10/19/2018	4:50:25 AM	2170.33	21.7	326.6
10/19/2018	5:34:09 AM	2214.06	21.5	330.7
10/19/2018	5:49:13 AM	2229.13	21.4	332.8
10/19/2018	8:26:45 AM	2386.66	21.2	336.9
10/19/2018	8:38:07 AM	2398.02	21	341
10/19/2018	8:45:53 AM	2405.79	20.9	343.1
10/19/2018	9:33:09 AM	2453.05	20.7	347.2
10/19/2018	10:49:52 AM	2529.77	20.5	351.4
10/19/2018	11:09:55 AM	2549.83	20.4	353.4
10/19/2018	12:06:35 PM	2606.5	20.2	357.6
10/19/2018	1:45:34 PM	2705.47	20	361.7
10/19/2018	2:20:57 PM	2740.86	19.9	363.8
10/19/2018	2:51:40 PM	2771.58	19.7	367.9
10/19/2018	3:59:37 PM	2839.53	19.5	372
10/19/2018	4:42:03 PM	2881.96	19.4	374.1
10/19/2018	5:22:21 PM	2922.26	19.2	378.2
10/19/2018	5:55:40 PM	2955.57	19	382.4

10/19/2018	6:15:44 PM	2975.64	18.9	384.4
10/19/2018	7:14:16 PM	3034.17	18.7	388.6
10/19/2018	8:06:35 PM	3086.49	18.5	392.7
10/19/2018	8:41:40 PM	3121.57	18.4	394.8
10/19/2018	9:29:59 PM	3169.9	18.2	398.9
10/19/2018	10:36:44 PM	3236.64	18	403.1
10/19/2018	11:02:18 PM	3262.21	17.9	405.1
10/19/2018	11:52:21 PM	3312.25	17.7	409.3
10/20/2018	12:42:33 AM	3362.46	17.5	413.4
10/20/2018	1:08:47 AM	3388.69	17.4	415.5
10/20/2018	1:49:34 AM	3429.48	17.2	419.6
10/20/2018	2:37:45 AM	3477.65	17	423.7
10/20/2018	2:57:21 AM	3497.26	16.9	425.8
10/20/2018	3:51:24 AM	3551.3	16.7	429.9
10/20/2018	4:41:53 AM	3601.8	16.5	434.1
10/20/2018	5:09:15 AM	3629.16	16.4	436.1
10/20/2018	5:56:22 AM	3676.27	16.2	440.3
10/20/2018	6:44:56 AM	3724.83	16	444.4
10/20/2018	7:15:02 AM	3754.94	15.9	446.5
10/20/2018	8:10:03 AM	3809.96	15.7	450.6
10/20/2018	8:56:49 AM	3856.73	15.5	454.7
10/20/2018	9:22:03 AM	3881.95	15.4	456.8
10/20/2018	10:27:37 AM	3947.53	15.2	460.9
10/20/2018	11:40:50 AM	4020.73	15	465.1
10/20/2018	12:03:22 PM	4043.27	14.9	467.1
10/20/2018	1:03:10 PM	4103.08	14.7	471.3
10/20/2018	2:22:18 PM	4182.2	14.5	475.4
10/20/2018	2:51:40 PM	4211.57	14.4	477.5
10/20/2018	3:42:09 PM	4262.06	14.2	481.6
10/20/2018	4:41:52 PM	4321.78	14	485.7
10/20/2018	5:16:30 PM	4356.4	13.9	487.8
10/20/2018	6:28:45 PM	4428.65	13.7	491.9
10/20/2018	7:18:53 PM	4478.78	13.5	496.1
10/20/2018	7:42:23 PM	4502.28	13.4	498.1
10/20/2018	8:37:59 PM	4557.88	13.2	502.3

10/20/2018	9:31:01 PM	4610.93	13	506.4
10/20/2018	9:53:06 PM	4633.01	12.9	508.5
10/20/2018	10:45:00 PM	4684.91	12.7	512.6
10/20/2018	11:36:55 PM	4736.82	12.5	516.7
10/21/2018	12:07:31 AM	4767.42	12.4	518.8
10/21/2018	1:05:43 AM	4825.63	12.2	522.9
10/21/2018	1:55:01 AM	4874.92	12	527.1
10/21/2018	2:17:48 AM	4897.71	11.9	529.1
10/21/2018	3:10:48 AM	4950.7	11.7	533.3
10/21/2018	4:00:46 AM	5000.68	11.5	537.4
10/21/2018	4:28:54 AM	5028.81	11.4	539.5
10/21/2018	5:13:36 AM	5073.51	11.2	543.6
10/21/2018	6:05:44 AM	5125.63	11	547.7
10/21/2018	6:32:07 AM	5152.03	10.9	549.8
10/21/2018	7:27:52 AM	5207.77	10.7	553.9
10/21/2018	8:33:30 AM	5273.41	10.5	558.1
10/21/2018	9:19:21 AM	5319.26	10.4	560.1
10/21/2018	3:04:26 PM	5664.35	10.2	564.3
10/21/2018	4:38:36 PM	5758.5	10	568.4
10/21/2018	5:26:39 PM	5806.56	9.9	570.5

Table E3: Pressure head results of sample SL-1-11 from falling head permeability test. Flow rate was calculated as 36.594 ml/min and K_{sat} was 7.97 meters/day

Date	Time	Elapsed Time (min)	Pressure (cmH2O)	Total Water Consumed (ml)
11/1/2018	4:21:13 PM	0	21.8	
11/1/2018	4:21:49 PM	0.6	21.7	2.1
11/1/2018	4:21:52 PM	0.66	21.5	6.2
11/1/2018	4:21:54 PM	0.69	21.4	8.3
11/1/2018	4:21:58 PM	0.76	21.2	12.4
11/1/2018	4:22:02 PM	0.82	21	16.5
11/1/2018	4:22:03 PM	0.83	20.9	18.6
11/1/2018	4:22:07 PM	0.91	20.7	22.7
11/1/2018	4:22:11 PM	0.98	20.5	26.9
11/1/2018	4:22:13 PM	1.01	20.4	28.9
11/1/2018	4:22:18 PM	1.08	20.2	33.1
11/1/2018	4:22:21 PM	1.13	20	37.2
11/1/2018	4:22:23 PM	1.17	19.9	39.3
11/1/2018	4:22:27 PM	1.24	19.7	43.4
11/1/2018	4:22:31 PM	1.31	19.5	47.5
11/1/2018	4:22:32 PM	1.33	19.4	49.6
11/1/2018	4:22:37 PM	1.4	19.2	53.7
11/1/2018	4:22:41 PM	1.48	19	57.9
11/1/2018	4:22:43 PM	1.51	18.9	59.9
11/1/2018	4:22:47 PM	1.58	18.7	64.1
11/1/2018	4:22:51 PM	1.64	18.5	68.2
11/1/2018	4:22:53 PM	1.68	18.4	70.3
11/1/2018	4:22:59 PM	1.78	18.2	74.4
11/1/2018	4:23:01 PM	1.81	18	78.5
11/1/2018	4:23:04 PM	1.85	17.9	80.6
11/1/2018	4:23:08 PM	1.92	17.7	84.7
11/1/2018	4:23:14 PM	2.02	17.5	88.9
11/1/2018	4:23:17 PM	2.07	17.4	90.9
11/1/2018	4:23:20 PM	2.12	17.2	95.1
11/1/2018	4:23:25 PM	2.2	17	99.2

11/1/2018	4:23:27 PM	2.24	16.9	101.3
11/1/2018	4:23:31 PM	2.31	16.7	105.4
11/1/2018	4:23:36 PM	2.39	16.5	109.5
11/1/2018	4:23:40 PM	2.45	16.4	111.6
11/1/2018	4:23:43 PM	2.51	16.2	115.7
11/1/2018	4:23:47 PM	2.58	16	119.9
11/1/2018	4:23:49 PM	2.61	15.9	121.9
11/1/2018	4:23:56 PM	2.72	15.7	126.1
11/1/2018	4:23:59 PM	2.77	15.5	130.2
11/1/2018	4:24:02 PM	2.83	15.4	132.3
11/1/2018	4:24:07 PM	2.9	15.2	136.4
11/1/2018	4:24:13 PM	3.01	15	140.6
11/1/2018	4:24:15 PM	3.03	14.9	142.6
11/1/2018	4:24:20 PM	3.12	14.7	146.8
11/1/2018	4:24:24 PM	3.19	14.5	150.9
11/1/2018	4:24:27 PM	3.25	14.4	153
11/1/2018	4:24:34 PM	3.35	14.2	157.1
11/1/2018	4:24:38 PM	3.42	14	161.2
11/1/2018	4:24:41 PM	3.47	13.9	163.3
11/1/2018	4:24:46 PM	3.56	13.7	167.4
11/1/2018	4:24:52 PM	3.66	13.5	171.6
11/1/2018	4:24:55 PM	3.7	13.4	173.6
11/1/2018	4:25:02 PM	3.82	13.2	177.8
11/1/2018	4:25:07 PM	3.91	13	181.9
11/1/2018	4:25:09 PM	3.94	12.9	184
11/1/2018	4:25:13 PM	4.01	12.7	188.1
11/1/2018	4:25:20 PM	4.13	12.5	192.2
11/1/2018	4:25:23 PM	4.18	12.4	194.3
11/1/2018	4:25:29 PM	4.27	12.2	198.4
11/1/2018	4:25:33 PM	4.34	12	202.6
11/1/2018	4:25:38 PM	4.43	11.9	204.6
11/1/2018	4:25:44 PM	4.53	11.7	208.8
11/1/2018	4:25:49 PM	4.6	11.5	212.9
11/1/2018	4:25:54 PM	4.69	11.4	215
11/1/2018	4:25:59 PM	4.77	11.2	219.1

11/1/2018	4:26:06 PM	4.89	11	223.2
11/1/2018	4:26:07 PM	4.91	10.9	225.3
11/1/2018	4:26:17 PM	5.07	10.7	229.4
11/1/2018	4:26:21 PM	5.14	10.5	233.6
11/1/2018	4:26:27 PM	5.24	10.4	235.6
11/1/2018	4:26:30 PM	5.3	10.2	239.8
11/1/2018	4:26:32 PM	5.33	9.8	248
11/1/2018	4:26:33 PM	5.35	9.7	250.1
11/1/2018	4:26:45 PM	5.54	9.6	252.2
11/1/2018	4:26:48 PM	5.59	9.5	254.2
11/1/2018	4:26:50 PM	5.62	9.4	256.3
11/1/2018	4:26:53 PM	5.67	9.3	258.4
11/1/2018	4:26:55 PM	5.71	9.2	260.4
11/1/2018	4:26:58 PM	5.76	9.1	262.5
11/1/2018	4:26:59 PM	5.77	9	264.6
11/1/2018	4:27:04 PM	5.86	8.9	266.6
11/1/2018	4:27:08 PM	5.93	8.8	268.7
11/1/2018	4:27:09 PM	5.94	8.7	270.8
11/1/2018	4:27:11 PM	5.98	8.6	272.8
11/1/2018	4:27:14 PM	6.03	8.5	274.9
11/1/2018	4:27:16 PM	6.06	8.4	277
11/1/2018	4:27:20 PM	6.12	8.3	279
11/1/2018	4:27:22 PM	6.15	8.2	281.1
11/1/2018	4:27:27 PM	6.24	8.1	283.2
11/1/2018	4:27:30 PM	6.29	8	285.2
11/1/2018	4:27:32 PM	6.32	7.9	287.3
11/1/2018	4:27:36 PM	6.39	7.8	289.4
11/1/2018	4:27:39 PM	6.44	7.7	291.4
11/1/2018	4:27:42 PM	6.49	7.6	293.5
11/1/2018	4:27:45 PM	6.54	7.5	295.6
11/1/2018	4:27:48 PM	6.59	7.4	297.6
11/1/2018	4:27:52 PM	6.66	7.3	299.7
11/1/2018	4:27:54 PM	6.7	7.2	301.8
11/1/2018	4:27:57 PM	6.75	7.1	303.8
11/1/2018	4:28:01 PM	6.8	7	305.9

11/1/2018	4:28:06 PM	6.88	6.9	308
11/1/2018	4:28:07 PM	6.9	6.8	310
11/1/2018	4:28:12 PM	6.99	6.7	312.1
11/1/2018	4:28:14 PM	7.02	6.6	314.2
11/1/2018	4:28:16 PM	7.06	6.5	316.2
11/1/2018	4:28:20 PM	7.12	6.4	318.3
11/1/2018	4:28:23 PM	7.18	6.3	320.4
11/1/2018	4:28:28 PM	7.26	6.2	322.4
11/1/2018	4:28:30 PM	7.3	6.1	324.5
11/1/2018	4:28:33 PM	7.35	6	326.6
11/1/2018	4:28:39 PM	7.43	5.9	328.6
11/1/2018	4:28:43 PM	7.5	5.8	330.7
11/1/2018	4:28:46 PM	7.55	5.7	332.8
11/1/2018	4:28:48 PM	7.59	5.6	334.8
11/1/2018	4:28:52 PM	7.65	5.5	336.9
11/1/2018	4:28:56 PM	7.72	5.4	339
11/1/2018	4:29:00 PM	7.79	5.3	341
11/1/2018	4:29:02 PM	7.83	5.2	343.1
11/1/2018	4:29:06 PM	7.89	5.1	345.2
11/1/2018	4:29:11 PM	7.98	5	347.2
11/1/2018	4:29:13 PM	8.01	4.9	349.3
11/1/2018	4:29:17 PM	8.06	4.8	351.4
11/1/2018	4:29:22 PM	8.15	4.7	353.4
11/1/2018	4:29:25 PM	8.2	4.6	355.5
11/1/2018	4:29:28 PM	8.25	4.5	357.6
11/1/2018	4:29:34 PM	8.36	4.4	359.6
11/1/2018	4:29:35 PM	8.37	4.3	361.7
11/1/2018	4:29:41 PM	8.48	4.2	363.8
11/1/2018	4:29:44 PM	8.53	4.1	365.8
11/1/2018	4:29:52 PM	8.66	3.9	370
11/1/2018	4:30:00 PM	8.78	3.7	374.1
11/1/2018	4:30:08 PM	8.92	3.5	378.2
11/1/2018	4:30:17 PM	9.07	3.3	382.4
11/1/2018	4:30:20 PM	9.13	3.2	384.4
11/1/2018	4:30:27 PM	9.24	3	388.6

11/1/2018	4:30:43 PM	9.5	2.8	392.7
11/1/2018	4:30:44 PM	9.52	2.7	394.8
11/1/2018	4:30:55 PM	9.71	2.5	398.9
11/1/2018	4:31:06 PM	9.89	2.3	403.1
11/1/2018	4:31:11 PM	9.98	2.2	405.1
11/1/2018	4:31:24 PM	10.19	2	409.3
11/1/2018	4:31:33 PM	10.34	1.8	413.4
11/1/2018	4:31:46 PM	10.56	1.6	417.5
11/1/2018	4:32:03 PM	10.84	1.4	421.7
11/1/2018	4:32:10 PM	10.96	1.3	423.7
11/1/2018	4:32:22 PM	11.16	1.1	427.9
11/1/2018	4:32:46 PM	11.55	0.9	432
11/1/2018	4:32:55 PM	11.7	0.8	434.1
11/1/2018	4:33:11 PM	11.98	0.6	438.2

APPENDIX F

Hyprop Results

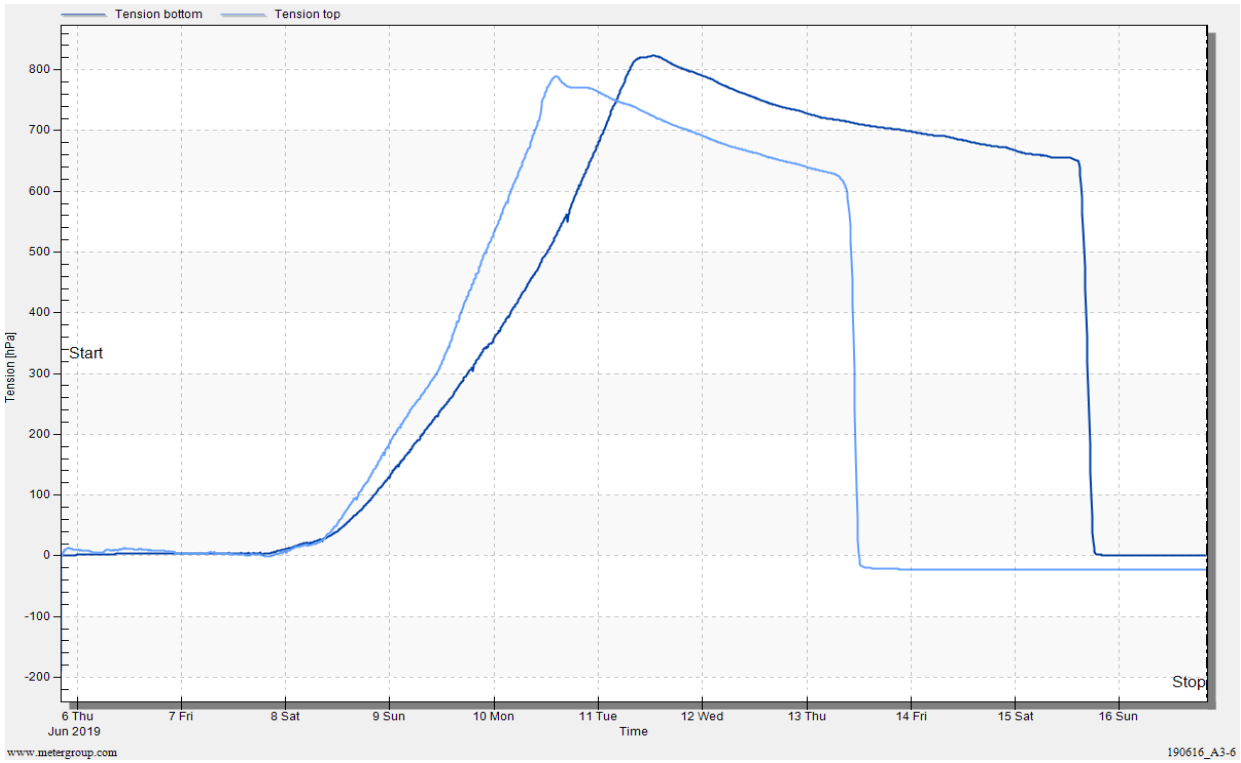

Figure F1: Tension data from 2 tensiometers

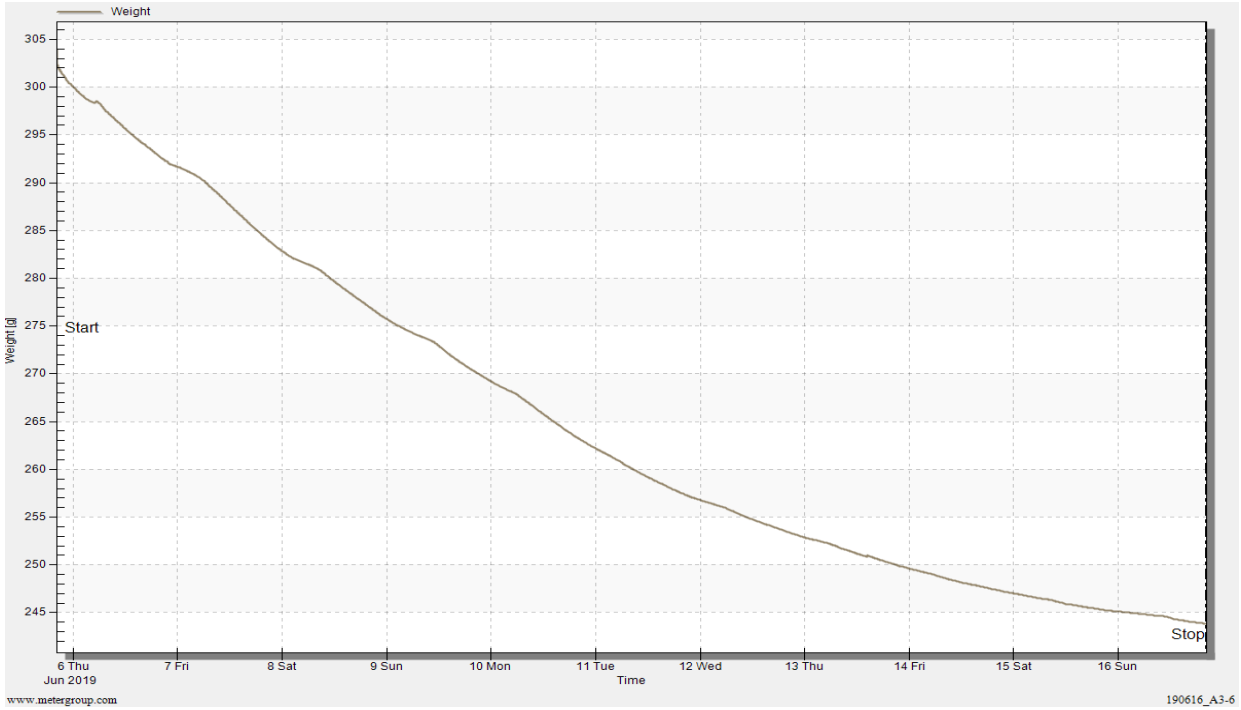

Figure F2: Weight data from Hyprop test

APPENDIX G

Hanging Water Column Data and van Genuchten Equation Fit

Table G1: Hanging water column data – draining curve

Suction head ψ (cm)	Increase of the water level in the burette, Δh (cm)	The loss of the water,	Moisture Content
		$A \cdot \Delta h$ (cm^3)	θ
5.1	3	0.1	0.329
7.1	0.1	-0.2	0.332
12.1	0	0	0.332
17.1	0	0	0.332
19.1	0.5	-0.6	0.342
25.1	0	0	0.342
30.1	1.9	3.6	0.284
30.2	0.8	1.1	0.266
31.4	0.6	0.9	0.251
31.8	0.4	0.3	0.246
33.4	0.9	1.2	0.227
34.5	0.5	1	0.210
36.1	0.9	0.8	0.198
37.1	0.7	0.9	0.183
38.1	0.3	0.4	0.177
39.8	0.7	0.8	0.164
41.1	0.7	0.8	0.150
43.1	0.7	0.4	0.144
45.1	-0.3	0.3	0.139
47.1	0.3	0.2	0.136
50.1	0.4	0.6	0.126
55.1	0.3	0.5	0.118
65.1	0.4	0.7	0.107
75.1	0.3	0.3	0.102
85.1	0.3	0.3	0.097
95.1	0.2	0.5	0.089
105.1	0	0	0.089
109.1	0	0	0.089

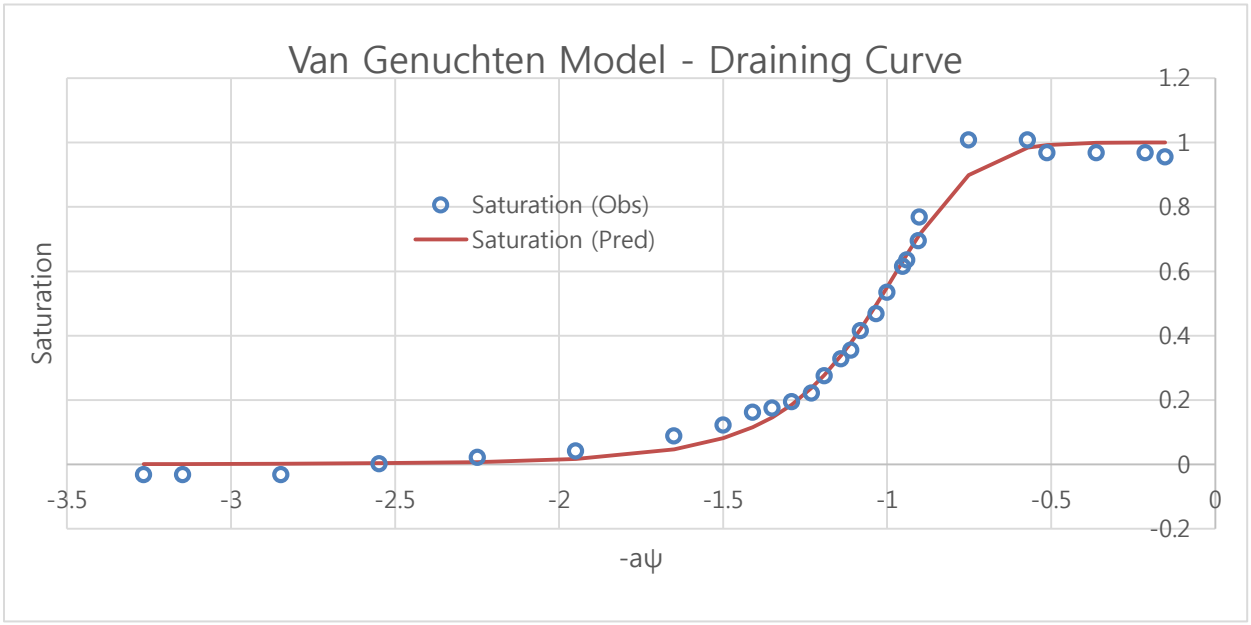

Figure G1: Van Genuchten model fit – draining curve

Table G2: Hanging water column data – wetting curve

Suction head ψ (cm)	The gain of the water, $A \cdot \Delta h$ (cm^3)	Moisture Content θ
109.1	0	0.089
85.1	0.3	0.094
65.1	0.9	0.108
45.1	1	0.125
35.1	1.7	0.152
30.1	1.3	0.173
25.1	1.7	0.201
20.1	3.2	0.253
15.1	3.6	0.311
10.1	2.2	0.330
5.1	1.1	0.330
0.1	0.9	0.330
-4.9	6.4	0.330
-9.9	6.4	0.330
-14.9	6.8	0.330
-24.9	0	0.330

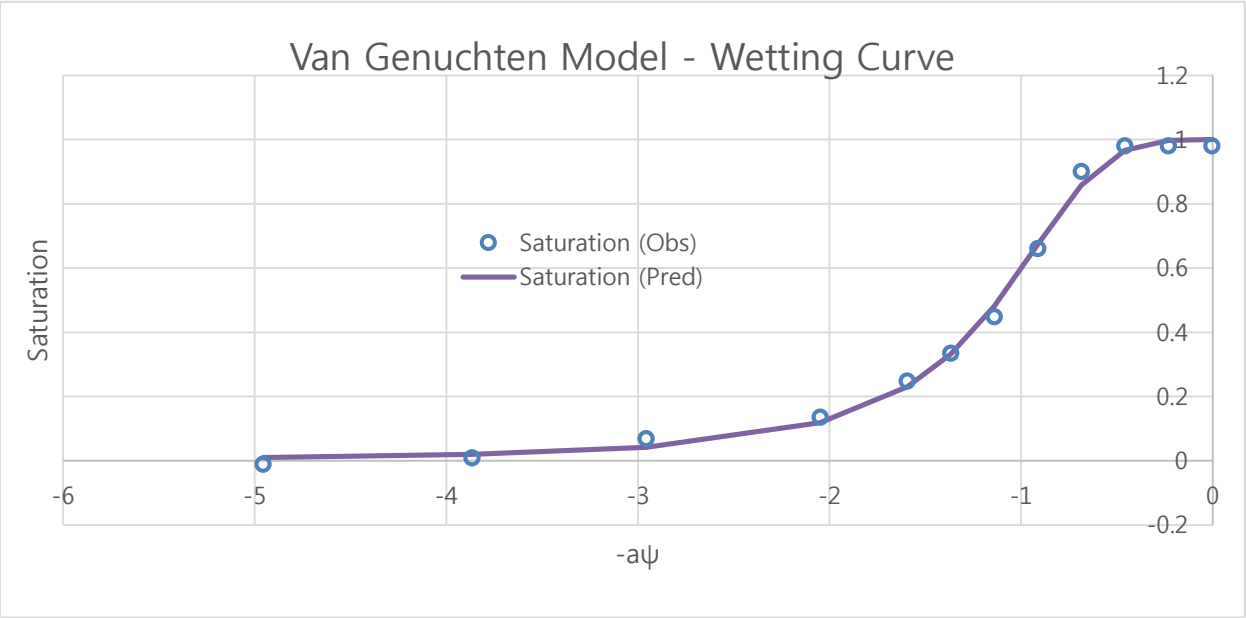

Figure G2: Van Genuchten model fit – wetting curve

APPENDIX H

Balance Error File from 3D Model using HYDRUS-3D

Time [T] 0.00000000E+00

Sub-region num. 1

Volume	[L3]	0.13093E+05 0.13093E+05
VolumeW	[L3]	0.40277E+04 0.40318E+04
InFlow	[L3/T]	0.00000E+00 0.00000E+00
hMean	[L]	0.11660E+02 11.660

Time [T] 0.0500

Sub-region num. 1

Volume	[L3]	0.13093E+05 0.13093E+05
VolumeW	[L3]	0.40320E+04 0.40359E+04
InFlow	[L3/T]	0.75252E+02 0.75252E+02
hMean	[L]	0.11676E+02 11.676
WatBalT	[L3]	0.43691E+01
WatBalR	[%]	96.744

Time [T] 0.1000

Sub-region num. 1

Volume [L3] 0.13093E+05 0.13093E+05

VolumeW [L3] 0.40340E+04 0.40377E+04

InFlow [L3/T] 0.21294E+02 0.21294E+02

hMean [L] 0.11684E+02 11.684

WatBalT [L3] 0.86910E+01

WatBalR [%] 77.943

Time [T] 0.1500

Sub-region num. 1

Volume [L3] 0.13093E+05 0.13093E+05

VolumeW [L3] 0.40348E+04 0.40384E+04

InFlow [L3/T] 0.10415E+02 0.10415E+02

hMean [L] 0.11688E+02 11.688

WatBalT [L3] 0.13031E+02

WatBalR [%] 68.174

Time [T] 0.2000

Sub-region num. 1

Volume [L3] 0.13093E+05 0.13093E+05

VolumeW [L3] 0.40352E+04 0.40388E+04

InFlow [L3/T] 0.65646E+01 0.65646E+01

hMean [L] 0.11691E+02 11.691

WatBalT [L3] 0.17386E+02

WatBalR [%] 63.446

Time [T] 0.2500

Sub-region num. 1

Volume [L3] 0.13093E+05 0.13093E+05

VolumeW [L3] 0.40355E+04 0.40390E+04

InFlow [L3/T] 0.46231E+01 0.46231E+01

hMean [L] 0.11693E+02 11.693

WatBalT [L3] 0.21746E+02

WatBalR [%] 60.740

Time [T] 0.3000

Sub-region num. 1

Volume [L3] 0.13093E+05 0.13093E+05

VolumeW [L3] 0.40357E+04 0.40392E+04

InFlow [L3/T] 0.35284E+01 0.35284E+01

hMean [L] 0.11695E+02 11.695

WatBalT [L3] 0.26110E+02

WatBalR [%] 59.033

Time [T] 0.3500

Sub-region num. 1

Volume	[L3]	0.13093E+05 0.13093E+05
VolumeW	[L3]	0.40358E+04 0.40394E+04
InFlow	[L3/T]	0.28140E+01 0.28140E+01
hMean	[L]	0.11696E+02 11.696
WatBalT	[L3]	0.30477E+02
WatBalR	[%]	57.793

Time [T] 0.4000

Sub-region num. 1

Volume	[L3]	0.13093E+05 0.13093E+05
VolumeW	[L3]	0.40359E+04 0.40395E+04
InFlow	[L3/T]	0.23260E+01 0.23260E+01
hMean	[L]	0.11697E+02 11.697
WatBalT	[L3]	0.34844E+02
WatBalR	[%]	56.865

Time [T] 0.4500

Sub-region num. 1

Volume [L3] 0.13093E+05 0.13093E+05

VolumeW [L3] 0.40361E+04 0.40396E+04

InFlow [L3/T] 0.19811E+01 0.19811E+01

hMean [L] 0.11698E+02 11.698

WatBalT [L3] 0.39214E+02

WatBalR [%] 56.204

Time [T] 0.5000

Sub-region num. 1

Volume [L3] 0.13093E+05 0.13093E+05

VolumeW [L3] 0.40361E+04 0.40396E+04

InFlow [L3/T] 0.17046E+01 0.17046E+01

hMean [L] 0.11699E+02 11.699

WatBalT [L3] 0.43584E+02

WatBalR [%] 55.704

Time [T] 0.5500

Sub-region num. 1

Volume [L3] 0.13093E+05 0.13093E+05

VolumeW [L3] 0.40362E+04 0.40397E+04

InFlow [L3/T] 0.14804E+01 0.14804E+01

hMean [L] 0.11700E+02 11.700

WatBalT [L3] 0.47955E+02

WatBalR [%] 55.274

Time [T] 0.6000

Sub-region num. 1

Volume [L3] 0.13093E+05 0.13093E+05

VolumeW [L3] 0.40363E+04 0.40398E+04

InFlow [L3/T] 0.13098E+01 0.13098E+01

hMean [L] 0.11701E+02 11.701

WatBalT [L3] 0.52326E+02

WatBalR [%] 54.902

Time [T] 0.6500

Sub-region num. 1

Volume [L3] 0.13093E+05 0.13093E+05

VolumeW [L3] 0.40364E+04 0.40398E+04

InFlow [L3/T] 0.11691E+01 0.11691E+01

hMean [L] 0.11702E+02 11.702

WatBalT [L3] 0.56697E+02

WatBalR [%] 54.605

Time [T] 0.7000

Sub-region num. 1

Volume [L3] 0.13093E+05 0.13093E+05

VolumeW [L3] 0.40364E+04 0.40399E+04

InFlow [L3/T] 0.10564E+01 0.10564E+01

hMean [L] 0.11702E+02 11.702

WatBalT [L3] 0.61068E+02

WatBalR [%] 54.334

Time [T] 0.7500

Sub-region num. 1

Volume [L3] 0.13093E+05 0.13093E+05

VolumeW [L3] 0.40365E+04 0.40399E+04

InFlow [L3/T] 0.95750E+00 0.95750E+00

hMean [L] 0.11703E+02 11.703

WatBalT [L3] 0.65440E+02

WatBalR [%] 54.104

Time [T] 0.8000

Sub-region num. 1

Volume [L3] 0.13093E+05 0.13093E+05

VolumeW [L3] 0.40365E+04 0.40399E+04

InFlow [L3/T] 0.87693E+00 0.87693E+00

hMean [L] 0.11703E+02 11.703

WatBalT [L3] 0.69812E+02

WatBalR [%] 53.920

Time [T] 0.8500

Sub-region num. 1

Volume [L3] 0.13093E+05 0.13093E+05

VolumeW [L3] 0.40366E+04 0.40400E+04

InFlow [L3/T] 0.81067E+00 0.81067E+00

hMean [L] 0.11704E+02 11.704

WatBalT [L3] 0.74185E+02

WatBalR [%] 53.787

Time [T] 0.9000

Sub-region num. 1

Volume	[L3]	0.13093E+05 0.13093E+05
VolumeW	[L3]	0.40366E+04 0.40400E+04
InFlow	[L3/T]	0.74375E+00 0.74375E+00
hMean	[L]	0.11705E+02 11.705
WatBalT	[L3]	0.78558E+02
WatBalR	[%]	53.690

Time [T] 0.9500

Sub-region num. 1

Volume	[L3]	0.13093E+05 0.13093E+05
VolumeW	[L3]	0.40366E+04 0.40401E+04
InFlow	[L3/T]	0.69362E+00 0.69362E+00
hMean	[L]	0.11705E+02 11.705
WatBalT	[L3]	0.82931E+02
WatBalR	[%]	53.611

Time [T] 1.0000

Sub-region num. 1

Volume [L3]	0.13093E+05	0.13093E+05
VolumeW [L3]	0.40367E+04	0.40401E+04
InFlow [L3/T]	0.64544E+00	0.64544E+00
hMean [L]	0.11706E+02	11.706
WatBalT [L3]	0.87304E+02	
WatBalR [%]	53.525	

VITA

Kyungwon (Won) Kwak

Master of Science in **Hydrology** August 2017 - August 2019
Department of Geology and Geological Engineering, University of Mississippi, University, MS
THESIS: “Examining the Use of Vadose-Zone Recharge Wells in the Mississippi River Valley Alluvial Aquifer as an Artificial Recharge Method”
Advisor: Dr. Andrew M. O’Reilly

Bachelor of Science in **Geological Sciences** March 2012 - February 2016
Department of Earth Systems & Environmental Sciences, Chonnam National University, Gwangju, South Korea
GPA: 4.24/4.5 *summa cum laude* Top Student in College of Natural Sciences
THESIS: “The Hydrologic Causes of Sinkhole Formation in an Urban Area”